Seismological Studies of the 1983 Japan Sea Earthquake Tsunami

Kenji Satake

Ph.D. Thesis submitted to University of Tokyo

July 3, 1987

TABLE OF CONTENTS

Abstract

The Japan Sea earthquake of May 26, 1983 was accompanied by a destructive tsunami. This tsunami is important not only because it is recorded on many tide gauge stations but also it occurred in the closed Japan Sea and continued for a long time. In this thesis, seismological studies are made to infer the source process of the Japan Sea earthquake and the long-period features of the tsunamis in the Japan Sea.

In Part 1, the heterogeneous fault motion of the 1983 Japan Sea earthquake is inferred from the tsunami record. The inversion of tsunami waveforms is formulated in Chapter 1. Since the velocity of tsunami wave depends on water depth which is a well-known geophysical quantity, the propagation effect can be evaluated by making a finite-difference computation on actual bathymetry. Thus the information on tsunami source can be retrieved from tide gauge records. Several numerical experiments are made to confirm the effectiveness of the method.

Chapter 2 deals with tide gauge responses. The tsunami waveforms on tide gauge records are affected by the response of the tide gauge system. The *in situ* measurements are made for 18 tide gauge stations and the corrections are made for the observed tsunami waveforms. The corrected amplitude of the tsunami becomes more than twice of the tide gauge records for several stations.

In Chapter 3, the fault heterogeneity of the Japan Sea earthquake is estimated by the inversion of the corrected data for the tide gauge response. The result shows that the slip on the fault is larger at just north of the epicenter than other parts of the fault, indicating the existence of an asperity.

In Part 2, the free oscillations of the Japan Sea excited by large earthquakes are examined. The tsunamis in the closed Japan Sea continued more than two days probably due to the multiple reflections on the coasts. The analysis of the tide gauge records of the 1983 Japan Sea and the 1964 Niigata earthquakes is made in Chapter 1. The spectra of the tsunami show several distinct peaks above the noise level in the period range between 40 min and 3.5 hours. The finite-difference computations are made to reproduce the observed spectra and to separate the whole and regional oscillatons of the Japan Sea.

In Chapter 2, the modal approach for the free oscillation is discussed. The equivalence of the finite-differece computation and a superposition of normal mode solutions is indicated with a simple example.

The modal approach is applied to the Japan Sea in Chapter 3. One hundred normal mode solutions of the Japan Sea with the eigen period longer than 50 min are computed. These include the whole and the regional oscillations. The synthetic tsunamis by a superposition of the normal modes are compared with the observations. It is found that the excitation of the free oscillaton is different for the 1983 Japan Sea and the 1964 Niigata earthquakes because of the different ocean depth at the source area.

In Chapter 4, the detectability of a very slow crustal movement from tide gauge records is discussed. Since the period of the free oscillation of the ocean basin such as Japan Sea is much longer than that of the free oscillation of the solid Earth, it can be used for the detection of the slow crustal movements possibly preceding a large earthquake.

The ray tracing of tsunamis is presented in Appendix. The ray tracing is usuful for a preliminary evaluation of the tsunami propagation. The bathymetric effect is found to be significant for the tsunamis in the Japan Sea.

Acknowlegements

I thank my thesis adviser Kunihiko Shimazaki for critically reviewing the manuscripts and stimulus discussions throughout the course of this study. Part 2 of this thesis is a co-operative work with him which I enjoyed very much.

I also thank Katsuyuki Abe for continuous advise and discussion since I was an undergraduate student at Hokkaido University. My work on tsunami began with a field survey of the 1983 Japan Sea earthquake tsunami which was led by him.

My graduate study for the last 5 and half years has been made at Dept. Geophysics, Hokkaido Univ., Earthquake Reseach Inst., Univ. Tokyo and Dept. Applied Physics, Tokyo Inst. Tech. Too many colleagues and friends to mention here must be acknowledged for their advices, discussions, and encouragements. Among them, discussions with Toshiyuki Hibiya, Toshihiko Hashida, Shin'ichi Iwasaki, Shigeru Yamaki, Isamu Aida and Yoshinobu Tsuji have been directly improved the contents of the thesis.

The works in this thesis were supported by Grant-in-Aid for Natural Disasters and for Encouragement of Young Scientists from the Ministry of Education, Science and Culture. I have enjoyed to attend the meetings and field trips of the Natural Disasters group. Most of the measurements of chapter 1.2 were made with Kuniaki Abe and Masami Okada. I also thank Chiaki Goto, Fumihiko Imamura and Nobuo Shuto for their comments and discussions from a view point of civil engineering.

Takashi Fujii helped me prepare the manuscript, Masanori Saito, Masaru Kono and Yoshimori Honkura have continuously encouraged me.

Numerical Computations were made at the Computer Centre, Univ. Tokyo, and the Computer Center of Tokyo Inst. Technology. The database system at Earthquake Predicition Observation Center, Earthquake Research Inst. is also used.

Part 1

Fault Heterogeneity of the 1983 Japan Sea Earthquake Estimated by an Inversion of Tsunami Waveforms

Chapter 1

Inversion of Tsunami Waveforms : Method and Numerical Experiments

Abstract

A method for estimating fault heterogeneity by an inversion of tsunami waveforms is presented. The ocean bottom bathymetry, by which the velocity of tsunami wave is determined, is more accurately known than the seismic velocity structure, so that the effect on the propagation path can be precisely evaluated by means of numerical computation. Since the propagation velocity of tsunami is much smaller than any kind of seismic wave or rupture velocity, only a final slip distribution on a fault can be estimated. The slip amount on each segment of the fault is obtained by an inversion of the observed tsunami waveforms by using the numerically computed waveforms from each segment as the Green's function. Several numerical experiments are carried out to examine the spatial resolution of the fault heterogeneity by the present method. It is clarified that the size of the segment needs to be more than eight times the grid size used for the computation of the Green's function, indicating that accurate bathymetric data and large computation are required to get a fine picture of the heterogeneous fault motion. Simulation of the inversion shows that the slip distribution on the fault can be estimated stably. The effect of tide gauge response is the only unknown parameter contained in tsunami records besides the source information, so it is necessary to investigate it before the present method is applied to actual tsunami records.

1. Introduction

The rupture process on a fault is one of the most important problems in earthquake seismology and have been studied mainly by analyzing seismograms. For example, KIKUCHI and FUKAO (1985) made an iterative deconvolution of long-period body waves to study the source process of the 1968 Tokachi-oki earthquake and MORI and SHIMAZAKI (1985) made an inversion of intermediate Rayleigh waves for the same event. Seismograms contain information not only on the source process but also on the propagation path. Figure 1 is a schematic diagram showing the various information included in seismograms. Recent studies on mantle structure revealed the large scale heterogeneity in both the upper and lower mantle (*e.g.* WOODHOUSE and DZIEWONSKI, 1984). The correction for such heterogeneity on the propagation path is necessary even for the long-period surface waves (SATAKE, 1985). For detailed study of the source process, shorter-period seismic wave with shorter wavelength must be used. The shorter the wavelength of the seismic wave is, the effect of heterogeneity on the propagation path becomes more dominant. However, the Earth's lateral structure has not been known in such a small scale.

In this paper, use of tsunami as an alternative tool for seismic waves is proposed. Shallow large submarine earthquakes are usually accompanied by tsunamis which are clearly recorded on tide gauges. The size of earthquakes we are interested in here is $M > 7$ or $M_0 > 10^{27}$ dyne·cm, the corresponding fault size is more than several tens of km (KANAMORI and ANDERSON, 1975). Tsunami records contain information not only on source but also on the effects of propagation path, bay or harbor near tide gauge, and the response of tide gauge system (Fig.1). The propagation velocity of tsunami depends only on water depth as far as tsunami is regarded as linear long-wave. Since the bathymetry is one of the well-known quantities among the geophysical data, the propagation effect can be evaluated more precisely than the seismic waves by means of numerical computation. If the other effects are also known, source process can be retrieved from tide gauge records.

The purpose of this paper is to formulate the waveform inversion of tsunamis and to examine the reliability of the method.

2. Computation of Tsunami Waveforms

The tsunami waveforms have been computed either analytically for a uniform depth (*e.g.* TAKAHASHI, 1942; KAJIURA, 1963) or numerically for an actual topography (AIDA, 1978; SATAKE, 1985). Since our interest is in large earthquakes occurring at tectonically complicated regions such as subduction zone, the assumption of uniform depth or simple topography is not valid. The effect of bathymetry on tsunami propagation is found to be very significant (SATAKE, 1988).

We first discuss on the validity of linear long-wave approximation. When the amplitude of tsunami is small compared to the water depth, the advection term can be neglected so that the equation of motion becomes linear (*e.g.* MURTY, 1977). The linearity holds except for the very shallow region near the coast. The inversion is much easier for linear problems because of the superposition principle.

The phase velocity c of a small amplitude, or linear, gravity wave is given as (*e.g.* LAMB, 1932),

$$c = \sqrt{g/k \tanh kD} = \sqrt{g\lambda/2\pi \tanh (2\pi D/\lambda)} \qquad (1)$$

where g is the gravitational acceleration, k the wavenumber, D the water depth, and λ is the wavelength. If the water is shallow, or $2\pi D/\lambda$ is small, the function $y = \tanh x$ is close to $y = x$ as shown in Fig.2. In this case the velocity becomes $\sqrt{gD}$, which corresponds a long-wave approximation. As can be seen in Fig.2, this approximation is valid for small values of x or D/λ. On the other hand, the function $\tanh x$ becomes almost unity if D/λ is larger than 0.3. In this case the phase velocity is given as $\sqrt{g\lambda/2\pi}$ which corresponds a deep water or short-wave approximation. Since this wave shows a dispersive character, the

treatment must be totally different. Figure 2 shows that the error associated with the long-wave approximation is less than 0.07 if $D/\lambda = 0.1$ and less than 0.01 if $D/\lambda = 0.05$. This means that when the wavelength of tsunami is as long as 10 times the water depth, the error is 7 % and when the ratio is 20 the error is less than 1 %. The fault size of earthquakes of our interest is more than several tens of km and the ocean depth around the source area is at most a few km. Therefore the long-wave approximation is valid in the present study and the associated error is less than several per cent. This amount of error is considered as negligible in the present study. However, we must keep in mind that tsunamis from small earthquakes in deep ocean may be considered as short-waves.

The method of numerical computation is very similar to that used by AIDA (1978) and SATAKE (1985), so we describe it briefly. The basic equations are the linear long-wave equation and the equation of continuity, both integrated vertically from the bottom to the water surface. They are

$$\frac{\partial Q_x}{\partial t} = -gD \frac{\partial H}{\partial x}$$

$$\frac{\partial Q_y}{\partial t} = -gD \frac{\partial H}{\partial y} \tag{2}$$

and

$$\frac{\partial H}{\partial t} = -\left(\frac{\partial Q_x}{\partial x} + \frac{\partial Q_y}{\partial y}\right) \tag{3}$$

where Q_x and Q_y are the flow rate in x and y directions respectively, and H is the surface elevation of water. Equations (2) and (3) are solved by a finite-difference method in a staggered grid system. The time step of integration is chosen so as to satisfy a stability condition.

3. Inversion of Tsunami Waveforms

The velocity of tsunami, or linear long-wave, is much smaller than any kind of seismic waves or rupture velocity of the fault. The *P* wave velocity in the upper mantle is about 8 km/s whereas the velocity of tsunami for a depth of 3000m, for example, is 0.17km/s. This difference is essential in formulating the inversion. We discuss it in a representative example. Figure 3 is a travel time diagram for a representative earthquake. The fault length is 100 km and the source process time is 30 sec since the rupture velocity is about 3 km/s. The travel time of *P* and tsunami waves from three different points in time and space are shown in the figure. One phase (phase 1) leaves the epicenter at the origin time. The other two phases are from the epicenter (phase 2) and the other end of the fault (phase 3) after the source process is completed. Since the *P* wave velocity is larger than the rupture velocity, the time lag of phase 3 arrival to phase 2 at the observation point is smaller than that of phase 2 to phase 1, or the source process time. This means that the temporal resolution in the source process is better than the spatial resolution if seismic waves are used. On the other hand, the velocity of tsunami wave is much smaller than the rupture velocity so that the arrival time of phases 2 and 3 differ significantly. Since the resolution of the observed tsunami waveform is about 1 min (SATAKE *et al.*, 1988), it is impossible to infer the temporal change in the source process. However, the spatial resolution in the fault area is good as the large separation of arrivals of phases 2 and 3 indicates. Therefore we make our formulation to estimate the final spatial distribution of slip on the fault.

The source of tsunami is the ocean bottom deformation, which can be computed from fault parameters (*e.g.* MANSINHA and SMYLE, 1971). If the slip on a fault plane is not uniform, the resultant crustal deformation must be also heterogeneous. KAJIURA (1970) discussed on the energy exchange between the bottom and the water on the basis of the long-wave approximation and showed that if the deformation is completed in less than

several minites it can be treated as an abrupt change. Since the source process time of earthquakes of our interest is less than a few minutes, the water surface is considered to be uplifted exactly the same as the bottom deformation and it can be regarded as an initial condition for tsunami propagation. We divide the source area into small segments and compute waveforms from each segment by the numerical method described in the previous section. These are used as the Green's function in the inversion.

The observational equation is written as

$$A_{ij}(t) \cdot x_j = b_i(t) \tag{4}$$

where $A_{ij}(t)$ is the Green's function at the i-th station from the j-th segment, x_j is a weight or the slip amount for the j-th segment, and $b_i(t)$ is the tide gauge record at the i-th station. Equation (4) is a set of simultaneous linear equations (Fig.4) and the solution x_j can be inverted readily by a least-squares method. Each time point of waveform consists of data points so that a large amount of data are available from each station. This is the major difference from the previous trial and error method of tsunami analysis (*e.g.* SATAKE, 1985). AIDA (1972) tried a similar approach to estimate an initial water elevation distribution without assuming a fault model, but he could not get a reasonable solution since the crustal deformation caused by a fault motion is too complicated to be presented by a coarse grid. In this study, assuming a fault model, we intend to estimate the slip distribution on a fault.

To investigate a heterogeneity on a fault, a fine segmentation of fault is desirable. On the other hand, since the Green's function is computed numerically, the fine segmentation requires large memories and long computation time. To get an idea of optimum grid size for computation, numerical experiments are carried out for a very simple case.

4. Effect of Grid Size : Simple Numerical Experiment

In this section, the effect of grid size is examined by a simple numerical experiment in a rectangular area with a uniform depth (Fig.5). The uniform rise in a square whose lateral dimension is 40 km is used as a source. Waveforms are computed at 6 points shown in Fig.5. The computation is made for four different grid sizes; 20, 10, 5, and 2.5 km as shown in the figure. Figure 6 shows the waveforms at the 6 points. They contain short-period oscillations whose period is determined by the grid size. The spectra of these waves are shown in Fig.7. The corresponding wavelength to frequency is shown on the top of each figure. Although a total reflection is assumed at the right hand side of the area, very similar spectra at the all points indicate that the echo does not affect the spectrum structure and quefrency (BOGERT *et al.*, 1963) is constant. Since a box-car type source is assumed, the resultant power spectrum should have a shape of the function $(\sin x / x)^2$ which has many side lobes in a high frequency range (*e.g.* BRACEWELL, 1978). The spectrum obtained from 2.5 km grid shows such a character. The spectrum from 5 km grid is very similar up to 0.9 mHz to that from 2.5 km grid. The spectrum from 10 km grid also has a similar character up to 0.4 mHz. It is found that the spectra are very similar down to the wavelength of about 4 times the grid size. This feature indicates that the shorter wavelength component than 4 times of the grid size is affected by the grid sampling, which is known as an aliasing effect.

To remove the effect of aliasing, the waveforms are low-pass filtered and are shown in Fig.8. The cutoff frequency is 0.5 mHz, corresponding wavelength is the same as the source size (40 km). The filtered waveforms for 5 km and 2.5 km grids show very similar waveforms: one pulse propagating and coming back after reflection. The waveform for 10 km grid is somewhat distorted as it propagates. In the case of 20 km grid, the waveform does not show the feature of one pulse any more. Such a distortion is likely to be caused by a numerical dispersion. The amplitude of main pulse is plotted in Fig.9 against the distance. KAJIURA (1963) showed that the amplitude of tsunami in the ocean with a uniform

depth is proportional to $R^{-1/2}$ for large R where R is the distance from the source. The amplitudes in 5 km and 2.5 km grids are proportional to $R^{-1/2}$, however, the slope is larger for 10 km and 20 km grids because of the dispersion. The agreement of amplitude in 5 km and 2.5 km grids indicate that the grid size must be less than one eighth of the source size to prevent numerical dispersion in a practical view point.

ALFORD *et al.* (1976) examined the numerical dispersion and showed that the phase velocity in numerical computation, c_p, is given as

$$c_p = cG/p\pi \sin^{-1}(p \sin \pi/G) \tag{5}$$

where G is the number of grids in one wavelength, p is a parameter determined by spatial grid size and time step of computation. To satisfy a stability condition, p must be less than $1/\sqrt{2}$ and the larger value is desirable for an efficient computation. When one wavelength is divided into 8 grids, the relative error of c_p is less than 2 %. IMAMURA and GOTO (1986) discussed on the truncation error of the finite-difference computation of tsunamis, combining the aliasing and numerical dispersion. They showed that the error is larger for shorter wavelength component. As a result of simple experiment in this section, an optimum number of grids is more than eight over a dimension of the segment of the fault, then the associated error will be a few per cent if the aliasing effect is properly removed.

5. Simulation of Inversion : Numerical Experiment for Actual Bathymetry

In this section, a more realistic numerical experiment is made to simulate the inversion for the 1983 Japan Sea earthquake tsunami. The purpose is to examine whether or not the inverse problem formulated in this paper is solved stably when the Green's functions computed in the optimum size of grid are used. Since the numerical computation for this tsunami was made by SATAKE (1985), his computed waveform are used as the data for the simulation of inversion. The area for computation and location of the tide gauge

stations are shown in Fig.10. The grid size for computation is basically 5 km, but finer grid system is employed near the tide gauge stations being the smallest grid size 625 m. The topographic effect of harbor and bay near tide gauge stations is taken into account. Therefore the initial part of the wave is accurately computed. However, the quality for the later phase such as reflected wave may be lower.

The model *D2* in SATAKE (1985) consists of 2 segments, the slip on the northern part is 4 m while in the southern part is 5m (Fig.12). Using computed waveforms from this model as the data, we simulate the inversion dividing a fault into 2 segments, each of them is 60×40 km^2 in size. Figure 11 shows the Green's functions at 7 stations computed from each segment. The period of the wave is longer than 10 min, long enough for the aliasing effect to be excluded. Considering that the quality of the computed wave is lower in the later part, we use only the earlier part than the vertical bar shown in the figure. The result of inversion is shown in Fig.12. The exact input value is obtained for this case, showing that the inverse problem can be solved stably. To see the effect of the numerical dispersion, we also tried 4 segments model in which each of the segment in the 2 segments model is further divided into two parts. The number of grids in each segment is only 6 in this case. The Green's functions are computed from 4 segments, but the data are again the computed waveforms from the model *D2*. The result is also shown in Fig.12, which is somewhat different from the input value. The numerical dispersion produces the discrepancy as expected.

The result of simulation is encouraging for the estimation of final slip distribution on a fault by an inversion of tsunami waveforms. If bathymetric data in 5 km grid as used by SATAKE (1985) are used, spatial resolution of the fault heterogeneity is half of the whole fault for the 1983 event, that is, 60×40 km^2. For more detail study of fault heterogeneity, finer grid system must be used.

6. Discussion

So far we have formulated the inversion of tsunami waveforms for the estimation of fault heterogeneity and made several numerical experiments to see the optimum grid size and the stability of the inversion. The bathymetric data are available by 5′ grid for the whole globe (LOUGHRIDGE, 1986) today. Considering the optimum grid size, the slip distribution can be estimated in resolution of less than 1° . Since the fault size of large earthquakes with seismic moment of 10^{28} dyne·cm is several hundreds of km (KANAMORI and ANDERSON, 1975), the fault heterogeneity for larger earthquakes than this moment can be estimated by tsunami waveforms. For some regions such as around Japan, the bathymetry is known more accurately. Therefore the lower limit of the earthquake size becomes smaller and more detail of the heterogeneity can be obtained if fine grid system is used for the computation of the Green's function. However, when grid size becomes small, more memory is required for the computation of the Green's function. Ray tracing of tsunami (SATAKE, 1988) would be useful to solve this dilemma. Since ray paths are visible very quickly before the finite-difference computation, the required area for the computation is known *a priori* and the memory can be saved.

Another problem comes from the structure of tide gauge system. In the case of seismic waves, instrumental response is known by calibration and the waveforms can be deconvolved before the analysis. Most of the tide gauge systems in Japan are originally designed to monitor the crustal deformation or the ocean tide. Since the period of tsunami is much shorter than these movements, the response for tsunami is not known. Recently, both theoretical computation and *in situ* measurements are made for many tide gauge stations in Japan (SATAKE *et al.*, 1988). They show that the correction of tide gauge is necessary for tsunami waveforms. Once the response is evaluated, all the information included in tide gauge records (Fig.1) besides the source are known, so that the fault heterogeneity can be retrieved from tsunami waveforms. The application of the present

method will be presented in a separate paper after the correction for the tide gauge system is made.

Acknowledgements

I thank K. Shimazaki, K. Abe and T. Hibiya for critically reviewing the manuscript and making valuable comments, C. Goto, F. Imamura, I. Aida, Y. Tsuji, Y. Nagata and H. Ohnishi for suggestion and discussion. I used HITAC M280H computer system at the Computer Centre, University of Tokyo. This work was partially supported by the Grand-in-Aid for Scientific Research from Ministry of Education, Scince and Culture of Japan (No. 60020009) by courtesy of K. Abe and N. Shuto.

REFERENCES

AIDA, I., Numerical estimation of a tsunami source, Zisin 2, 25, 343-352, 1972 (in Japanese).

AIDA, I., Reliability of a tsunami source model derived from fault parameters, J. Phys. Earth, 26, 57-73, 1978.

ALFORD, R.M., K.R. KELLY, and D.M. BOORE, Accuracy of finite-difference modeling of the acoustic wave equation, Geophysics, 39, 834-842, 1974.

BOGERT, B.P., M.J.R. HEALY, and J.W. TUKEY, The quefrency alanysis of time series for echoes: cepstrum, pseudo-autocovariance, cross-cepstrum and saphe cracking, in Time Series Analysis, pp.209-243, John Wiley and Sons, 1963.

BRACEWELL, R.N., The Fourier transform and its applications, 444pp., McGrow-Hill, 1978.

IMAMURA, F. and C. GOTO, Truncated error of tsunami numerical simulation by the finite difference method, Proc. Japan Soc. Civil Eng., 375, 241-250, 1986 (in Japanese).

KAJIURA, K., The leading wave of a tsunami, Bull. Earthq. Res. Inst. Univ. Tokyo, 41, 535-571, 1963.

KAJIURA, K., Tsunami source, energy, and the directivity of wave radiation, Bull. Earthq. Res. Inst. Univ. Tokyo, 48, 835-869, 1970.

KANAMORI, H. and D.L. ANDERSON, Theoretical basis of some empirical relations in seismology, Bull. Seismol. Soc. Am., 65, 1073-1095, 1975.

KIKUCHI, M. and Y. FUKAO, Iterative deconvolution of complex body waves from great earthquakes - the Tokachi-oki earthquake of 1968, Phys. Earth Planet. Inter., 37, 235-248, 1985.

LAMB, H., Hydrodynamics, Cambridge University Press, 1932.

LOUGHRIDGE, M.S., Relief map of the Earth's surface, EOS Trans. Am. Geophys. Union, 67, 21, 1986.

MANSINHA, L. and D.E. SMYLIE, The displacement fields of inclined faults, Bull. Seismol. Soc. Am., 61, 1433-1440, 1971.

MORI, J. and K. SHIMAZAKI, Inversion of intermediate-period Rayleigh waves for source characteristics of the 1968 Tokachi-Oki earthquake, J. Geophys. Res., 90, 11374-11382, 1985.

MURTY, T.S., Seismic sea waves -tsunamis, Bull. Fish. Res. Board Canada, 198, 337pp., 1977.

SATAKE, K., The mechanism of the 1983 Japan Sea earthquake as inferred from long-period surface waves and tsunamis, Phys. Earth Planet. Inter., 37, 249-260, 1985.

SATAKE, K., Effects of bathymetry on tsunami propagation : application of ray tracing to tsunamis. PAGEOPH, 1988 (in press).*(Appendix of this thesis).*

SATAKE, K., M. OKADA and K. ABE, Tide gauge response: measurents and its effect to tsunami waveforms, to be submitted to Proc. PACON'88, 1988.*(Chapter 1.2 of this thesis).*

TAKAHASHI, R., On seismic sea waves caused by deformations of the sea bottom, Bull. Earthq. Res. Inst. Univ. Tokyo, 20, 377-400, 1942 (in Japanese).

WOODHOUSE, J.H., and A.M. DZIEWONSKI, Mapping the upper mantle: three-dimensional modeling of Earth structure by inversion of seismic waveforms, J. Geophys. Res., 89, 5953-5986, 1984.

Fig.1

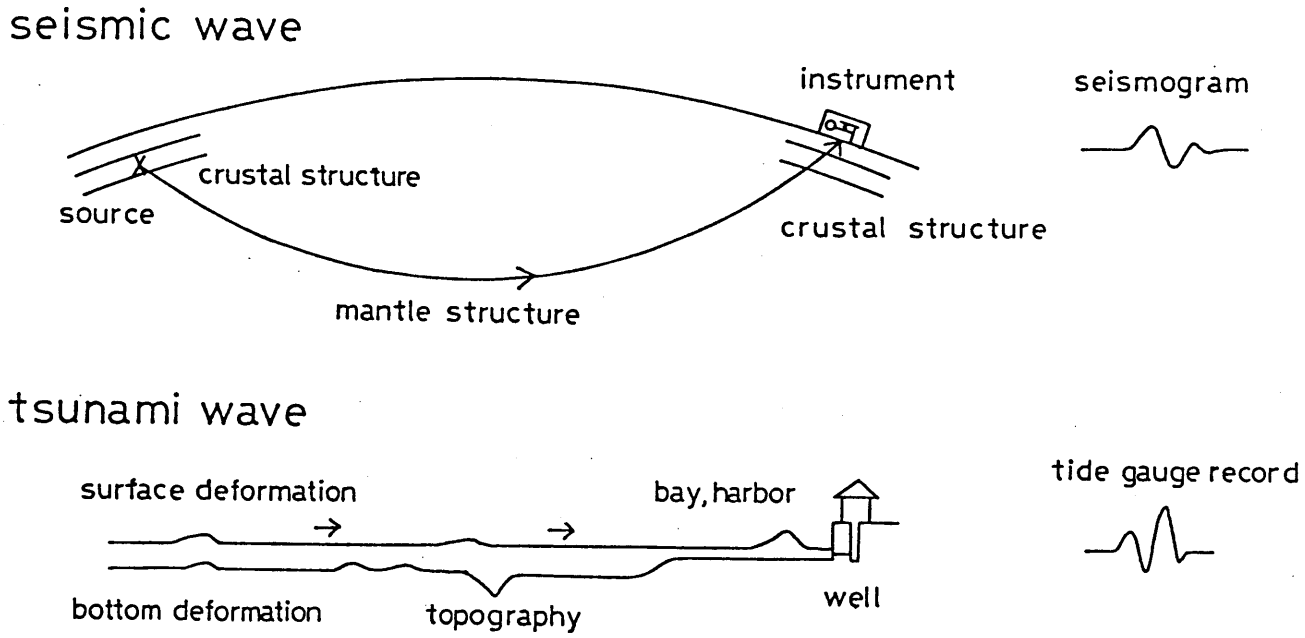

Fig.1. Schematic diagram showing various information included in seismic and tsunami waves.

Fig.2

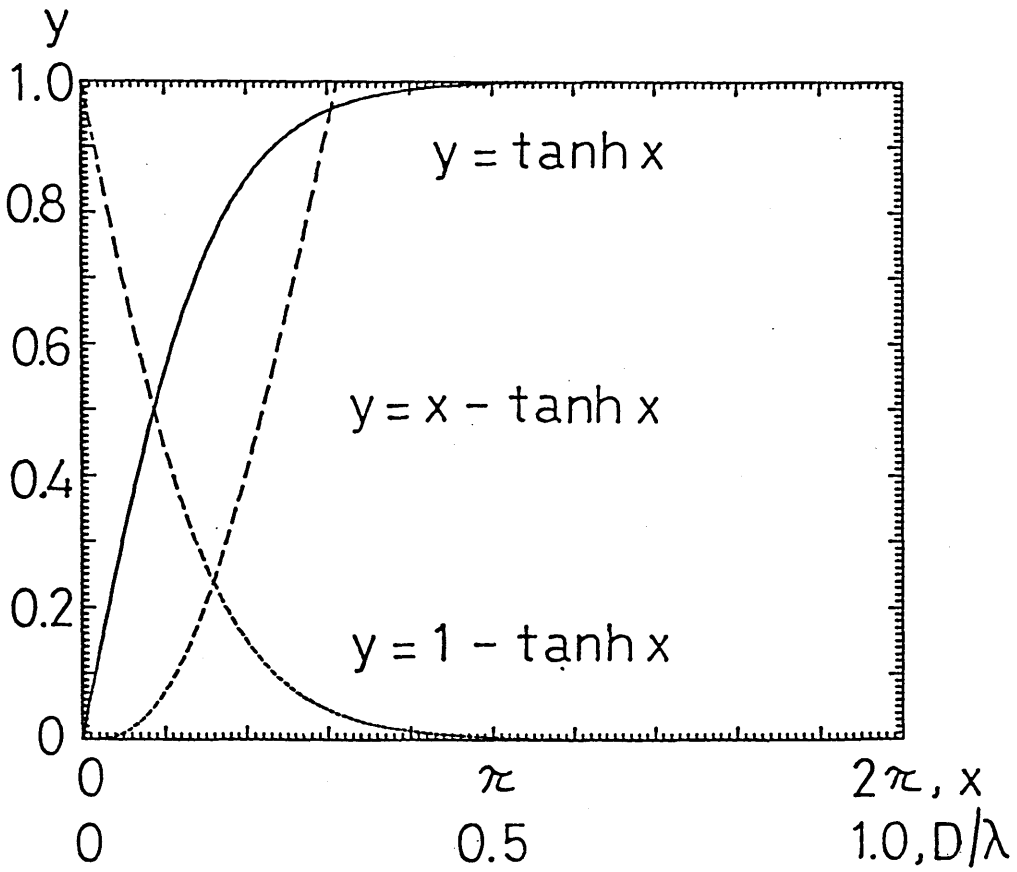

Fig. 2. Graph for a function $y = \tanh x$ (solid line) and the errors when it is approximated to x and 1 (dashed lines). The scale for D/λ is also shown, where D is the water depth and λ is the wavelength of tsunami.

Fig.3

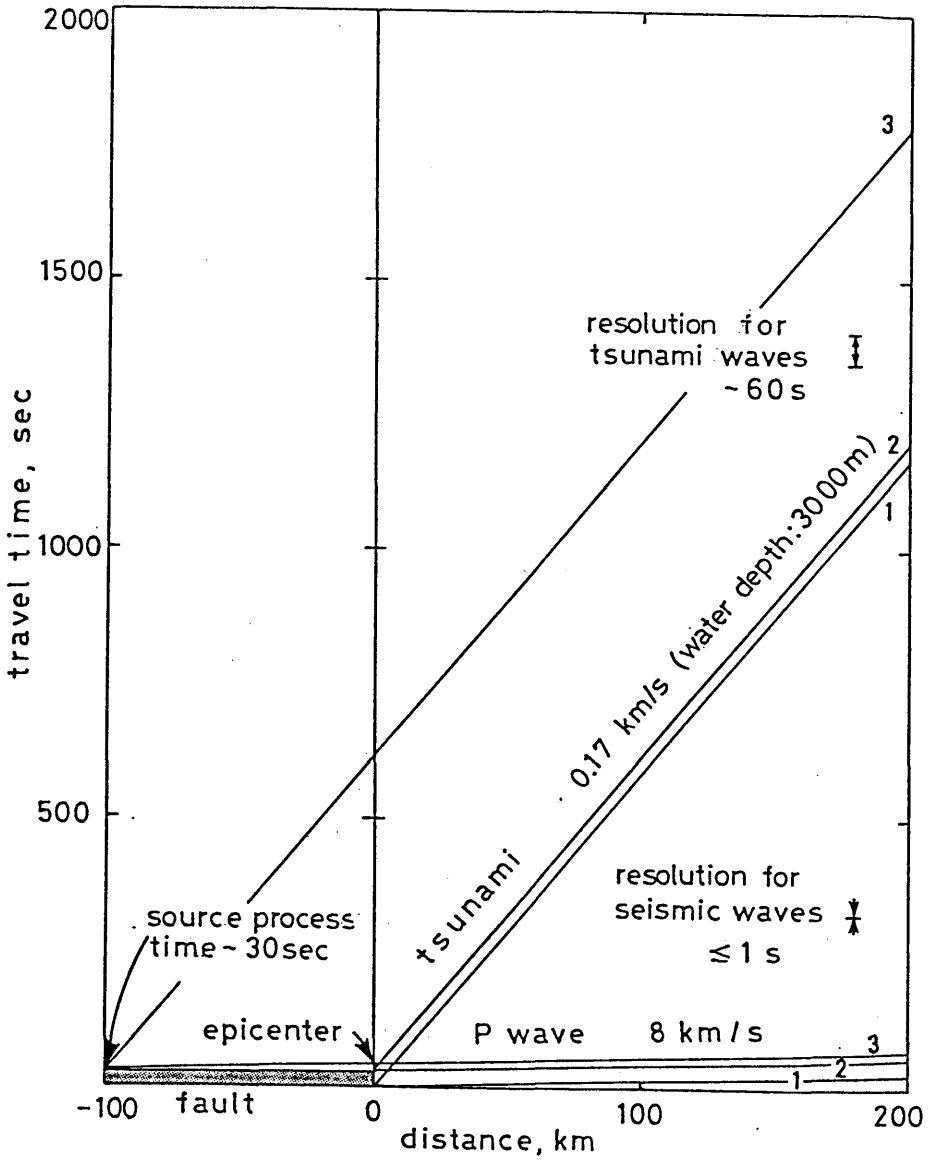

Fig.3. Travel time diagrams for a representative earthquake model. Three phases originated from different points in space and time are shown for both tsunamis and *P* waves. Phases 1 and 2 are from epicenter but 1 leaves at the origin time and 2 leaves later as the source process time. Phase 3 leaves the other end of the fault after the source process completed.

Fig.4

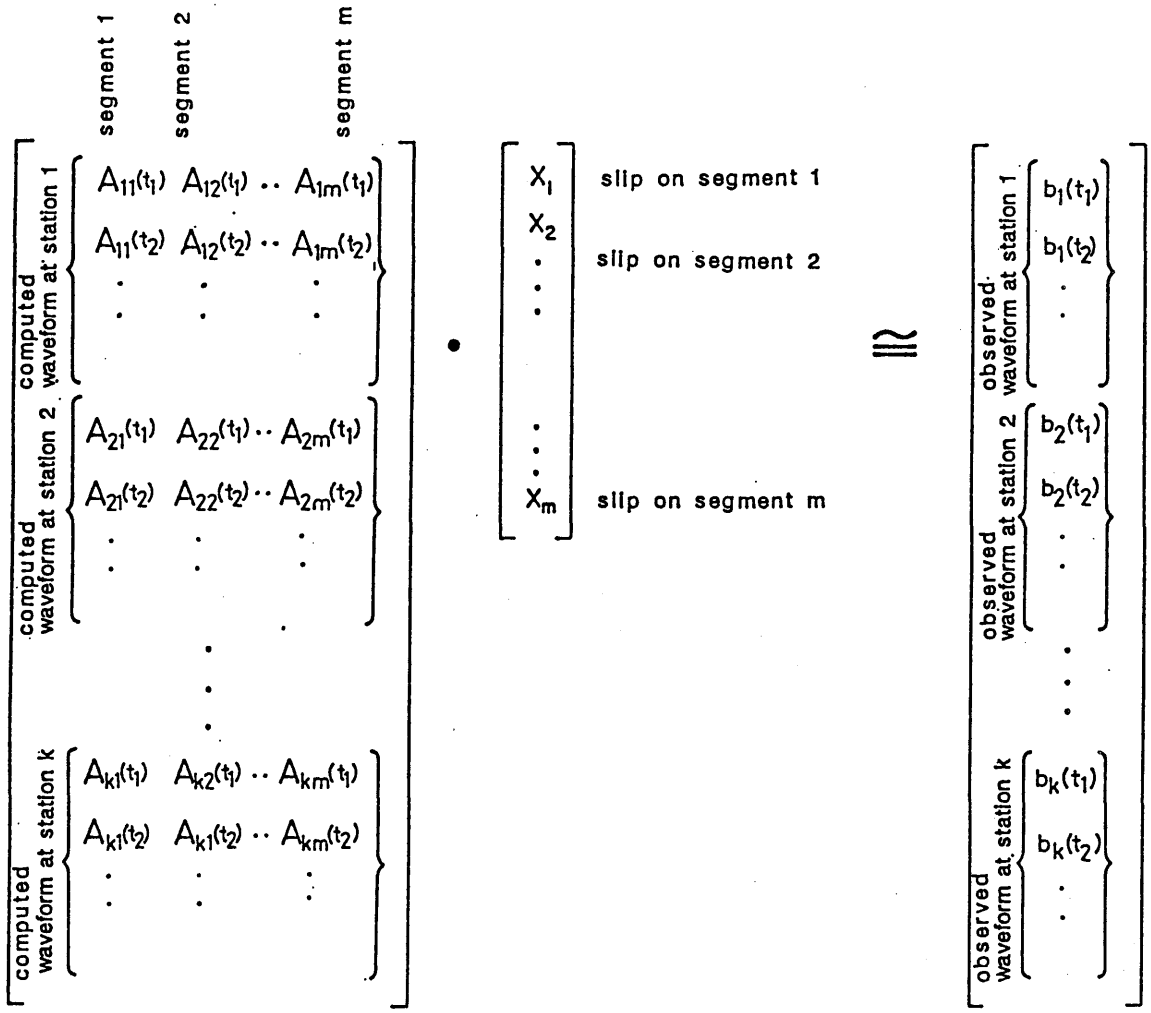

Fig.4. Matrix representation of equation (4).

Fig.5

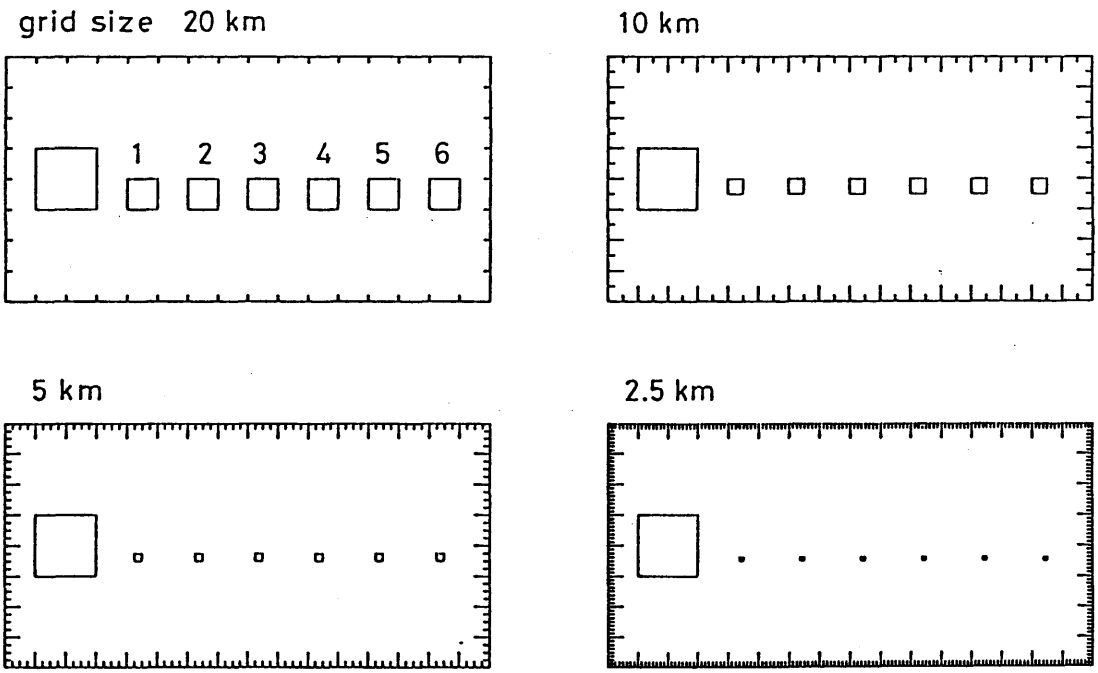

Fig.5. Four different grid systems used for the numerical experiment. The water depth is uniform (40 m). Larger boxes are the tsunami source where the water is uplifted (1 m). The stations where the waveforms are computed are also shown.

Fig.6

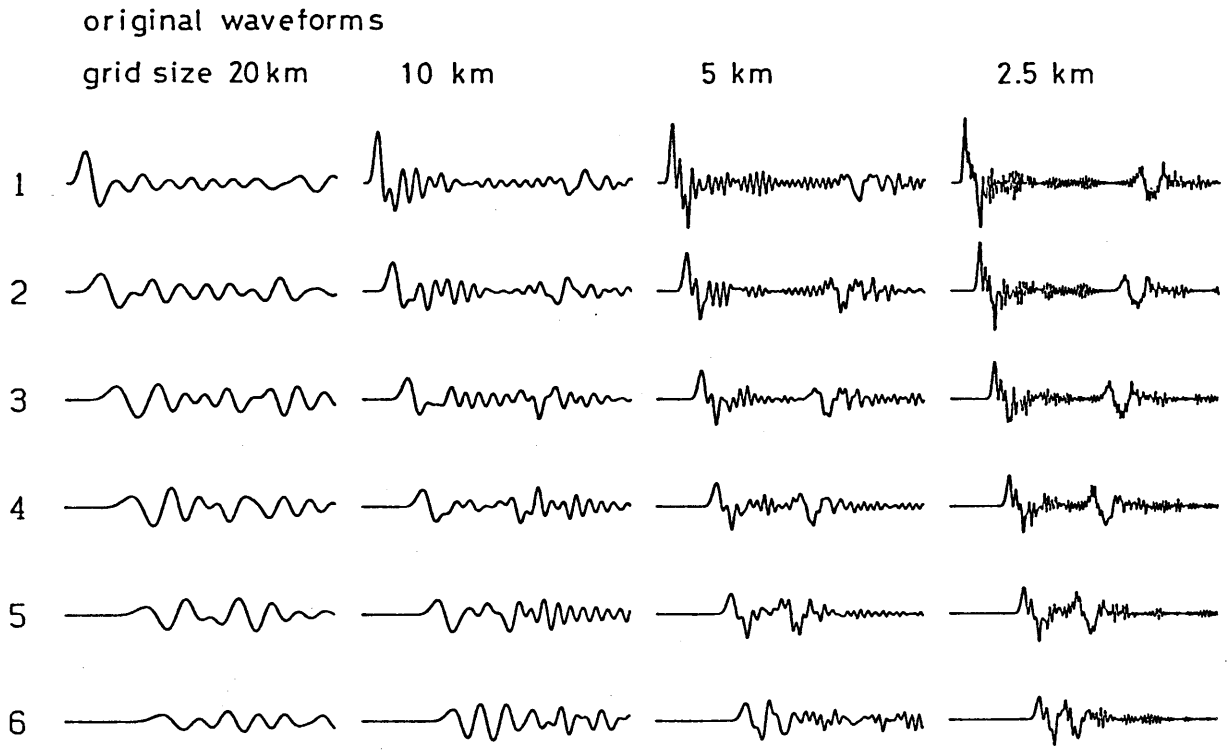

Fig.6. The waveforms at 6 stations shown in Fig.5 for 4 different grid sizes.

Fig.7

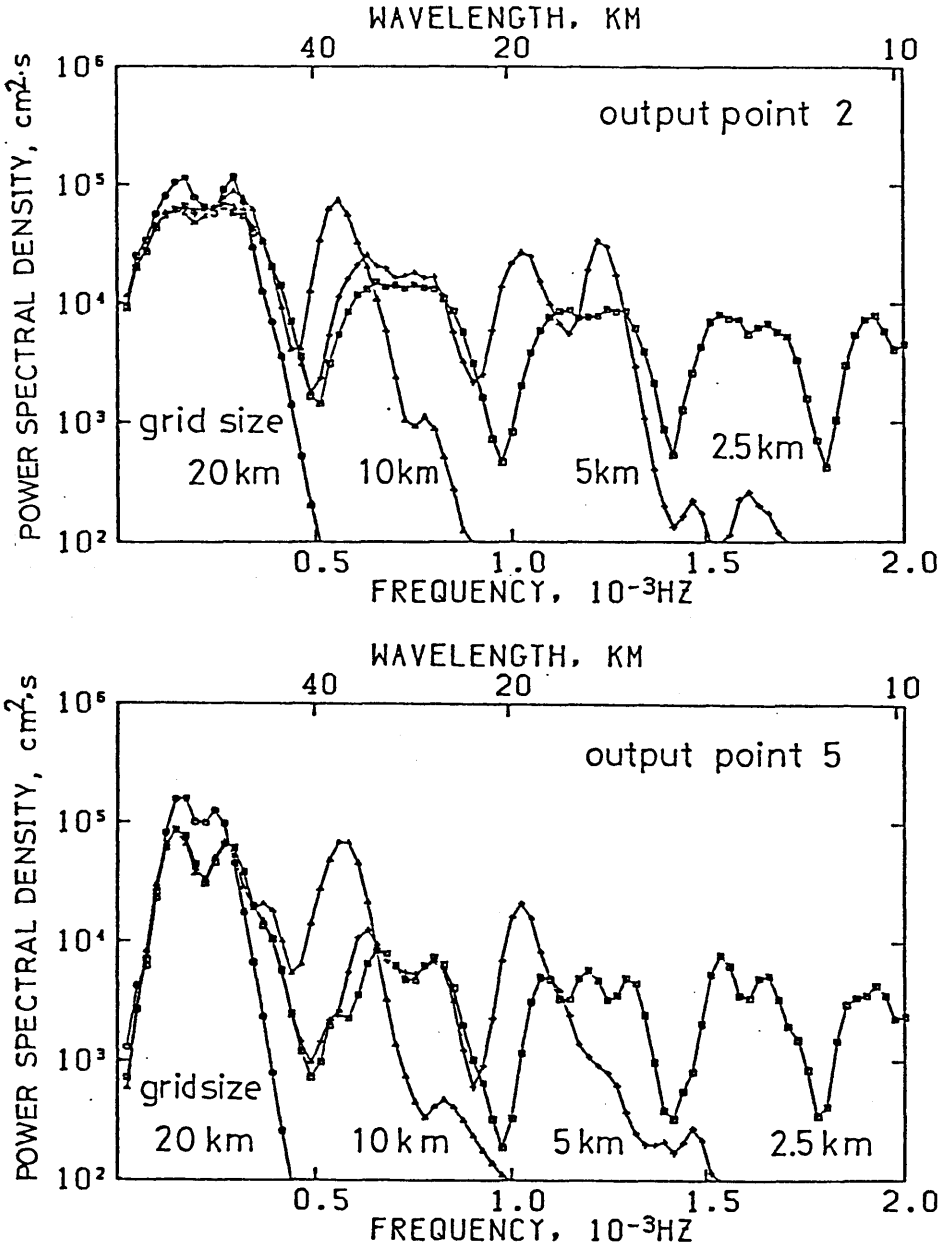

Fig.7. The power spectra for the waveforms in Fig.6 at two stations (Nos. 2 and 5).

Fig.8

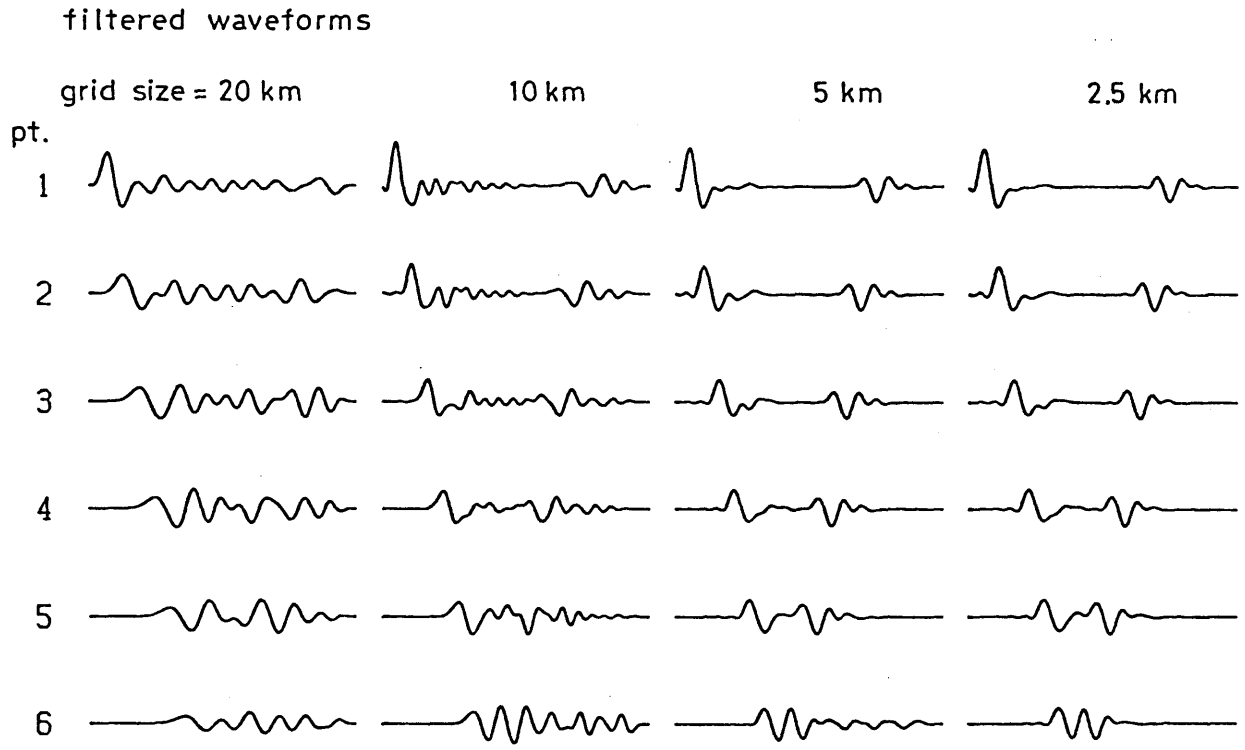

Fig.8. The low-pass filtered waveforms of Fig.6.

Fig.9

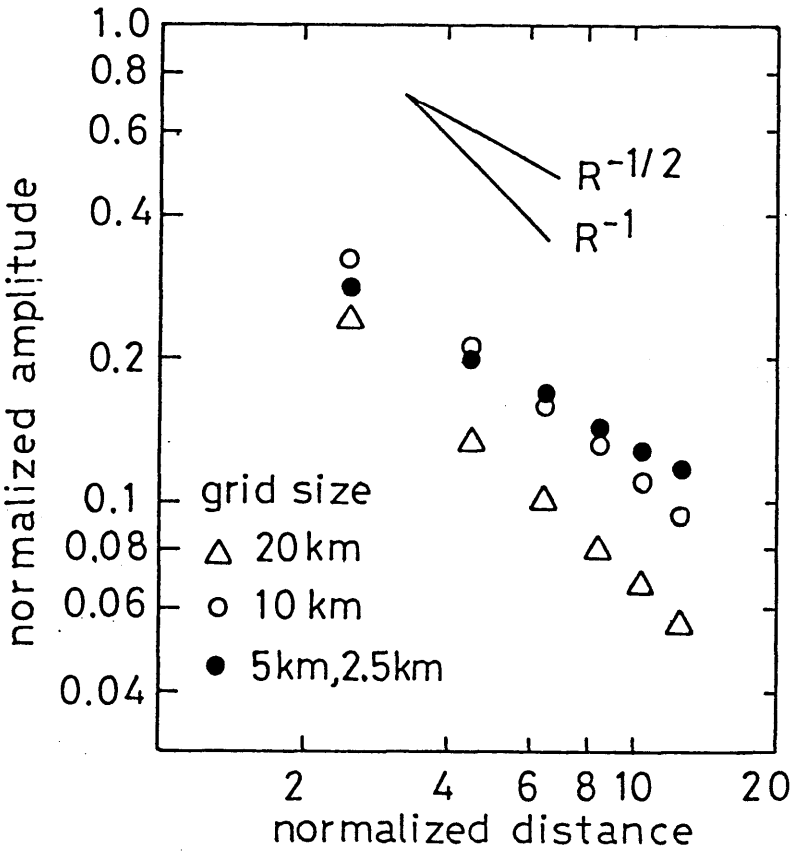

Fig.9. The maximum amplitude of waveforms in Fig.8 as a function of distance from the source. Both amplitude and distance are normalized by the wave height at the source and the size of source, respectively.

Fig.10

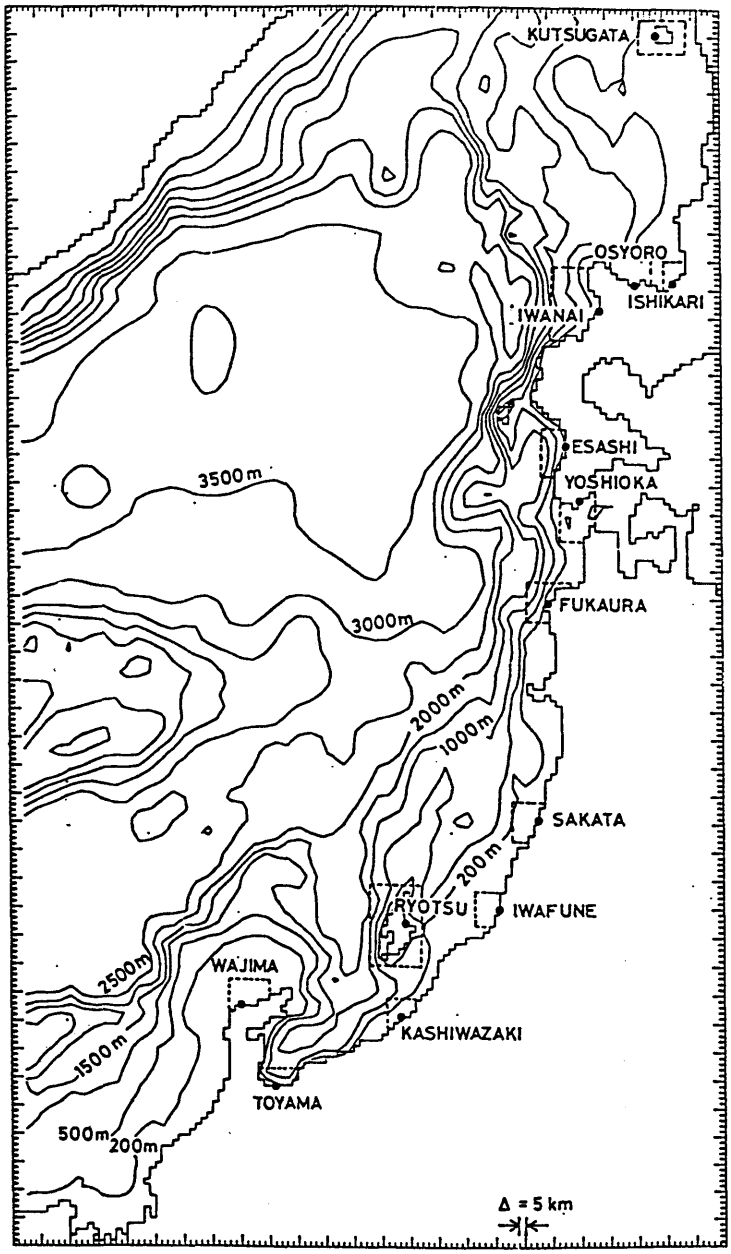

Fig.10. Map showing the computation area used for the simulation of inversion (SATAKE, 1985). Finer grid systems are used inside the dashed lines near tide gauge stations.

Fig.11

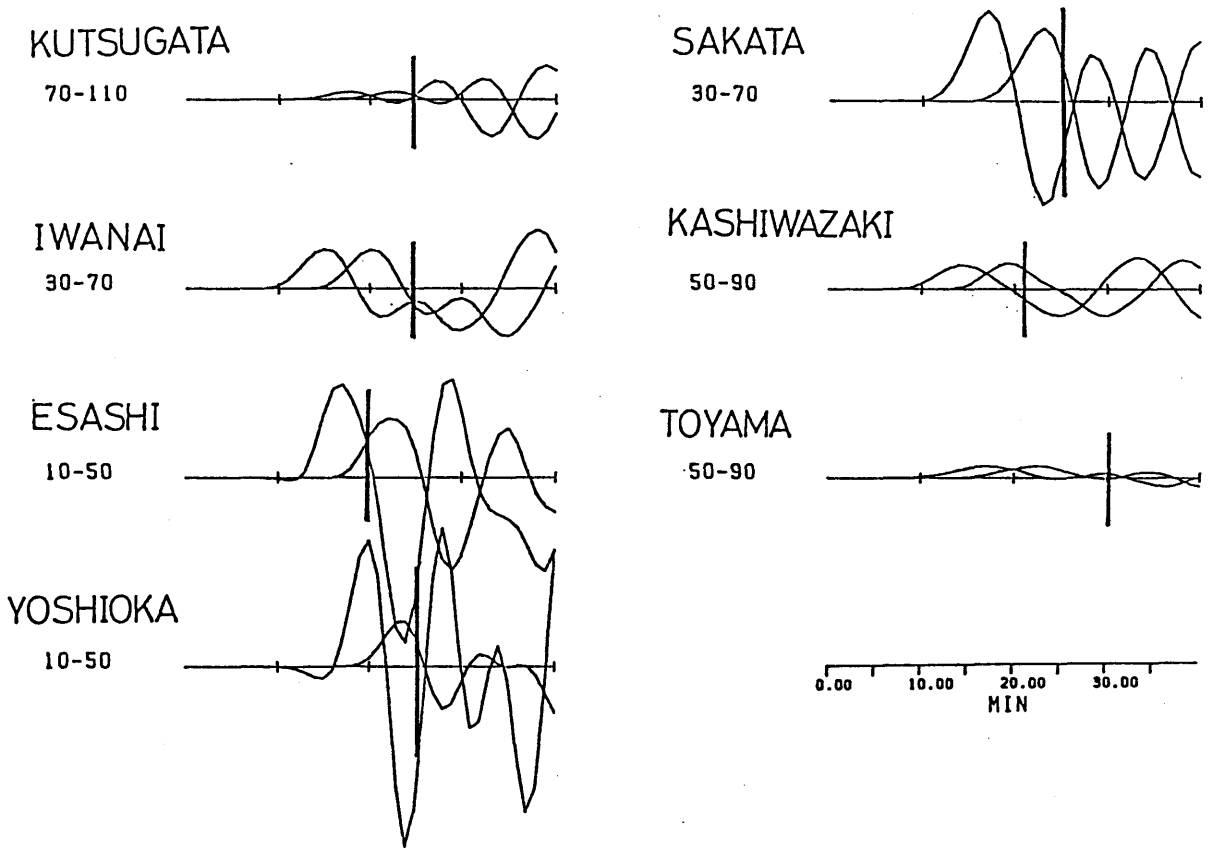

Fig.11. The waveforms computed from two segments of the 1983 earthquake fault. Only a part before the vertical bar is used for as the Green's functions. Numbers indicate the time after the origin time in min.

Fig.12

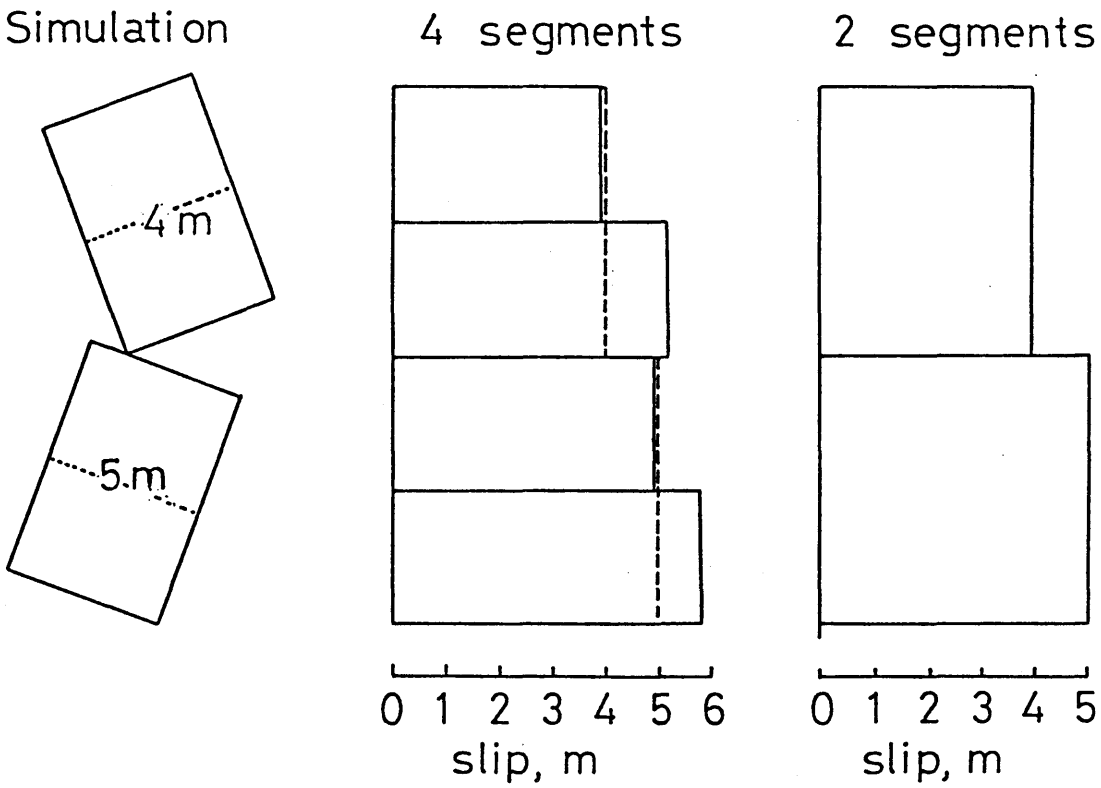

Fig.12. (*left*) The segmentation and the slip distribution on the fault for the 1983 Japan Sea earthquake (SATAKE, 1985). The waveforms computed from this model is used as the data for simulation of inversion. (*center*) The input (solid line) and the obtained (dashed line) slip distribution by simulation of inversion for 4 segments model. (*right*) The same as the middle figure for 2 segments model. The exactly the same values as input one are obtained by inversion.

Chapter 2

Tide Gauge Response : Measurements and its Effect on Tsunami Waveforms

Abstract

Earthquake source process can be retrieved from the tsunami records since the propagation effect of tsunami can be accurately evaluated. The tsunami waveforms are usually recorded by tide gauges and are affected by the response of a tide gauge system. A large discrepancy between the amplitude of the tide gauge records and inundation heights was pointed out at the time of the 1983 Japan Sea earthquake tsunami. It is necessary to examine the response of tide gauge system before the analysis of tsunami waveforms. In this paper, the responses of 18 tide gauge systems in Japan are examined by *in situ* measurements. The observed recovery time after the water is drained from the well or poured into the well differs from station to station and is generally longer than the theoretically calculated time. The difference between the observed and calculated time is due to the environmental change after the tide gauge was constructed. Tide gauge stations are classified into two groups by the recovery time. In the first group, the observed recovery time is less than 5 min and the ratio of the observed to the calculated recovery time is less than 5. In the second group, the observed recovery time is longer than 5 min and the ratio is also larger. The corrected waveforms by the observed response for the 1983 tsunami reproduce the inundation heights at the tide gauge stations.

1. Introduction

Most of the large earthquakes on the Earth occur under the ocean and they are often accompanied by tsunamis. Tsunami waveforms are useful to study the earthquake source process, since the propagation effect can be accurately evaluated compared with seismic waves (Satake, 1987). However, the response of tide gauge system on which tsunami waveforms are recorded is not well known. At the time of the 1983 Japan Sea earthquake tsunami, a large discrepancy between the tsunami amplitude on tide gauge records and the inundation heights is reported. For example, the observed inundation heights are about 1.5 m at the two tide gauge stations near the source area, Yoshioka and Fukaura, whereas the maximum tsunami heights on the tide gauge records are 0.96 and 0.65 m, respectively at these stations (Okada and Amino, 1984; JMA, 1984; Kinoshita *et al.*, 1984). The discrepancy is due to the response of the tide gauge system to tsunamis. For the study of seismic source by tsunami waveforms, the measurements of the tide gauge response and the correction to the recorded waveforms are essential.

Several studies have been made on the frequency response of the tide gauge system (Cross, 1968; Noye, 1974; Loomis, 1983). All of these studies treat a tide gauge of a stilling well type set in the water with an orifice. The Japanese tide gauge systems, which are originally designed to monitor crustal deformation or ocean tides, have different structure from those studied by the above authors. Generally, tide well is dug on a wharf and it is connected with the ocean by an intake pipe (Fig.1). A long and narrow intake pipe strongly affects the response of the system to tsunamis. After the 1983 tsunami, theoretical computation (Murakami, 1983) and an *in situ* measurement (Okada, 1985) of tide gauge response were made for a few tide gauge stations. The computed response differs significantly from the measured one and it could not account the discrepancy between the inundation heights and the tsunami heights on the tide gauges. Okada and Amino (1984) showed that the

inundation height at Fukaura was reproduced by correcting the waveforms by using the measured response. In this paper, we extensively measure the *in situ* tide gauge responses for 14 tide gauge stations, compare them with theoretical computations, and make the corrections for the waveforms from the 1983 Japan Sea earthquake tsunami.

2. Theory

We take a similar approach to Cross (1968) and Loomis (1985) who discussed on a non-linear response of the tide gauge system. According to the Bernoulli's theorem, the velocity of water in the intake pipe, u (taking positive for incoming water) is proportional to a square root of the difference in water level outside the well, H, and that inside the well, h,

$$u = sgn(H-h)\sqrt{2g\,|H-h| \,/\, F} \tag{1}$$

where sgn means the sign function, either 1 or -1 depending on the sign of $(H-h)$, g the gravitational acceleration, and F is a non-dimensional friction coefficient. The equation of continuity requires a relation between the velocities in the pipe and the well,

$$D^2\frac{dh}{dt} = id^2u \tag{2}$$

where D and d are the diameters of the well and the intake pipe assuming that both have circular cross sections, and i is a number of the intake pipe which is generally one. From equations (1) and (2), we have

$$\frac{dh}{dt} = Wsgn(H-h)\sqrt{2g\,|H-h|} \tag{3}$$

where

$$W = i(d/D)^2/\sqrt{F} \tag{4}$$

is a non-dimensional constant for the tide gauge system. We call it 'well constant' hereafter.

If the temporal variation of water level in the well is recorded on tide gauges, the tsunami waveform outside the well can be computed from equation (3) as

$$H = h + sgn(\frac{dh}{dt})\cdot(\frac{dh}{dt})^2 / 2gW^2. \tag{5}$$

This is the equation for the correction of tide gauge records. Although W is a quantity describing the response of the tide gauge system, we define another quantity T as

$$T = \sqrt{2/g} / W \tag{6}$$

which represents a time necessary to recover the 1 m difference in water level inside and outside the well.

The well constant W or the recovery time T can be calculated from the size and the material of the intake pipe and the well (Murakami, 1983). The calculated values are referred as W_{cal} and T_{cal}. The frictional coefficient F is a sum of the losses due to sudden changes in cross section and a surface resistance along the stream line,

$$F = f_e + f\, l/d + f_o \tag{7}$$

where f_e is a loss for a sudden contraction, f_o is a loss due to a sudden expansion, l the length of the intake pipe, and f is a frictional loss on the surface. For a geometry of the tide gauge shown in Fig.1, f_e is 0.5, f_o is 1.0, and f is given for a circular section as

$$f = 8gn^2\ (4/d)^{1/3} \tag{8}$$

where n is the Manning's roughness coefficient (*e.g.* Streeter, 1950). A kind of concrete, namely Hume tube, is generally used for the intake pipe and n is 0.013 ($m^{-1/3}$ sec) for this material (Murakami, 1983). However, the environmental change after the construction of

the tide gauge system such as attachment of shells or deposition of sand may change the effective roughness.

Another way to estimate the well constant W is to make an *in situ* measurement at the tide gauge stations. By draining the water from the well or pouring into the well, the water level difference inside and outside the well is artificially given. Fitting equation (3) to the following water level change, W can be estimated. The values of W and T obtained in this way are referred as W_{obs} and T_{obs} and distinguished from those calculated.

3. In situ Measurements of Tide Gauge Responses

We made measurements of W_{obs} and T_{obs} at 14 tide gauge stations on the Japan Sea coast as shown in Fig.2. At each station, the water is drained from the well and poured into the well by using a small pump. After stopping the pump, we measure the recovery of the water level. The paper speeds of tide gauges are very slow, generally 2 cm/hour, and the scale is 1/10 or 1/20, so that it is much more accurate to observe the movement of the float directly. We observe the movement of the wire suspending the float at a time interval of 3 to 10 sec depending on the recovery time.

Figure 3 shows the water level change after the water is drained from the well at Yoshioka. The recovery time is long at this station and the water level difference near 50 cm between outside and inside the well could be given. Figure 4 is a result of two sets of drain and pour test made at Esashi. Since the recovery time is short at this station, the small difference in water level could be given. At such a station the pour and drain tests are repeated. At both stations, the water level changes as a quadratic function of time. By fitting equation (3) to these data, the best-fitting W_{obs} is obtained by a trial and error approach. The temporal change of the water level outside the well, H, during the pouring and draining process is assumed to be a linear function of time and shown by dashed lines

in the figures. This is estimated from the tide gauge records (inset of Fig.3) when the recovery time is long or also by trial and error when the recovery time is short (Fig.4).

To estimate the error of W_{obs} and T_{obs}, three curves for different values of W are shown in Fig.3. The best-fit W_{obs} is estimated to be 9×10^{-3}. If the value is changed by about 10 %, the computed curves don't fit the data anymore. Therefore the estimation error of W_{obs} is regarded as less than 10 %. Since the recovery time T_{obs} is relatively large for this station, the error for other stations may be larger. We assign the error to be less than 30 % for any station. The two sets of drain and pour test at Esashi give a constant value of W_{obs}, indicating that the reproducibility of the measurement is good.

For some of the stations, the recovery time for the drain test significantly differs from that for the pour test. Shells or sediments in the pipe might cause a sudden change of the effective diameter in a different way for inflow and outfolw. As a result, the recovery time and the well constant are different between inflow and outflow. When the difference is much larger than the estimation error, namely greater than 50 %, we assign different estimates for inflow and outflow.

4. Response of Some Japanese Tide Gauge Stations

The measured and computed tide gauge responses are compiled in Table I with the calculated values and the other parameters for the 14 tide gauge stations. Four stations studied by Okada (1985) are added in the table.

The period of tsunami near the tide gauge stations is usually several to several tens of min. Since the calculated recovery time T_{cal} ranges from 11 to 167 sec, the effect of tide gauge response will be small if we use the calculated recovery time. However, *in situ* measurements show that the observed recovery time T_{obs} ranges from 45 to 1300 sec, significantly longer than T_{cal}. It takes at most 20 min to recover the 1 m difference in

water level. Therefore, the recorded waveforms in tide gauges must be strongly affected by the response for such a station having a long recovery time.

The calculated and measured recovery times are plotted on Fig.5. The amount of estimation errors of T_{obs} is shown by a bar. For those stations whose T_{obs} are different for inflow and outflow, both values are shown by different symbols. The scatter of T_{obs} is much larger than that of T_{cal}. Eighteen tide gauge stations can be grouped into two by the values of T_{obs}. The first group includes those stations whose T_{obs} is less than 5 min. The second group includes the stations whose T_{obs} is more than 5 min. In the first group the ratio T_{obs} / T_{cal} is less than 5 whereas in the second group the ratio is more than 5.

5. Correction of Tsunami Waveforms by the Observed Response

In this section, the waveforms outside the tide well is estimated by correcting the tide gauge records using the observed response. Okada (1985) made such an estimate for the record of the 1983 Japan Sea earthquake tsunami at Fukaura (Fig.6). The estimated amplitude is significantly larger than the tide gauge record for the first several peaks. The third peak, the amplitude is smaller than the first peak in the tide gauge record, becomes about 1.2 m and shows the maximum height. Since the inundation height near the tide gauge station is estimated as 1.5 m, the corrected waveforms roughly reproduces the actual tsunami. Five other tide gauge records from the 1983 tsunami are collected and digitized at an interval of 1 min. This corresponds to 1/30 cm in the tide gauge records. To reduce the digitization error, Hanning window is applied three times to the digitized time series. This operation is a kind of low-pass filtering and the shorter period component than 4 min is reduced to less than 10 % of the original amplitude (Blackman and Tukey, 1958). Figure 7 shows the original (solid curves) and corrected (dashed curves) waveforms by using equation (5) at 5 tide gauge stations. Original and corrected waveforms almost coincide at

Iwanai, Esashi and Sakata. These stations belong to the first group in which the recovery time T_{obs} is less than 5 min. The corrected waveforms differ from the original one at Yoshioka and Iwafune. These stations belong to the second group where T_{obs} is longer than 5 min.

At Yoshioka, the amplitude of the first cycle becomes significantly larger by the correction of tide gauge response. Especially the first trough which was positive in the original waveform becomes negative in the corrected waveform. The abnormal shift in the original waveform to the positive side is due to the response of the tide gauge system. The maximum amplitude becomes 1.5 m, consistent with the inundation height at this station.

6. Discussion and Conclusion

The discrepancy between the calculated and the observed responses of tide gauge should be due to the environmental change after the construction of the tide gauge system. Attachment of shells or deposition of sediments cloggs the intake pipe and the effective roughness changed. There are two lines of evidences for this. The first one is result from a repeated measurement at Fukaura. The measurements of tide gauge response have been made in November 1983, six months after the 1983 tsunami and in June 1986, about three years after the tsunami. As shown in Table I and Fig.5, the observed recovery time T_{obs} was 411 sec in 1983 and it becomes 807 sec in 1986, roughly doubled in two and a half years. Nothing besides the environmental change causes this temporal change of T_{obs}. Another evidence is the agreement of T_{obs} and T_{cal} at Funakawa. At this station, a new tide gauge system was constructed about 6 months before our measurement. The environment has not change so much after the construction, so that the observed values agree well with those calculated.

In this paper, the response of tide gauge system is obtained for 14 Japanese tide gauge

stations by both the theoretical computation and *in situ* measurements. The results show that the tide gauge stations are classified into two groups. In the first group, the observed recovery time is less than 5 min and the ratio of the observed to the measured recovery time is less than 5. In the second group, the recovery time is longer than 5 min and the ratio is also larger. The corrected waveforms by the observed response almost agree with the original records for the first group but differ significantly for the second group.

For a seismological study by using tsunami waveforms, the examination of tide gauge response is found to be important for the second group. The *in situ* measurement of the response is necessary. It is better to make measurements immediately after the tsunami is recorded, since the environmental change greatly affects the response. Further, a more suitable tide gauge system for tsunami is expected. A design of the well and intake pipe with short recovery time and a digital recording system will be a great benefit for a seismological study of tsunamis. A tsunami gauge instead of tide gauge is desirable for a study of seismic source, since the tsunami has a potential advantage that the propagation effect can be more accurately evaluated than seismic waves.

References

Blackman, R. B. and J. W. Tukey, 1958. The Measurement of Power Spectra. Dover, 190pp., New York.

Cross, R. H., 1968. Tide gage frequency response. J. Waterways Harbor Div. Proc. Am. Soc. Civil Eng., 94, 317-330.

Japan Meteorological Agency (JMA), 1984. Report on the Nihonkai- Chubu earthquake, 1983. Tech. Rep. JMA, 106, 253pp. (in Japanese).

Kinoshita, T., S. Kumagai, Y. Tsuji, N. Ogawa, N. Numano, O. Abe, and T. Konishi, 1984. Survey research report of the disaster of the Nihonkai-Chubu earthquake. Principal Disaster Report, 23, Nat. Res. Cent. Dis. Prev., 164pp. (in Japanese).

Loomis. H. G., 1983. The nonlinear response of a tide gage to a tsunami. Proc. 1983 Tsunami Symp., 177-185.

Murakami, K., 1983. The response of tide gage to the tsunami. Tech. Note Port Harbour Res. Inst., 470, 217-223 (in Japanese).

Noye, B. J., 1974. Tide-well systems I: Some non-linear effects of the conventional tide well. J. Mar. Res., 32, 129-153.

Okada, M., 1985. Response of some tide-wells in Japan to tsunamis. Proc. Int. Tsunami Symp. 1985, 208-213.

Okada, M. and Amino, M., 1984. On the response characteristics of the tide gauge at Fukaura. Progr. Abstr. Oceanogr. Soc. Japan, 1, 135-136 (in Japanese).

Satake, K., 1987. Inversion of tsunami waveforms for the estimation of a fault heterogeneity: method and numerical experiments. submitted to J. Phys. Earth.*(Chapter 1.1 of this theis).*

Streeter, V. L., 1950. Steady flow in pipes and conduits. in: Rouse, H. (ed.), Engineering Hydraulics. pp. 387-443. John Wiley and Sons, New York.

TABLE I Tide Gauge Responses

No.	Station	Well D (m)	Intake Pipe d (m)	l (m)	Calculated Wcal	Tcal (s)		Observed Wobs	Tobs (s)	Observed Date
1	Ishikari	1.0	0.15	12.48	1x10-2	44		6 x 10-3	75	'86 9 17
2	Otaru	1.2	.125	15	4.2x10-3	107		5.5x10-4	821	'86 9 16
3	Oshoro	0.8	0.10	10	6.4x10-3	71		2.8x10-3	161	'86 9 16
4	Iwanai	1.2	0.15	16.74	6.4x10-3	70		3 x 10-3	151	'86 9 18
5	Esashi	0.9	0.05 * 4	2.1	6.3x10-3	72		5 x 10-3	90	'86 6 9
6	Yoshioka	1.0	0.06	0.3	2.7x10-3	167	in	9 x 10-4	502	'86 6 9
							out	5 x 10-4	904	
7	Hakodate	0.8	0.10	3.7	8.8x10-3	52	in	7.4x10-4	610	'86 6 8
							out	1.7x10-3	266	
8	Fukaura	1.0	0.15	6.96	1.2x10-2	37		5.6x10-4	807	'86 6 10
								1.1x10-3	411	'83 11 ?
9	Noshiro	1.2	0.15	10.615	7.5x10-3	60	in	4.3x10-3	105	'86 6 11
							out	2.3x10-3	196	
10	Oga	1.0	0.10	3.0	5.9x10-3	76		4.5x10-4	1004	'86 6 11
11	Funakawa	1.2	0.15	5.0	9.3x10-3	49		1x 10-2	45	'86 6 12
12	Sakata	1.2	0.15 *2	24	1.1x10-2	40	in	4 x 10-3	113	'86 6 12
							out	2 x 10-3	226	
13	Iwafune	1.2	0.30	6.1	4.3x10-2	11		1.2x10-3	376	'86 6 13
14	Niigata	1.2	0.10 *2	0.7	1.0x10-2	44		5 x 10-3	90	'86 6 13
15	Maizuru	1.2	0.2	4.7	1.8x10-2	25		6.6x10-4	684	
16	Choshi	1.2	0.1	4.2	3.8x10-3	120		3.4x10-4	1329	
17	Tokyo	1.0	0.1	2.0	6.4x10-3	70	in	4.0x10-3	113	
							out	2.2x10-3	205	
18	Omaezakil	1.2	0.1	2.4	4.3x10-3	105		4.0x10-3	113	

* Number of intake pipe is shown when it is not 1.

Fig.1

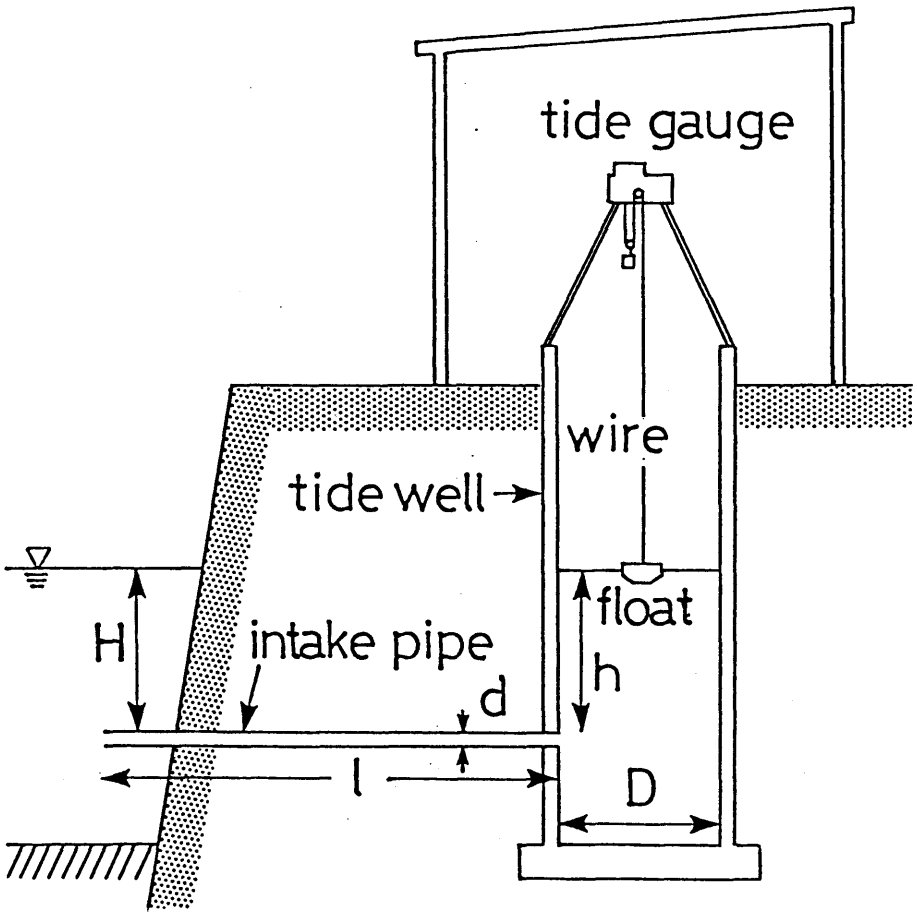

Figure 1. Structure and parameters of a typical tide gauge system in Japan.

Fig.2

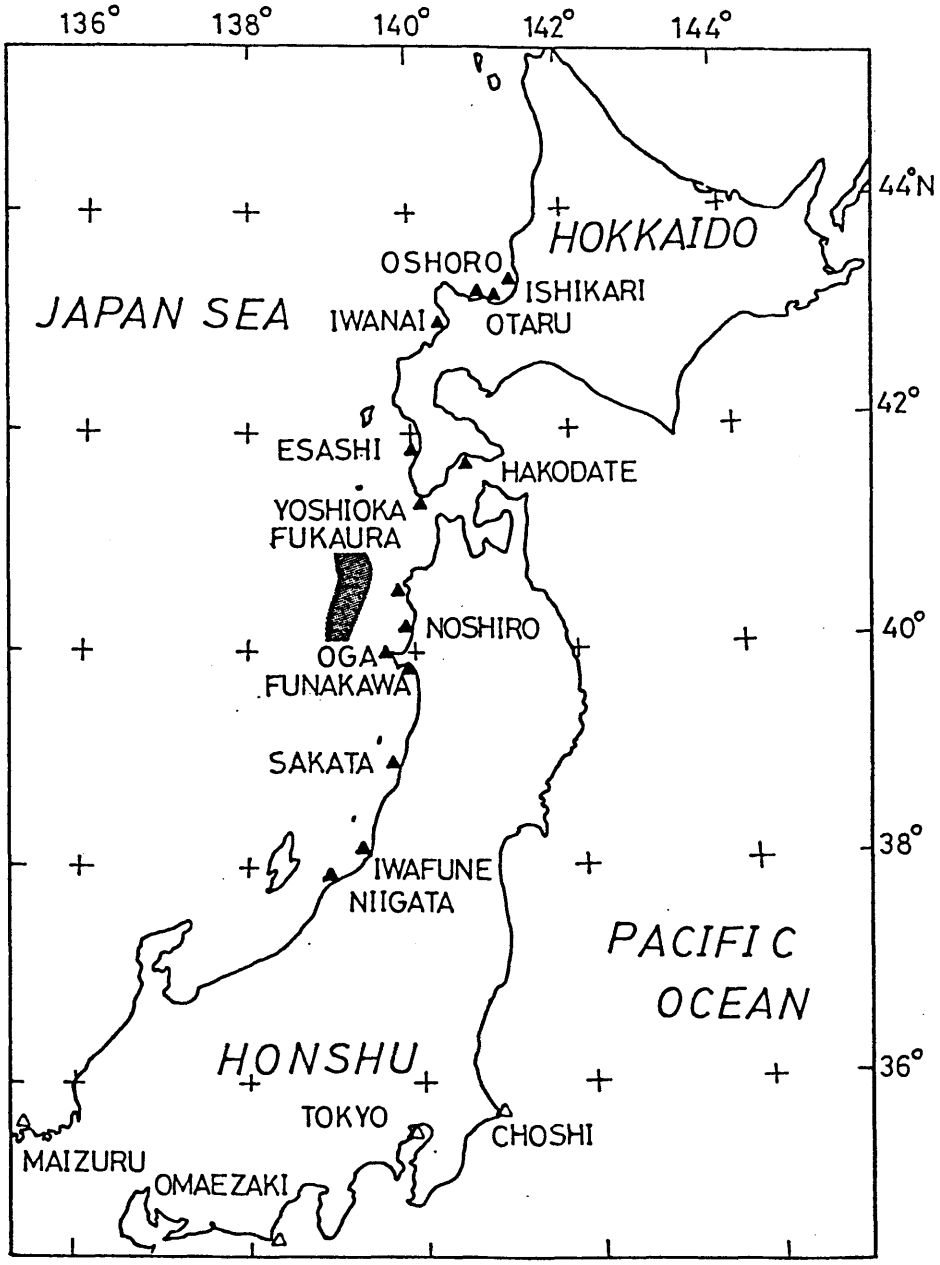

Figure 2. Tide gauge stations whose responses are compiled in this paper. Solid triangles are the measured stations in this study while open triangles are by Okada (1985). Shaded area is the source area of the 1983 Japan Sea earthquake tsunami.

Fig.3

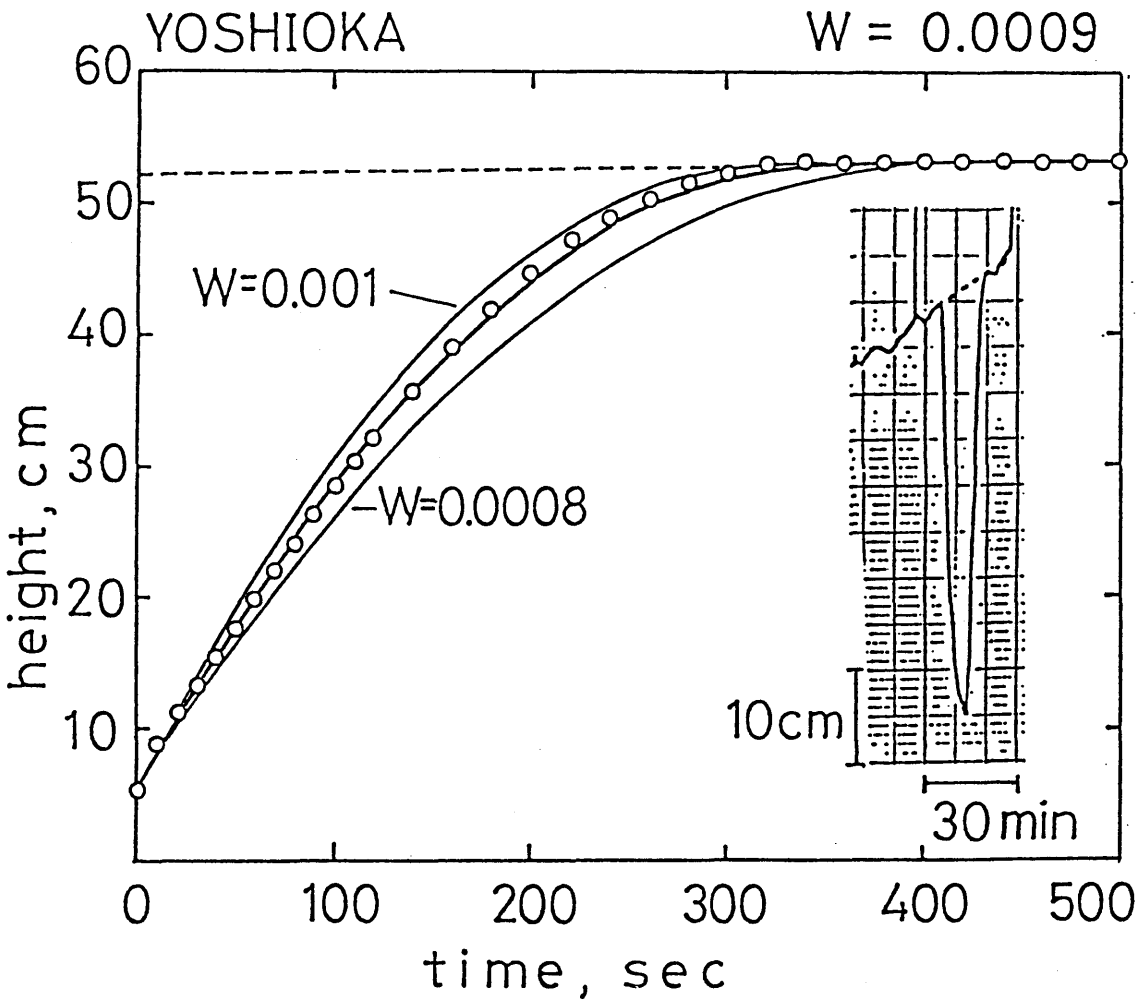

Figure 3. The temporal change of the water level inside the well after the water is drained from the well at Yoshioka. Computed curve for three different Well Constants are shown by solid lines. Dashed line is an estimated water level outside the well from the inset tide gauge record.

Fig.4

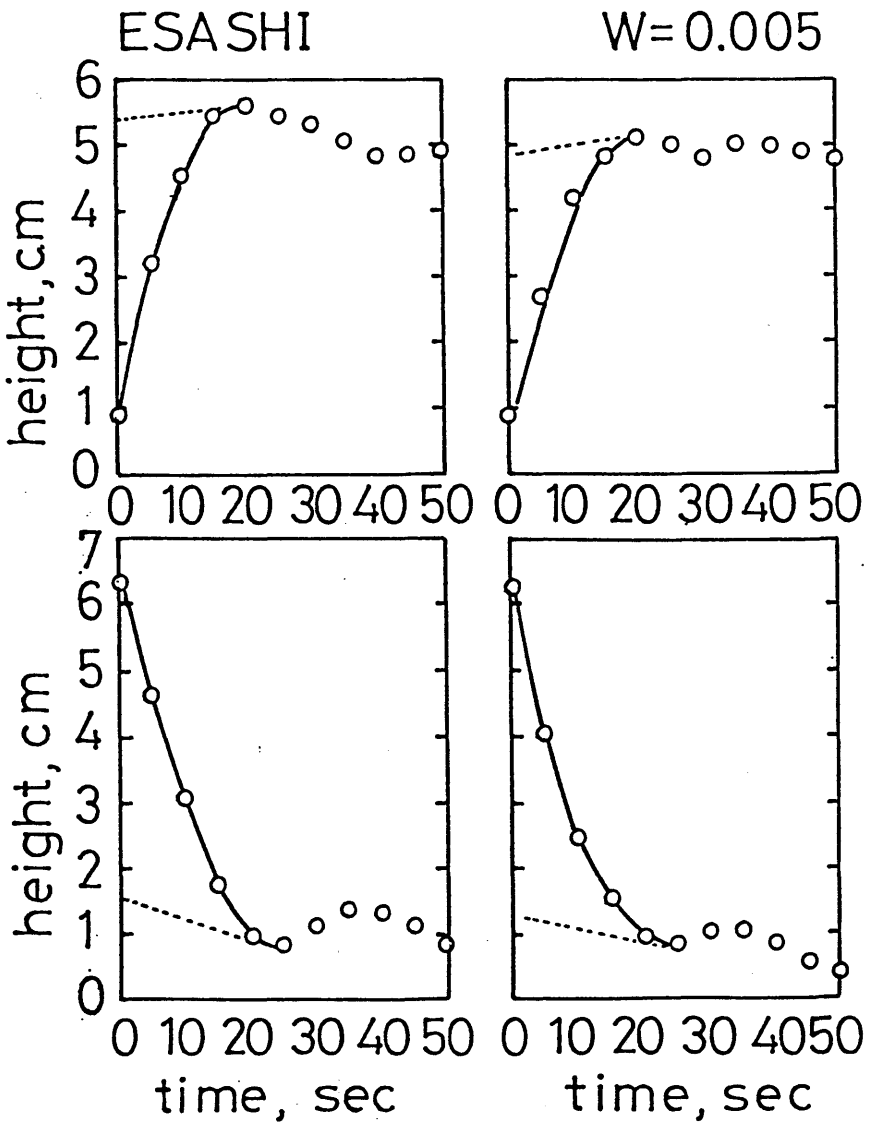

Figure 4. The water level change inside the tide well for the drain (*top*) and the pour (*bottom*) tests at Esashi. Dashed lines are the estimated water levels outside the well.

Fig.5

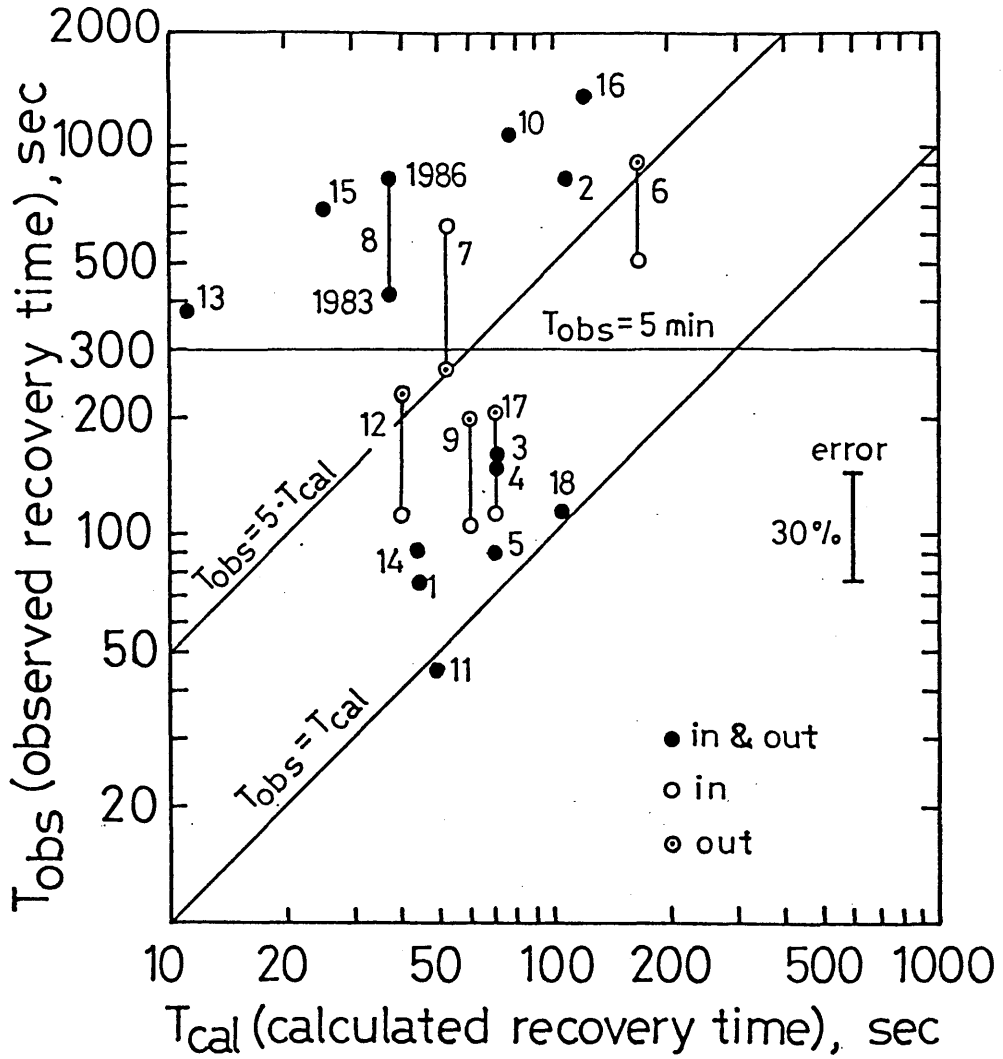

Figure 5. Comparison of the calculated and observed recovery times. The attached numbers correspond to the station number in Table I. The error bar for the estimation of T_{obs} is also shown. When T_{obs} for the inflow and outflow differ by more than 50 %, both are shown by different symbols. For Fukaura (No.8), the results of the two measurements in 1983 and 1986 are shown.

Fig.6

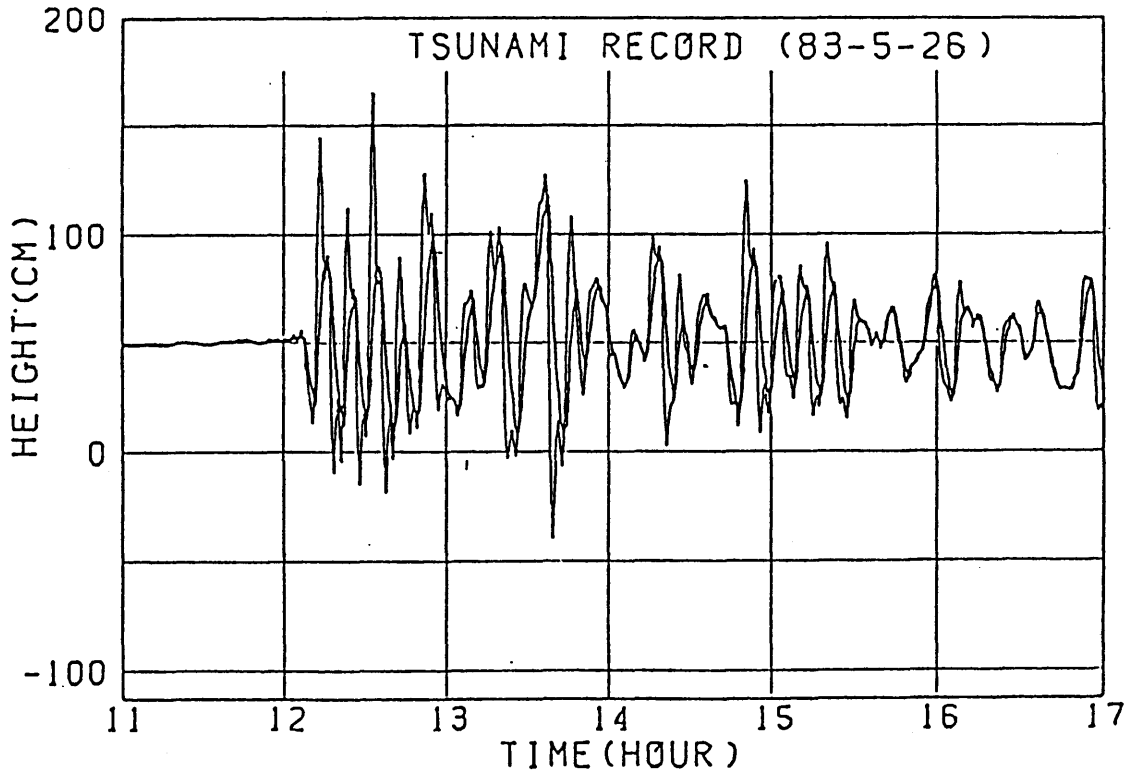

Figure 6. The tide gauge record at Fukaura from the 1983 Japan Sea earthquake tsunami (thick trace) and the corrected waveform for the tide gauge response (thin trace) taken from Okada (1985).

Fig.7

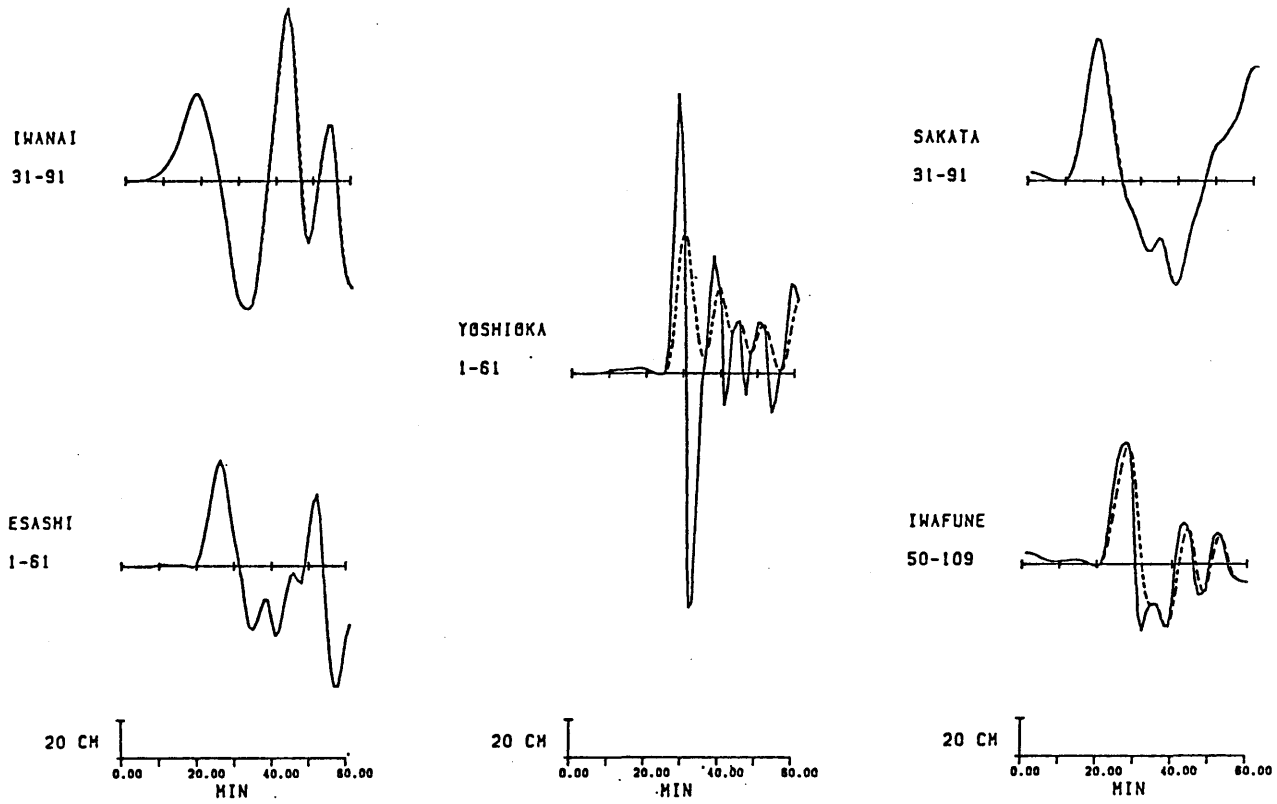

Figure 7. The tide gauge records from the 1983 Japan Sea earthquake tsunami (solid trace) and the corrected waveforms for the tide gauge response (dashed trace). The number below the station is the time from the origin time of the earthquake in min.

Chapter 3

Fault Heterogeneity of the 1983 Japan Sea Earthquake

Abstract

The fault heterogeneity of the 1983 Japan Sea earthquake is investigated by an inversion of tsunami waveforms. The propagation effect of tsunami is accounted by the finite-difference computation on actual bathymetry and the response of the tide gauge system is corrected by using the results of *in situ* measurements. Simulation of the inversion clarifies that the heterogeneity of the faulting can be resolved to a fourth of the total fault length when the grid size of the bathymetric data used for the computation of the Green's functions is 2.5 km and the observed waveforms are digitized at 1 min interval. The obtained slip distribution shows that the third segment from the north among the four slips 3.9 m whereas the slip on the other three segments are about 2 m. The estimated total seismic moment is smaller than the previous study as a result of using the total waveforms. The largest slip corresponds to the first sub-event of the multiple shock analyzed by seismic waves and it indicates the existence of an asperity.

1.Introduction

The heterogeneity of the faulting process of large earthquakes is one of the most important problems in earthquake seismology and is usually studied by using seismic waves. Satake (1987a) showed that the heterogeneity can be revealed by an inversion of tsunami waveforms. The propagation effect of tsunami waves can be more accurately evaluated than seismic waves since the velocity of tsunami depends only on the water depth and the bathymetry is the most well-known geophysical parameter.

The fault models of the 1983 Japan Sea earthquake of May 26, 1983 have been proposed from tsunami data (Aida, 1984; Satake, 1985; Kosuga *et al.*, 1986). Satake (1985), having constraints from the moment tensor inversion of seismic surface waves, made finite-difference computations of tsunami waveforms for several fault models. The best model was chosen by judging the amplitude ratio and the time difference of the observed and computed tsunami waveforms by a trial and error method. The final model, model *D*2 in Satake (1985), consists of two segments of 60×40 km^2 in size and the slip amount is 4 m and 5 m for the northern and southern parts, respectively. This result already showed the heterogeneous fault motion. The analyses of seismic waves (Shimazaki and Mori, 1983; JMA, 1984; Ishikawa *et al.*, 1984; Sato, 1985; Fukuyama and Irikura, 1986) showed that this event was a multiple shock. To obtain a more detailed picture of the faulting process from tsunami, the trial and error approach is not appropriate because of the non-uniqueness. In this paper, the inversion of tsunami waveforms proposed and examined for its effectiveness by Satake (1987a) is applied to the 1983 Japan Sea earthquake.

2. Method and Data

The method of inversion of tsunami waveforms is described briefly here because it is

already presented in Satake (1987a). The fault plane is divided into small segments and crustal deformation is computed for a unit amount of slip (1m in this study) on each segment. Assuming that the surface water height distribution is the same as that of the bottom deformation, and having it as an initial condition, tsunami waveforms are computed by a finite-difference method. The computed waveforms at tide gauge stations are used as the Green's functions. The observational equation is

$$A_{ij}(t) \cdot x_j = b_i(t)$$

where $A_{ij}(t)$ is the Green's function at the i-th station from the j-th segment, x_j is the slip amount of the j-th segment and $b_i(t)$ is the observed tide gauge record at the i-th station. The slip amount on each segment is obtained by a linear least-squares inversion.

Numerical experiments made by Satake (1987a) showed that the grid size for the finite-difference computation must be smaller than one eighth of the segment size. Since the estimate of finer heterogeneity that studied by Satake (1985) is the purpose of the present study, the grid size of bathymetric data for the computation of the Green's function is taken as 2.5 km. Variable grid system with the smallest size 612.5 m is employed near the tide gauge system as made by Satake (1985).

The region required for the finite-difference computation is determined by ray-tracing of tsunami waves from four end points of the source area (Satake, 1987b). The area and grid system for the computation are shown in Fig.1. The number of grids is about 110,000 including the land part. The time step for the computation is set to 5 sec to satisfy the stability condition. The waveforms are output in 1 min interval at 8 tide gauge stations shown in Fig.1.

Tide gauge records from the 1983 tsunami at these 8 stations are digitized in 1 min interval. The paper speed of Japanese tide gauges is usually 2 cm/hr, so that 1 min corresponds to 1/30 cm. The correction for the response of tide gauge system is made to

the observed tsunami records (Satake *et al.*, 1987). The correction does not change the waveforms so much except at Yoshioka where the corrected amplitude becomes twice of the original amplitude. The corrected waveforms are used as the data for the inversion.

3. Simulation of Inversion

A set of simulation is made to estimate the resolution of the inversion as made in Satake (1987a). Computed waveforms for the model *D*2 in Satake (1985) are used for the observed waveforms. The Green's function are computed for three kinds of segmentation as shown in Fig.2. The two-segment model shows the same segmentation as the model *D*2. Each of the segment is further divided into two for the 4-segment model and three for the 6-egment model. The area of each segment is 60×40 km^2 which contains 24×16 grids for the 2-segment model, 30×40 km^2 or 12×16 grids for the 4-segment model and 20×40 km^2 or 8×16 grids for the 6-segment model.

The results of simulation are shown in Fig.3. The slip distribution (4 m in the northern and 5 m in the southern part) is reproduced by both the 2- and 4-segment models. The error, probably caused by the numerical dispersion (Satake, 1987a), is less than 5 %. The covariance matrix whose diagonal and off-diagonal elements indicate the variance and covariance of the estimate of the slip amount, respectively, is also shown in the figure. Since the covariance matrix is a symmetric matrix, only a upper half is shown. The correlation coefficients, defined as the covariance normalized by the variance, are shown in the lower half. This is sometimes called as a correlation matrix.

The results of the simulation for the 6-segment model is totally different from the assumed model. The estimate is unstable and unreliable. The large negative correlation coefficients between neighboring segments, for example -0.85 for the 5 th and 6 th segments from the north, indicate that the estimated parameters are strongly and negatively

correlated each other. The spatial resolution of the fault heterogeneity is limited by both the numerical dispersion of the finite-difference computation and a finite sampling of the tide gauge records. The number of grid in each segment is 8×16, which indicates that the smaller grid size would cause the numerical dispersion (Satake, 1987a). Sampling interval of tide gauge records is 1 min. The first arrival of tsunami waves propagates along a deeper part of the Japan Sea, namely 2000 to 3000 m (Fig.1) where the tsunami propagates 8 to 10 km in 1 min. Since this distance is only a half of the segment size, the information from the neighboring segments may be included in the same sampling of the tide gauge records. This is also a reason of the instability.

As a result of simulation of the inversion, a fourth of the total fault size, or 30 km, is found to be an appropriate spatial resolution of the heterogeneity for the 1983 Japan Sea earthquake when the grid size of the finite-difference computation is 2.5 km and the sampling interval of the observed tide gauge records is 1 min. The 4-segment model is applied to the observation and the slip distribution is estimated in the next section.

4. Fault Heterogeneity of the 1983 Event

The heterogeneity of the fault motion is estimated for the 4-segment model of the previous section. The location of segments and the fault parameters are fixed to those of the model *D*2 of Satake (1985). Since the purpose of this paper is to estimate the relative slip distribution on the fault, the choice of the fault model doesn't seem to affect the result severely. The size of each segment is 30×40 km^2, dip angle is 30° and the top of the fault is 1 km below the ocean bottom. The northern two segments strike N20°W whereas the southern two segments strike N20°E. The Green's functions are shown in Fig.4. Though we use the variable grid system, the accuracy of the computation is worse for the later part of the tsunami because of the contamination of the reflected waves from the

region with coarse grids. Therefore the first two cycles of the waveforms are mainly used. The length of the record varies from station to station as shown in Fig.4 and ranges 23 to 44 min. The number of total data points at the 8 stations is 283. Considering that the digitizing interval is 1 min, the temporal separation of each Green's function is good.

The result of the inversion is shown in Fig.5 with the covariance and correlation matrices. The slip on the third segment from the north is largest, 3.9 m, and the others are about 2 m. The correlation matrix shows that the correlation between the neighboring segments is small so that the solution is well resolved. The moderate positive correlation, 0.66, between the first and third segments from the north is due to the simultaneous arrival of the first peak and the following trough of the Green's function from these segments (Fig.4). If the average slips for the northern and southern halves are calculated, they are 2.0 m and 3.0 m, respectively. The slip amount is much smaller than the model *D*2 of Satake (1985). However, the fact that the southern part of the fault slips more than the northern part is consistent with the model *D*2.

Figure 6 is the comparison of the observed and synthetic waveforms for the result of the inversion. The general agreement of the waveforms is fairly good. The RMS residual of the synthetic wave is 21.3 cm. The amplitude of the synthetic wave is smaller than the observed amplitude at Iwanai, Yoshioka and Sakata.

5. Discussion

The estimated slip amount on the fault becomes smaller than the previous model *D*2. The average slip for the total fault is 2.5 m and the seismic moment is 4.2×10^{27} dyne·cm assuming that the rigidity is 3.5×10^{11}dyne·cm^{-2}. This value is smaller than the moment obtained by long-period surface waves (Satake, 1985; Kanamori and Astiz, 1985) which ranges 5.9 to 7.6×10^{27} dyne·cm. The differences between this study and the previous one

(Satake, 1985) are the data and a criterion of fitting synthetic waves to the observed waveforms.

The correction of tide gauge records by the measured response is essential in the present study. The inversion is also performed for the tide gauge records corrected by the hydraulically computed response. This correction doesn't change the original tide gauge records so much, thus it is considered to be uncorrected data (Satake *et al.*, 1987). The estimated slip distribution is also shown in Fig.5 by dashed lines. The slip amount on each segment or the seismic moments are much smaller than the result from the corrected data for the response. In the previous trial and error approach, the amplitude of the first cycle of the wave is matched whereas in this study the difference of the total waveforms between the observed and synthetic waves is minimized. More applications of the present method to the earthquakes whose seismic moments are seismologically estimated are necessary to calibrate the estimation of the absolute value of the seismic moment.

Studies of the seismic waves showed that this event was a multiple shock (Fig. 7). JMA (1984) and Ishikawa *et al.*(1984) made an inversion of long-period body waves to estimate a spatio-temporal distribution of sub-events. They show that the initial pre-event was followed by two major sub-events. The first sub-event is located near the pre-event which is probably occurred at the hypocenter. The location of the second sub-event is about 50 km north of the first sub-event. The seismic moment is largest for the first sub-event. Shimazaki and Mori (1983) also analyzed long-period body waves and obtained a similar sub-event distribution. The largest slip in the third segment from the north obtained in this study may correspond to the first sub-event in these analyses although the frequency range of the seismic body waves and tsunamis are different. This part can be considered to be an asperity in which the slip amount is larger than the other area of the fault plane.

Sato (1985) made an analysis of strong-motion records at near-field stations and showed that there are three sub-events with similar moments. Fukuyama and Irikura (1986)

made a waveform inversion of strong-motion records and estimated the distribution of the moment release. The heterogeneity inferred from the seismic wave analyses does not agree each other because of the difference in the method and the type of the seismic waves used. For example, JMA (1984) assumed a laterally homogeneous Earth model whereas Fukuyama and Irikura (1986) used the seismograms from the aftershocks as the Green's functions. In this study, the propagation effect of the tsunami is taken account by making the finite-difference computation on actual bathymtery and the response of the tide gauge is corrected. Therefore the obtained slip distribution does not include any ambiguity. Although the resolution is not good enough, the reliability is considered as better than those seismic wave analyses.

References

Aida, I., 1984. A source model of the tsunami accompanying the 1983 Nihonkai-Chubu earthquake. Bull. Earthq. Res. Inst., 59, 93-104 (in Japanese).

Fukuyama, E. and Irikura, K., 1986. Rupture process of the 1983 Japan Sea (Akita-Oki) earthquake using a waveform inversion method. Bull. Seism. Soc. Am., 76, 1623-1640.

Ishikawa, Y., Takeo, M., Hamada, N., Katsumata, M., Satake, K., Abe, K., Kikuchi, M., Sudo, K., Takahashi, M., Kashiwabara, S. and Mikami, N., 1984. Source process of the 1983 Japan Sea earthquake. Chikyu, 6, 11-17 (in Japanese).

Japan Meteorological Agency (JMA), 1984. Report on the Nihonkai-Chubu earthquake, 1983. Tech. Rep. JMA, 106, 253pp. (in Japanese).

Kanamori, H. and Astiz, L., 1985. The 1983 Akita-Oki earthquake (M_W=7.8) and its implications for systematics of subduction earthquakes. Earthq. Pred. Res., 3, 305-317.

Kosuga, M., Sato, T., Tanaka, K. and Sato, H., 1984. Aftershock activities and fault model of the Japan Sea earthquake of 1983. Sci. Rep. Hirosaki Univ., 31, 55-69.

Kosuga, M., Ikeda, H., Kamazuka, Y. and Sato, H., 1986. Static fault model of the 1983 Nihonkai-Chubu (Japan Sea) earthquake as inferred from aftershock distributions, crustal deformation, and tsunami data. J. Geod. Soc. Japan, 32, 290-302 (in Japanese).

Satake, K., 1985. The mechanism of the 1983 Japan Sea earthquake as inferred from long-period surface wave and tsunamis. Phys. Earth Planet. Inter., 37, 249-260.

Satake, K., 1987a. Inversion of tsunami waveforms for the estimation of a fault heterogeneity: method and numerical experiments. submitted to J. Phys. Earth.*(Chapter 1.1 of this thesis).*

Satake, K., 1987b. Effects of bathymetry on tsunami propagation: application of ray tracing

to tsunamis. Pure Appl. Geophys. (in Press).*(Appendix of this thesis).*

Satake, K., Okada, M. and Abe, K., 1987. Measurements and correction of tide gauge response to tsunamis. to be submitted to Proc. PACON '88 (Pacific Congress on Marine Technology).*(Chapter 1.2 of this thesis).*

Sato, T., 1985. Rupture characteristics of the 1983 Nihonkai-Chubu (Japan Sea) earthquake as inferred from strong motion accelerograms. J. Phys. Earth, 33, 525-557.

Shimazaki, K. and Mori, J., 1983. Focal mechanism of the May 26, 1983 Japan Sea earthquake. Progr. Abstr. Seism. Soc. Japan, 2, 15.

Fig.1

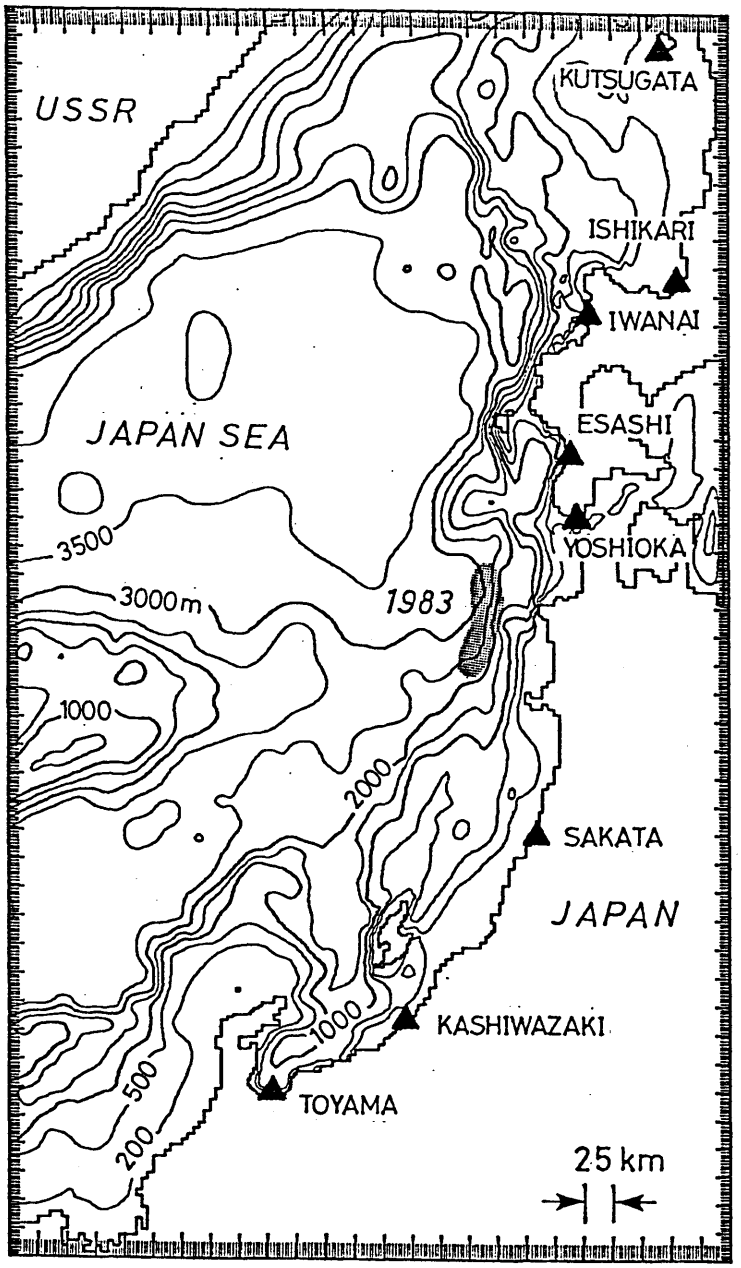

Figure 1. The area and grid system used for the finite-difference computation of the Green's function. Finer grid systems are employed near the tide gauge stations shown by solid triangles. The hatched area is the source area of the 1983 Japan Sea earthquake.

Fig.2

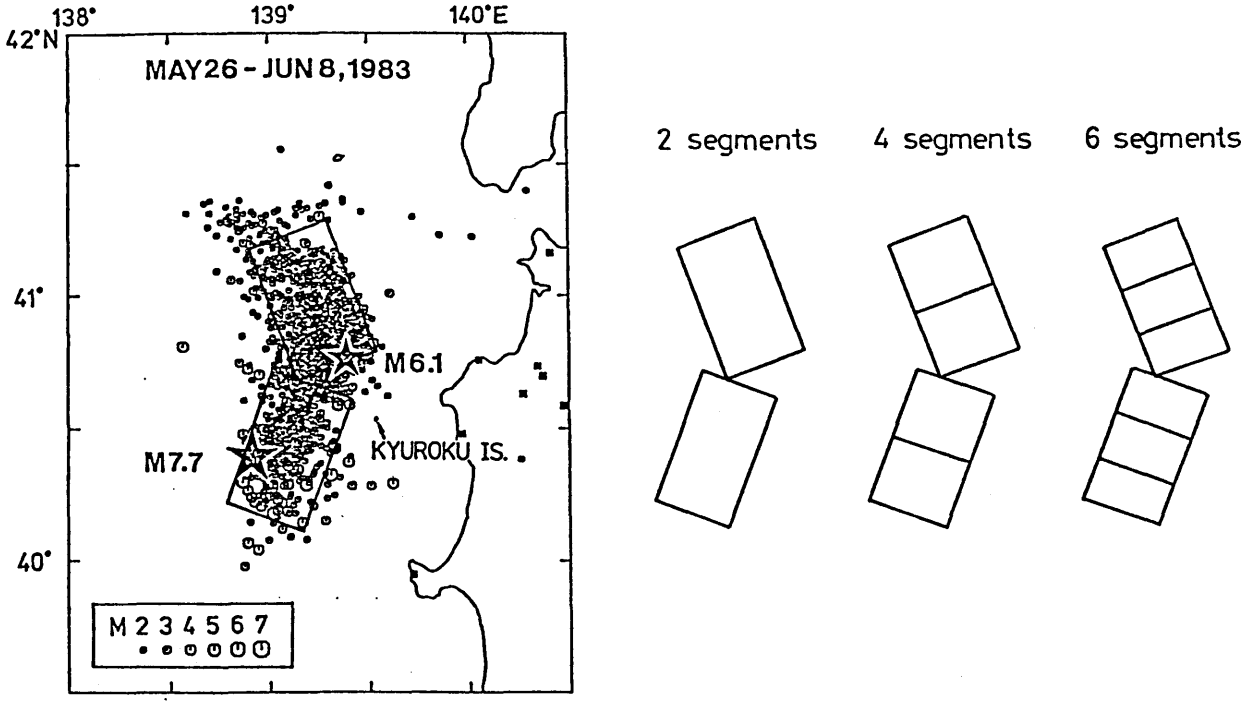

Figure 2. (*left*) Surface projection of the faults of the model *D*2 of Satake (1985) with the aftershock distribution determined by Kosuga *et al.*(1984). (*right*) Configuration of the three kinds of model used for the simulation of the inversion.

Fig.3

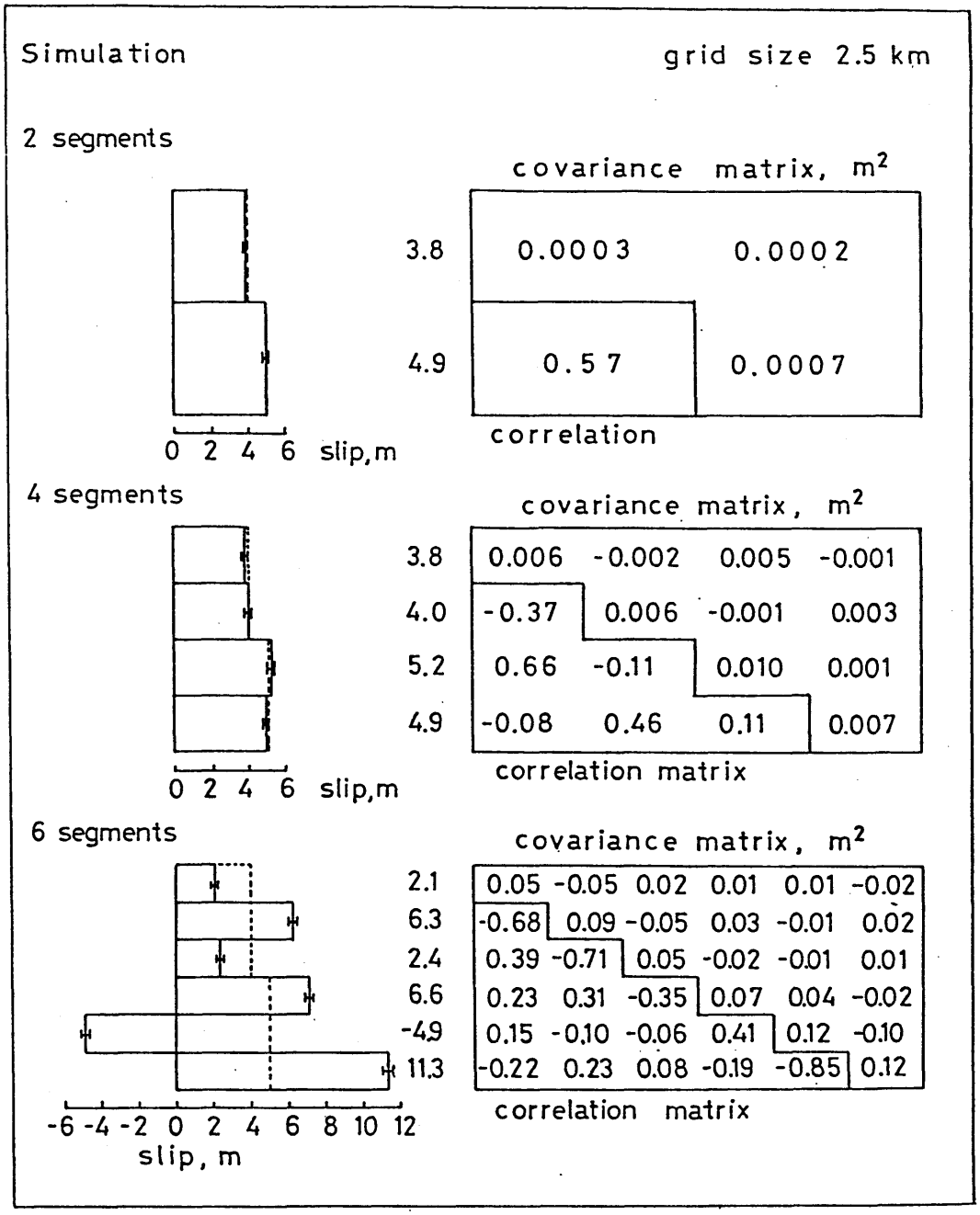

Figure 3. The result of simulation of inversion. The tsunami waveforms from the model *D*2 of Satake (1985) are used as data. The obtained slip distributions are shown in the left whereas in the right the covariance and correlation matrices are shown.

Fig.4

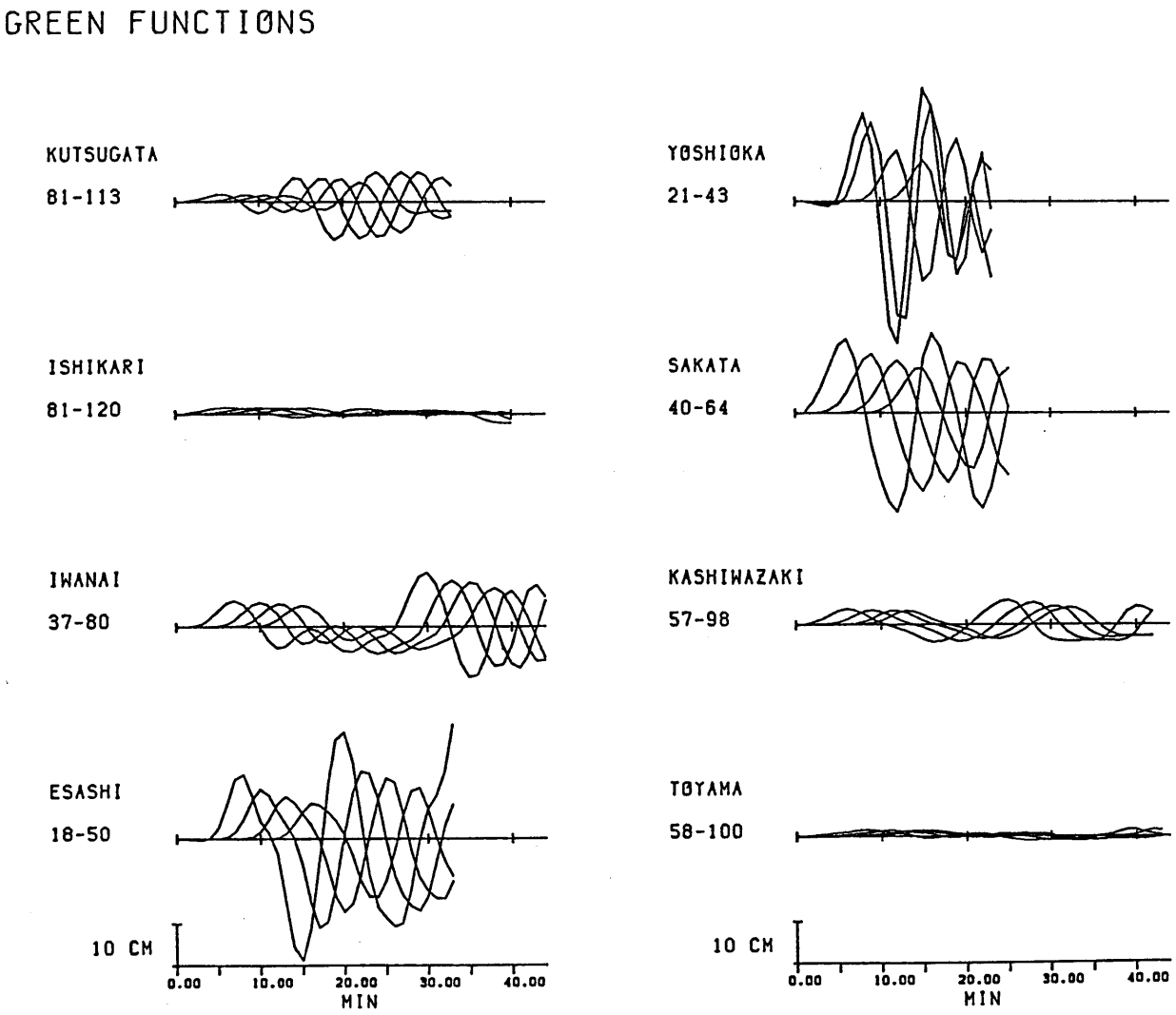

Figure 4. The Green's functions used for the waveform inversion. The time range measured from the origin time is shown below the station name.

Fig.5

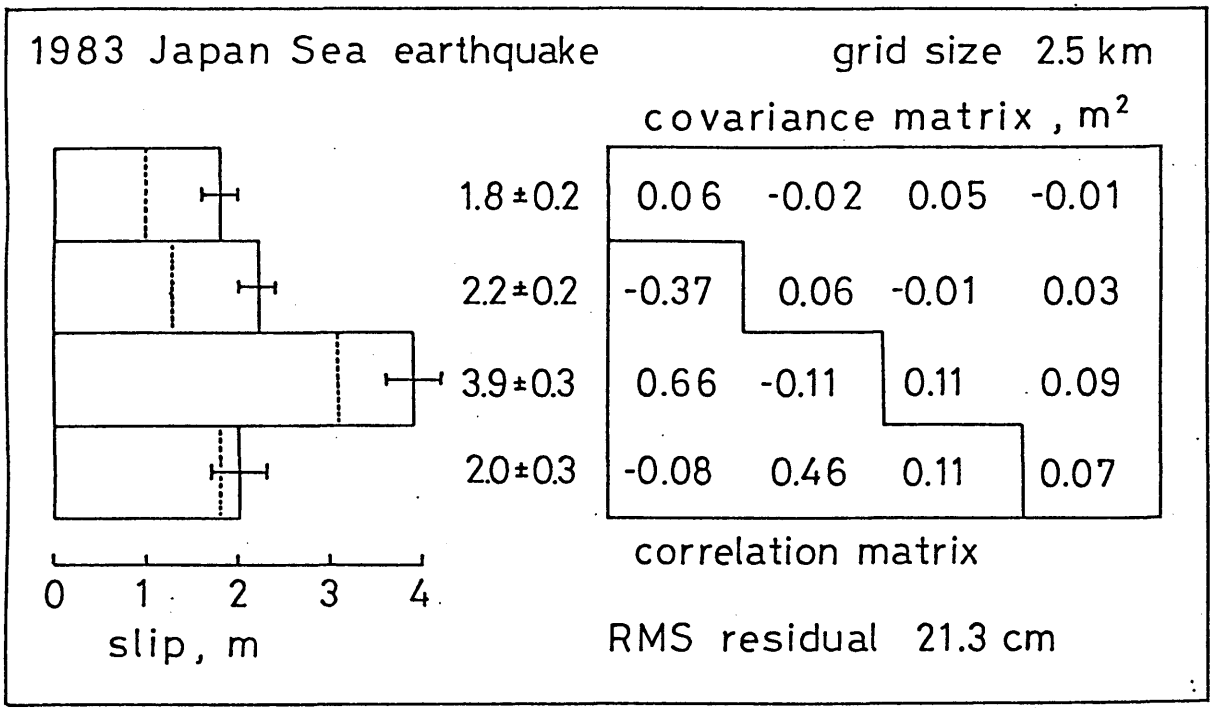

Figure 5. The result of the inversion for the 1983 Japan Sea earthquake. In the left, the obtained slip distribution from the waveforms corrected by the observed tide gauge response is shown. The dashed lines indicate the result by using the uncorrected data. The covariance and correlation matrices of the estimated parameters are shown in the right.

Fig.6

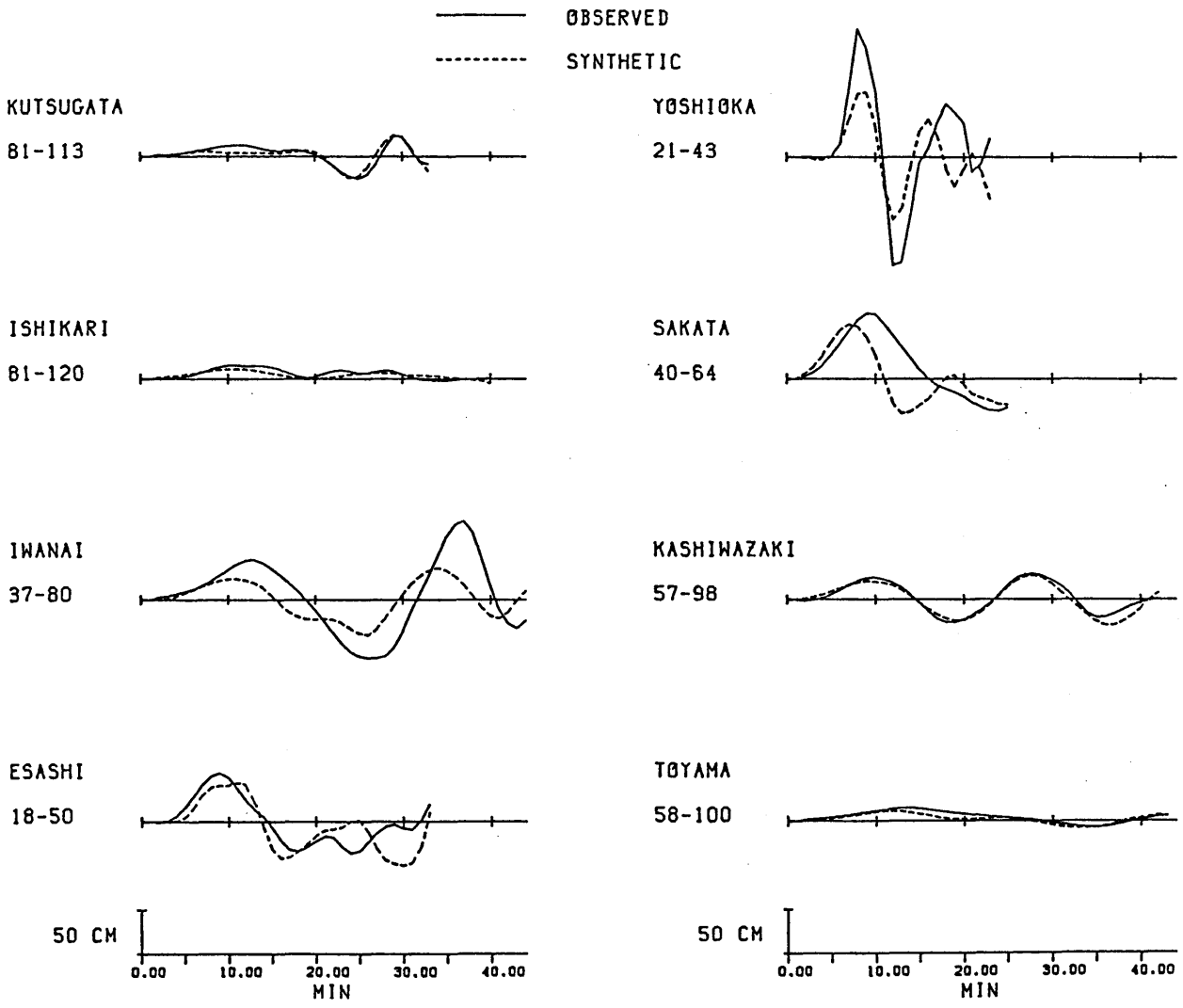

Figure 6. Comparison of the observed (solid curves) and synthetic (dashed curves) waves from the result of the inversion. The time range from the origin time is shown below the station name.

Fig.7

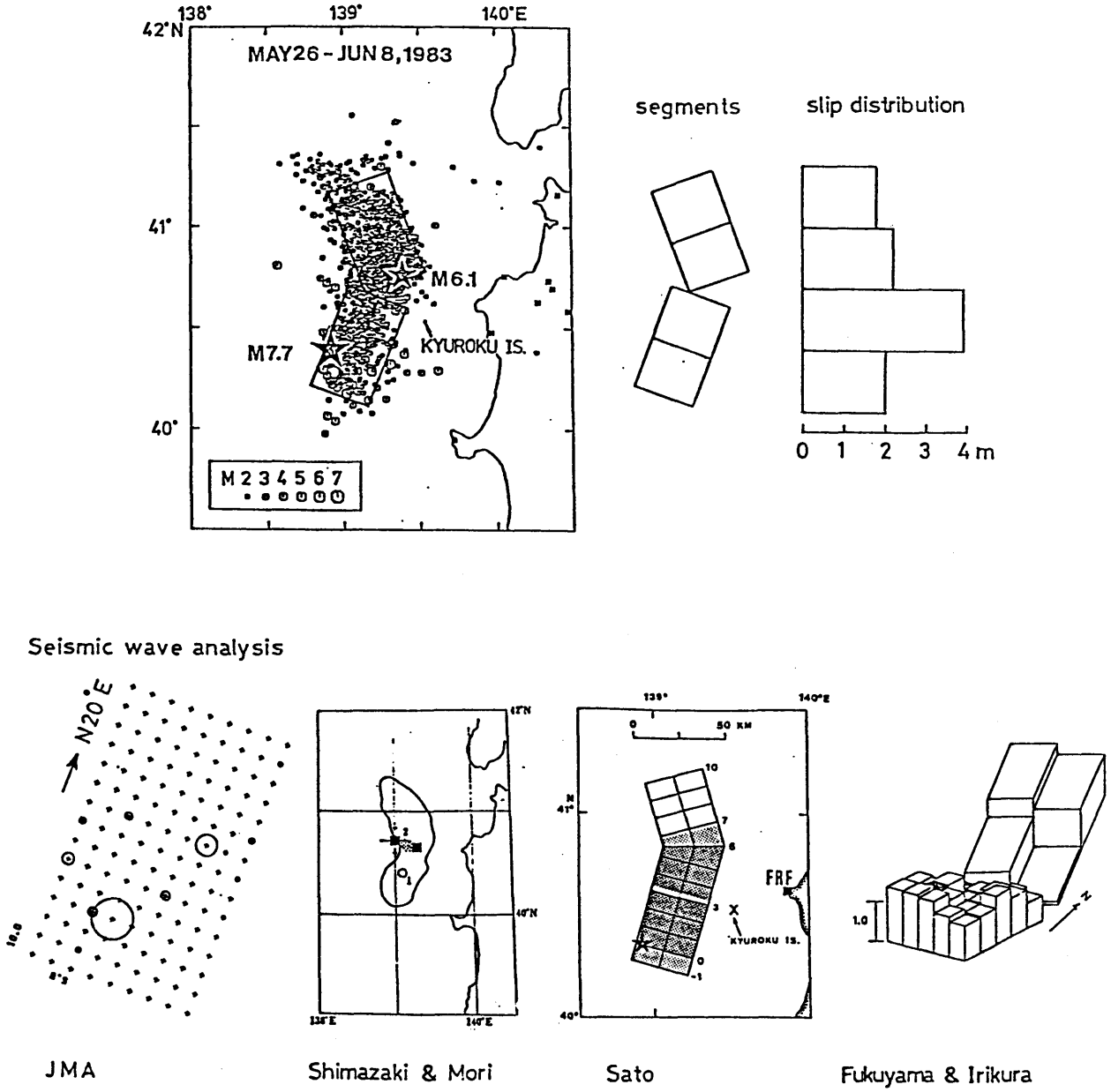

Figure 7. The heterogeneous fault motion obtained in the present study (*above*) and the results of the seismic wave analyses (*bottom*) made by JMA (1984), Shimazaki and Mori (1983), Sato (1985) and Fukuyama and Irikura (1986).

Part 2

Free Oscillation of the Japan Sea Excited by Earthquakes

Chapter 1

Observation and Wave-Theoretical Approach

Summary

Tsunamis accompanied by the 1964 Niigata and the 1983 Japan Sea earthquakes continued for a long time and appeared to have excited the free oscillation of the almost closed Japan Sea. The spectral analysis of the tide gauge records of those tsunamis shows that there are distinct peaks above the noise level in the frequency range between 0.08 and 0.4 mHz. Finite-difference computations of tsunami for the whole Japan Sea by using a supercomputer reproduce those peaks and confirm that they represent the free oscillation of the Japan Sea. The computation is also made for a region including only the south-eastern half of the Japan Sea with an artificial radiation condition on the north-western boundaries. A comparison between the results of these two computations shows the effect of reflections from the north-western coast or the geometry and size of the whole Japan Sea. The simulated spectrum from the south-eastern half region almost agrees with that from the whole Japan Sea for the Niigata tsunami indicating that the earthquake excites mainly the regional oscillations. For the 1983 Japan Sea earthquake, only a few peaks are reproduced by the computation for the south-eastern half region, indicating that the free oscillation of the whole Japan Sea is the essential part of the spectrum. Thus the excitation of the free oscillation is found to depend on the earthquake location.

1 Introduction

The Japan Sea, the marginal sea of the Japanese Islands, has an area of about $10^6 km^2$, with a mean depth of 1500 m and is an almost completely closed basin (Fig.1). It is connected with the outer sea by four straits: the Tatar, Soya, Tsugaru, and Tsushima (or Korea) straits. Several large earthquakes with accompanying tsunamis have occurred at the eastern margin of the Japan Sea (Hatori & Katayama 1977, Satake 1986). Among them the most recent one was the 1983 Japan Sea earthquake (M_W 7.9; Satake 1985) which caused a destructive tsunami. One of the characteristic features of this tsunami is its long duration. It was observed on tide gauge records for two days following the event (JMA 1984). This might be attributed to multiple reflections in the closed Japan Sea and the tsunami appears to have caused a free oscillation, or seiche in oceanographical term, of the Japan Sea. The tsunami from the 1964 Niigata earthquake (M_W 7.6; Abe 1975, Satake & Abe 1983) also showed a similar character (Shimazaki 1976).

In this paper, a spectral analysis of the tide gauge records of those earthquake tsunamis is made to study the free oscillation of the Japan Sea. Finite-difference computation of the tsunami is made for the whole Japan Sea to reproduce the free oscillation. Also a computation is carried out only for its south-eastern half to examine the effect of the reflections from the north-western coast. Such a large computation has become possible by the use of supercomputer which becomes recently available.

2 Spectra of tide gauge records

The tide gauge records from the 1964 Niigata and the 1983 Japan Sea earthquake tsunamis are collected and digitized. The tsunami waveform is easily affected by the local topography such as small bay or harbor (*e.g.* Murty 1977). Three tide gauge stations (Fig.2) are selected to minimize such local effects. Those are located at a site where the off-shore is deep without a continental shelf (Iwasaki), at the tip of a peninsula (Wajima),

or on a remote island (Saigo).

Figure 3 shows the tide gauge records observed at Iwasaki at the time of the 1964 Niigata earthquake. The upper two traces are the records before the event while the bottom two traces are the records just after the earthquake (the origin time is 13:02 JST, June 16, 1964). The tide gauge records are digitized at a 1 min interval. The upper one in each pair is the original record. The bottom one is the band-pass filtered record with a pass band between 50 min and 5 hrs to remove the effects of tide and local topography such as small bay or harbor near the tide gauge stations. The short period limit, 50 min, corresponds to the fundamental period of a bay with a uniform depth of 20 m and a length of 10.5 km (*e.g.* Dietrich *et al.* 1980). The trace after the event shows a decaying oscillation. The trace before the event, indicating a noise level at this station, shows almost nothing in the band-passed record compared with the record after the event. The signal-to-noise ratio at this station is considered to be high.

The power spectra, more precisely power spectral density, of these traces are computed and plotted in Fig.4. All the spectra in this paper are obtained by making FFT on records of 48 hrs after the events. The power spectra for the frequencies below 0.4 mHz (corresponding to a period of 42 min) are shown. The vertical bar shows the range of the 90 % confidence limit. This estimate is made by smoothing the spectrum in the frequency domain (Bendat & Piersol 1971). In Fig.4, the spectra for the three different time intervals are shown. The waveforms of two of them are shown in Fig.3: a post-event one (June 16-18) and a pre-event one (June 12- 14). The spectrum for another pre-event record is also shown in Fig.4. The records for two different time intervals before the earthquake show almost the same spectra, indicating that these can be regarded as noise spectra for this station. The power spectrum after the event is about 100 times larger than, or 20 dB above, the noise level in the frequency range higher than 0.08 mHz (about 3.5 hrs). Below this frequency, the spectra are very similar for the three time

intervals, indicating that they have no relations with the tsunami but represent the tidal effects. Several distinct peaks exist around 0.15, 0.23, 0.27 and 0.3 mHz. These peaks probably represent modes of the free oscillation of the Japan Sea excited by the earthquake.

The observed spectra for other stations and other earthquakes are shown in Figs.5 and 6 with computed spectra which will be a subject of the next section. The spectrum at Saigo from the 1964 Niigata earthquake also shows peaks at 0.14, 0.23, 0.26 and 0.3 mHz, but there is a dominant trough between 0.16 and 0.21 mHz. The spectra from the 1983 Japan Sea earthquake tsunami are shown in Fig.6. At Wajima, a significant peak exists at 0.21 mHz. No distinct peaks are found at Saigo but there is a trough at 0.18 mHz in the spectrum. The spectral structure at Saigo is different for the 1964 and the 1983 tsunamis; the peaks and troughs do not coincide. The spectra are different at the same station from different earthquake or at the different station from the same earthquake. This means that the spectra are not determined by the local topography around the station or the tsunami source, but represent the free oscillation of the Japan Sea, since in such a case the waveform is determined by the combination of the source and the station.

3 Numerical computations of tsunamis

To reproduce and examine the nature of the free oscillation of the Japan Sea, we make numerical computations of tsunamis for a long time. The hydrodynamic equations for long-waves are solved by a finite-difference method on actual topography. The computation is made at a 10 sec interval for 48 hrs after the earthquake in the whole Japan Sea. The computed waveforms at the tide gauge stations are stored. Simulated spectra are obtained from these waveforms by the same way as the observed spectra.

The method of the numerical computation is basically the same as that of Aida (1978) and Satake (1985). The horizontal two components of the equation of motion for linear

long-waves, which have been integrated in the vertical direction, are

$$\frac{\partial Q_x}{\partial t} = - g D \frac{\partial H}{\partial x}$$

$$\frac{\partial Q_y}{\partial t} = - g D \frac{\partial H}{\partial y}$$

and the equation of continuity is

$$\frac{\partial H}{\partial t} = - \left(\frac{\partial Q_x}{\partial x} + \frac{\partial Q_y}{\partial y} \right)$$

where Q_x and Q_y are the flow rate, or the water transports, in x- and y-directions, D the water depth, H the water height and g is the gravitational acceleration. The bottom friction is neglected since the effect is dominant at only very shallow (less than 50m) water (Imamura *et al.*, 1987) while the average depth of the Japan Sea is 1500 m. The Coriolis term is also neglected since a half pendulum day at the latitude 40° is about 19 hrs (*e.g.* Dietrich *et al.* 1980), which is much longer than the periods of our discussion. The above equations are solved in a staggered grid system to keep a stability of numerical computation.

The ocean depth is given on a 5 km × 5 km grid throughout the region as shown in Fig.2. Total number of grids for ocean part is more than 40,000. Since the Tatar strait is very shallow, less than 10 m deep, it is considered to be a land boundary where the waves are totally reflected. The boundary condition at the other three straits is the radiation condition in which we assume that the wave goes out of the region at the velocity on the boundary. The initial condition is that the water is elevated by the same amount as the crustal deformation computed from the fault model. This is valid for the size and source process time for usual earthquakes (Kajiura 1970). The fault parameters are taken from Satake & Abe (1983) for the 1964 Niigata earthquake and from Satake (1985) for the

1983 Japan Sea earthquake. The crustal deformation is completed during the source process time with a uniform rate. The source process time is 30 s for the Niigata and 60 s for the Japan Sea earthquake (Satake 1986). The computation is made at a 10 s interval to satisfy the stability condition. The waveforms at the grid points corresponding to the tide gauge stations are sampled at a 60 s interval, so that the observed and simulated spectra can be directly compared.

Computed spectra are shown in Figs.5 and 6 with the observed spectra. The simulated spectra for the 1964 tsunami (Fig.5) show the same distinct peaks as the observed spectra. At Iwasaki, the frequencies of the peaks agree well between the observed and the simulated spectra, although the power of the simulated spectrum is somewhat larger. At Saigo, the power level of the both spectra is also similar. The disagreement below 0.08 mHz is due to the tide since the tidal effect is not included in the numerical computations. The simulated spectra are also very similar to the observed ones for the 1983 Japan Sea earthquake (Fig.6).

The agreement between the observed and the simulated spectra, both the shape and the power, confirms that the numerical computation made in 5 km grids can satisfactorily reproduce the actual tsunami spectra in the frequency range between 0.08 and 0.4 mHz. In other words the peaks and troughs in the observed spectra are due to the topography of the Japan Sea. In the present frequency range, the spectrum is determined by the topography whose wavelength longer than 10 km (Nyquist wavelength). We use the numerical computation to examine the characteristics of the free oscillation in the next section.

4 Separation of the whole and regional oscillations

Some of the periods of the free oscillation of the Japan Sea are detected from the observed spectra and reproduced by the numerical computation. However, the spatial

characteristics such as location of nodes and loops cannot be examined by wave- theoretical approach as made in this paper. For such a purpose, modal approach is superior and it will be discussed in a separate paper (Satake & Shimazaki 1987). However, some of the characteristics can be examined by the numerical computation used in this paper.

Two types of modes of the free oscillation are expected. First one is that determined mainly by a geometry and size of the whole Japan Sea. Second is mostly determined by the shallow part such as continental shelf extending along the coast where the energy is trapped (*e.g.* Murty 1977). To see the contribution of each type, we make a numerical computation on a modified topography. An artificial boundary is set in the Japan Sea as shown in Fig.2. The effective area of the ocean region is only half of the whole Japan Sea. On the northern and western boundaries, a radiation condition is assumed; the waves go out of the region and never come back again. The oscillation on the marginal shallow parts can be reproduced by this computation but the oscillation of the whole Japan Sea cannot be reproduced.

The computed spectra on the artificial topography are shown in Figs.7 and 8. with those from the previous computations on actual topography. Figure 7 is for the 1964 Niigata earthquake. At both stations, the power spectra for the two computations are very similar. The peaks agree well though the power is somewhat lower for the marginal region. This agreement indicates that the spectrum of the 1964 tsunami is mostly determined by regional oscillation of the shallow part along the eastern margin of the Japan Sea. Also smaller power of spectral peaks from the computation for the marginal region indicates that the power of these peaks is fed by the oscillation of the whole Japan Sea. More close comparison reveals that some of small peaks of the spectrum from the marginal region, *e.g.* peaks at 0.25 and 0.35 mHz at Saigo, are not reproduced in the result for the whole Japan Sea. These peaks probably correspond to locally trapped modes whose frequencies do not match the frequency of oscillation of the whole Japan Sea.

Figure 8 shows the spectra for both the actual and artificial topographies from the 1983 Japan Sea earthquake tsunami. Part of the peaks, those at 0.14 and 0.37 mHz at Wajima, 0.09, 0.33, and 0.38 mHz at Saigo, are reproduced by the computation for the marginal region. This indicates that these peaks also represent regional oscillations. The discrepancies between two spectra at the other peaks are due to the radiation boundary. Especially at 0.08, 0.16, and 0.27 mHz at Wajima and at 0.27 mHz at Saigo, the spectrum for the whole Japan Sea shows peaks whereas that for the marginal region shows troughs. The reflections at the other side of the Japan Sea are essential for those frequencies.

5 Discussion and Conclusion

The computations on the different topographies made clear that the 1964 tsunami causes mainly the regional oscillations whereas the 1983 Japan Sea tsunami excites both the regional and the whole oscillations of the Japan Sea. The different excitation is probably due to the location of the tsunami source. The 1964 Niigata earthquake occurred on a continental shelf, the water depth is around 100 m (Satake & Abe 1983) whereas the water depth around the 1983 Japan Sea earthquake source is about 2500 m (Satake 1985). The shallow source can easily excite the regional oscillation if the amplitude of the mode is large at shallow parts. The normal mode solutions of the Japan Sea is computed in a separate paper and the difference in excitation will be further examined (Satake & Shimazaki 1987).

The minimum size of earthquakes which can excite the observable free oscillation can be estimated from Fig.4. Since the signal is about 20 dB above the noise level, the tsunami spectrum of an earthquake of 10 % in seismic moment may be at the noise level. Since the moment magnitude (M_W) of the 1964 Niigata earthquake was 7.6, the detectable limit of the free oscillation is about 7.0 in the moment magnitude scale (Kanamori 1977) if a scaling can be applied and the spectral structure is the same. The large earthquakes as

accompanied by tsunamis are not common in the Japan Sea (Hatori & Katayama 1977). Only three earthquakes with magnitude 7.5 or greater occurred in this century (Satake 1986). Therefore the free oscillation of the Japan Sea is also rarely observed.

In conclusion, we found that the 1964 Niigata and the 1983 Japan Sea earthquakes excited the free oscillation of the Japan Sea. Numerical computations for 5 km × 5 km grids satisfactorily reproduce the observed spectra at a frequency range between 0.08 and 0.4 mHz. Some of the peaks in this frequency range are the regional oscillation in which the most of the energy is trapped in the regional shallow part, but the others represent the oscillation characterized by a geometry and size of the whole Japan Sea. Excitation of the free oscillation is different, depending on the location of the source.

Acknowledgements

This chapter is a manuscript submitted to *Geophysical Journal of the Royal astronomical Society* with Kunihiko Shimazaki. We thank anonymous referees for critical comments by which the contents and English of our paper is improved very much. One of the authors (Ku.S.) acknowledges encouragement from Hiroo Kanamori at the earliest stage of this study. The numerical computations were made at Computer Centre, University of Tokyo using HITAC S-810/20 and HITAC M280 computer system.

References

Abe, K., 1975. Re-examination of the fault model for the Niigata earthquake of 1964. *J. Phys. Earth,* **23**, 349-366.

Aida, I., 1978. Reliability of a tsunami source model derived from fault parameters. *J. Phys. Earth,* **26**, 57-73.

Bendat, J.S. & Piersol, A.G., 1971. *Random Data: Analysis and Measurement Procedures.*, John Wiley & Sons.

Dietrich, G., Kalle, K., Krauss, W., & Siedler, G., 1980. *General Oceanography* (translation from German), John Wiley & Sons.

Hatori, T. & Katayama, M., 1977. Tsunami behavior and source areas of historical tsunamis in the Japan Sea. *Bull. Earthq. Res. Inst. Univ. Tokyo,* **52**, 49-70 (in Japanese).

Imamura, F., Goto, C. & Shuto, N., 1987. Accuracy and speed of numerical simulation as a means of tsunami warning. *Proc. Japan Soc. Civil Eng.* in press (in Japanese).

Japan Meteorological Agency (JMA), 1984. Report on the Nihonkai- Chubu earthquake, 1983. *Tech. Rep. JMA, No.106,* Tokyo, 253pp. (in Japanese).

Kajiura, K., 1970. Tsunami source, energy and the directivity of wave radiation. *Bull. Earthq. Res. Inst. Univ. Tokyo,* **48**, 835-869.

Kanamori, H., 1977. The energy release in great earthquakes. *J. Geophys. Res.,* **82**, 2981-2987.

Murty, T.S., 1977. Seismic Sea Waves - Tsunamis. *Bull. Fish. Res. Board Canada, No.198.*

Satake, K., 1985. the mechanism of the 1983 Japan Sea earthquake as inferred from long-period surface waves and tsunamis. *Phys. Earth Planet. Inter.,* **37**, 249-260.

Satake, K., 1986. Re-examination of the 1940 Shakotan-oki earthquake and the fault parameters of the earthquakes along the eastern margin of the Japan Sea. *Phys. Earth Planet. Inter.,* **43**, 137-147.

Satake, K. & Abe, K., 1983. A fault model for the Niigata, Japan, earthquake of June 16, 1964. *J. Phys. Earth,* **31**, 217-223.

Satake, K. & Shimazaki, K., 1987. Free oscillation of the Japan Sea excited by earthquakes 2: modal approach ans synthetic tsunamis. submitted to *Geophys. J. R. astr. Soc. (Chapter 2.3 of this thesis)*

Shimazaki, K., 1976. Long-period power spectra of tsunamis in the Japan Sea (*abstract*). *EOS Trans. Am. Geophys. Union.*, **57**, 290.

Fig.1

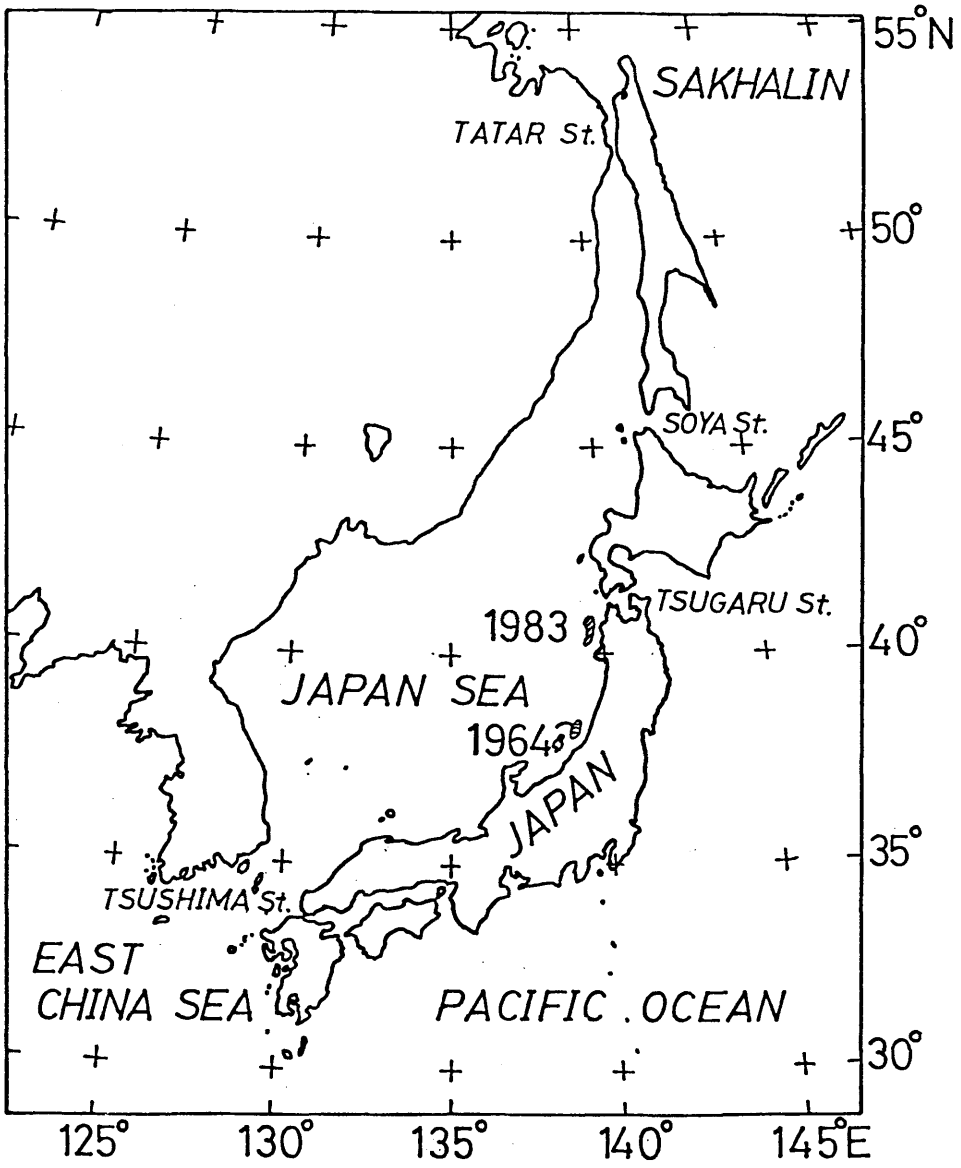

Figure 1. Map showing the location of the Japan Sea. The source areas of the two earthquakes used in this study are also shown.

Fig.2

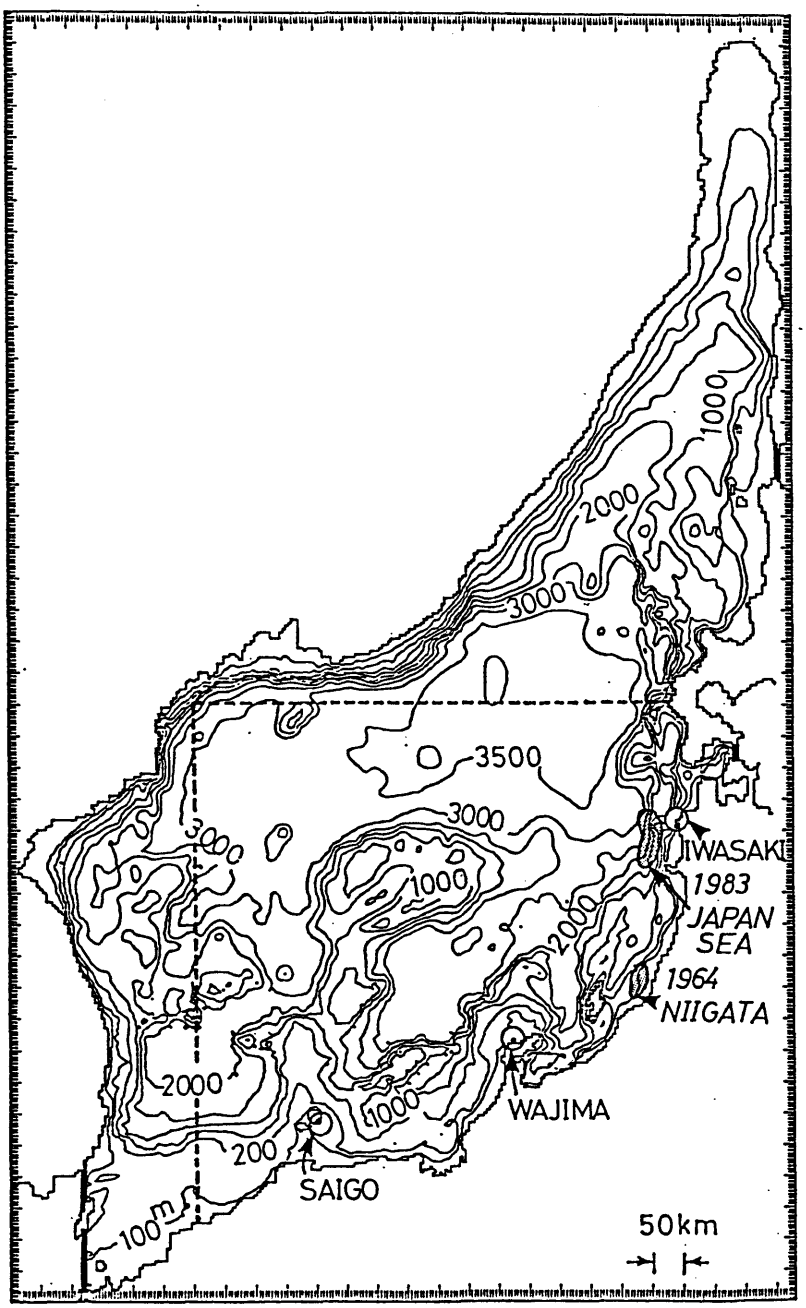

Figure 2. The grids and their depths used for the numerical computations. The tide gauge stations are circled and the source areas of the earthquakes are hatched. The thick solid lines are the boundaries to the outer sea. The dashed line is the artificial radiation boundary for the computation in the south-eastern half of the Japan Sea.

Fig.3

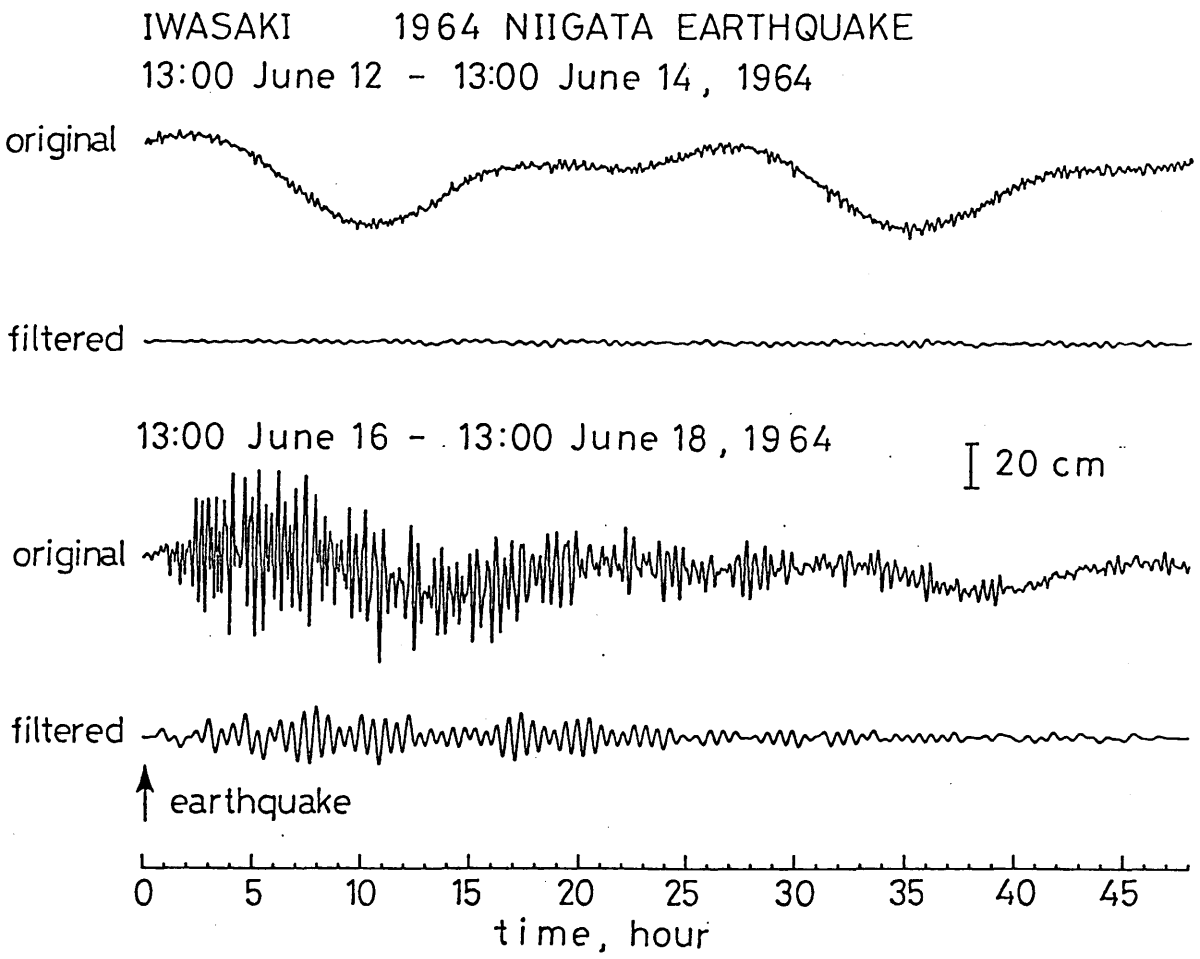

Figure 3. Digitized tide gauge records at Iwasaki before (*top*) and after (*bottom*) the 1964 Niigata earthquake. The upper trace in each time interval is the original record while the lower one is band-passed with a pass-band between 50 and 300 min.

Fig.4

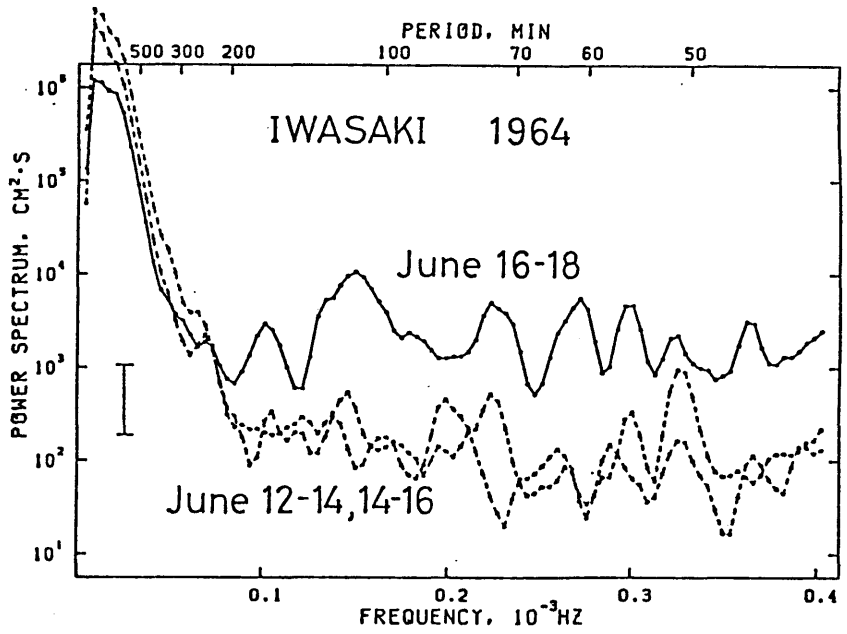

Figure 4. The spectra of the tide gauge records at Iwasaki at the time of 1964 Niigata earthquake. The solid line shows the spectrum after the event while two dashed lines are the spectra before the event indicating the noise level. The vertical bar at the left indicates the range of the 90 % confidence level.

Fig.5

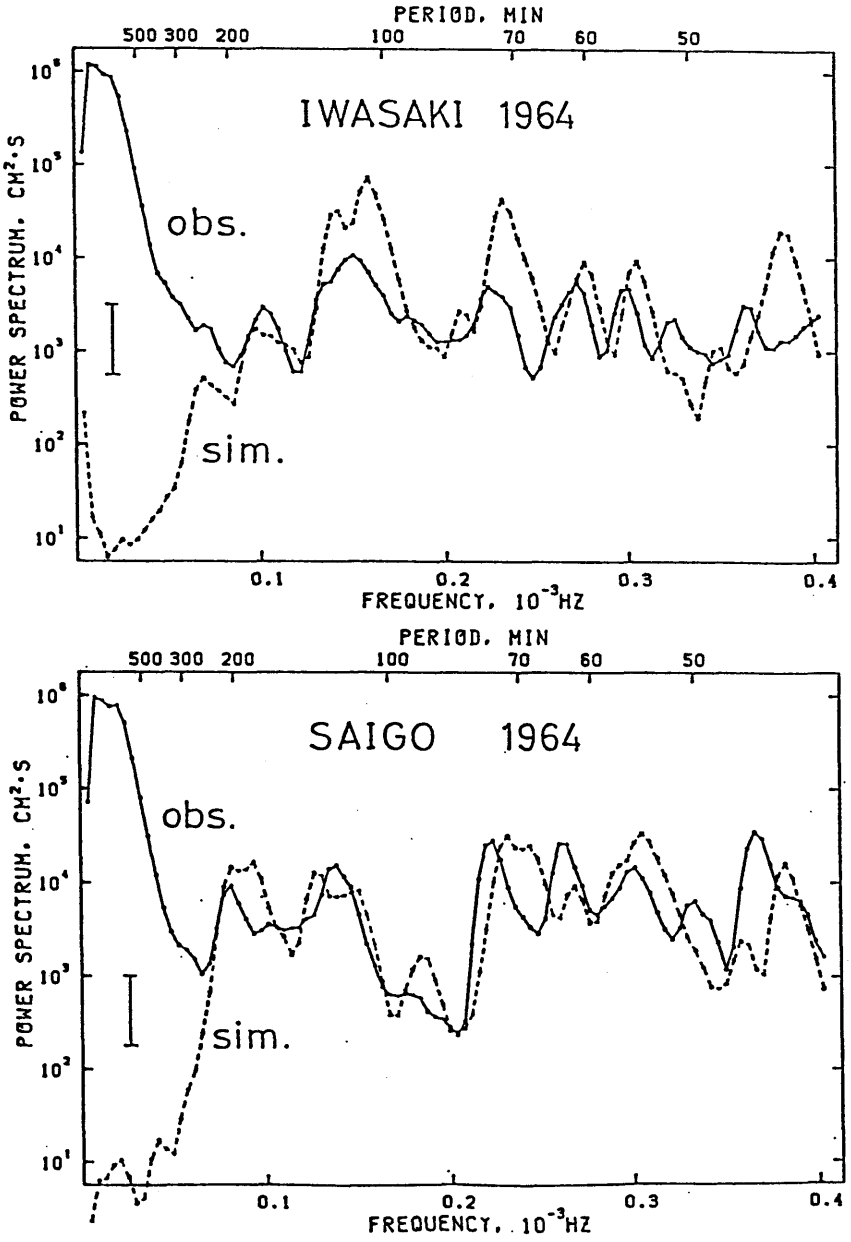

Figure 5. Comparison of the observed and simulated spectra for the 1964 Niigata earthquake tsunami at Iwasaki and Saigo. Solid lines show the observed spectra while the dashed lines show simulated ones. The vertical bar at the left indicates the range of the 90 % confidence level.

Fig.6

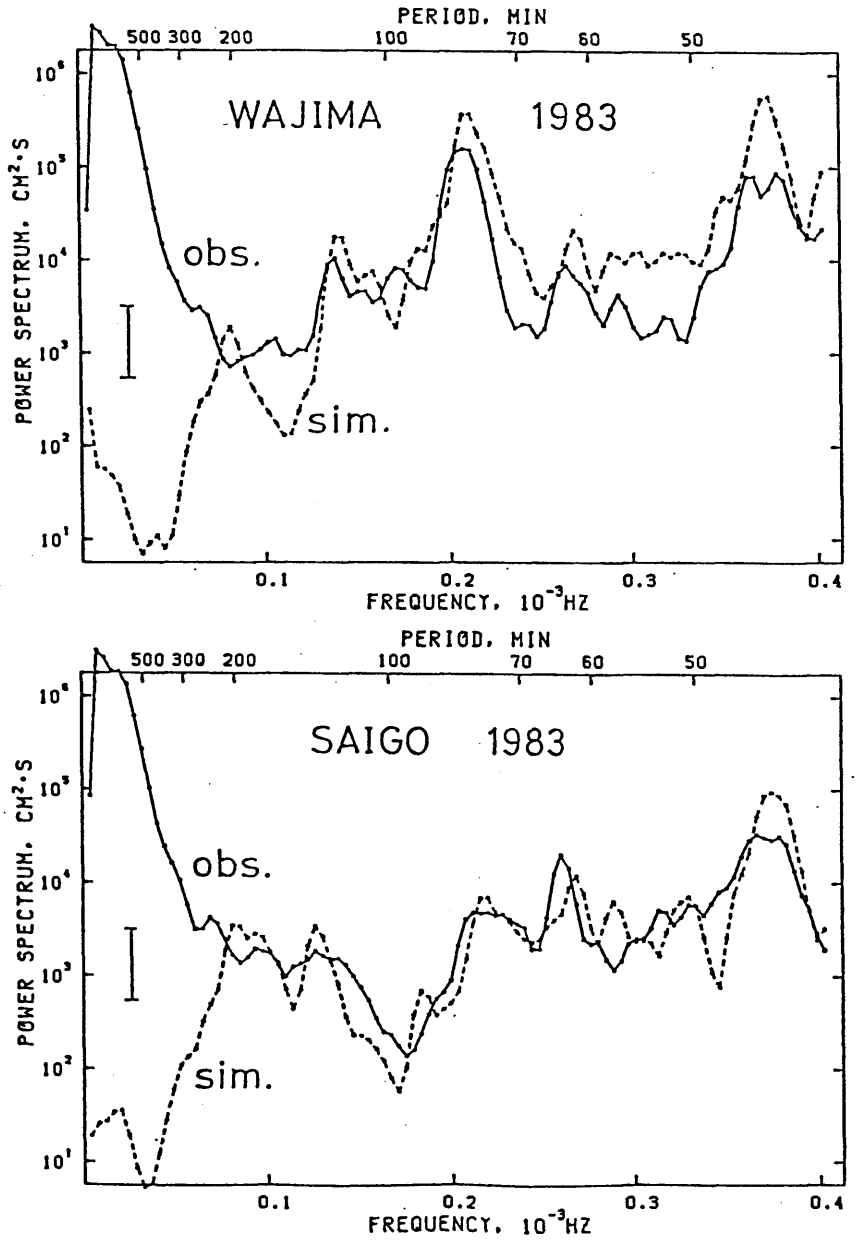

Figure 6. Comparison of the observed and simulated spectra for the 1983 Japan Sea earthquake tsunami at Wajima and Saigo. The symbols are the same as those of Fig.5.

Fig.7

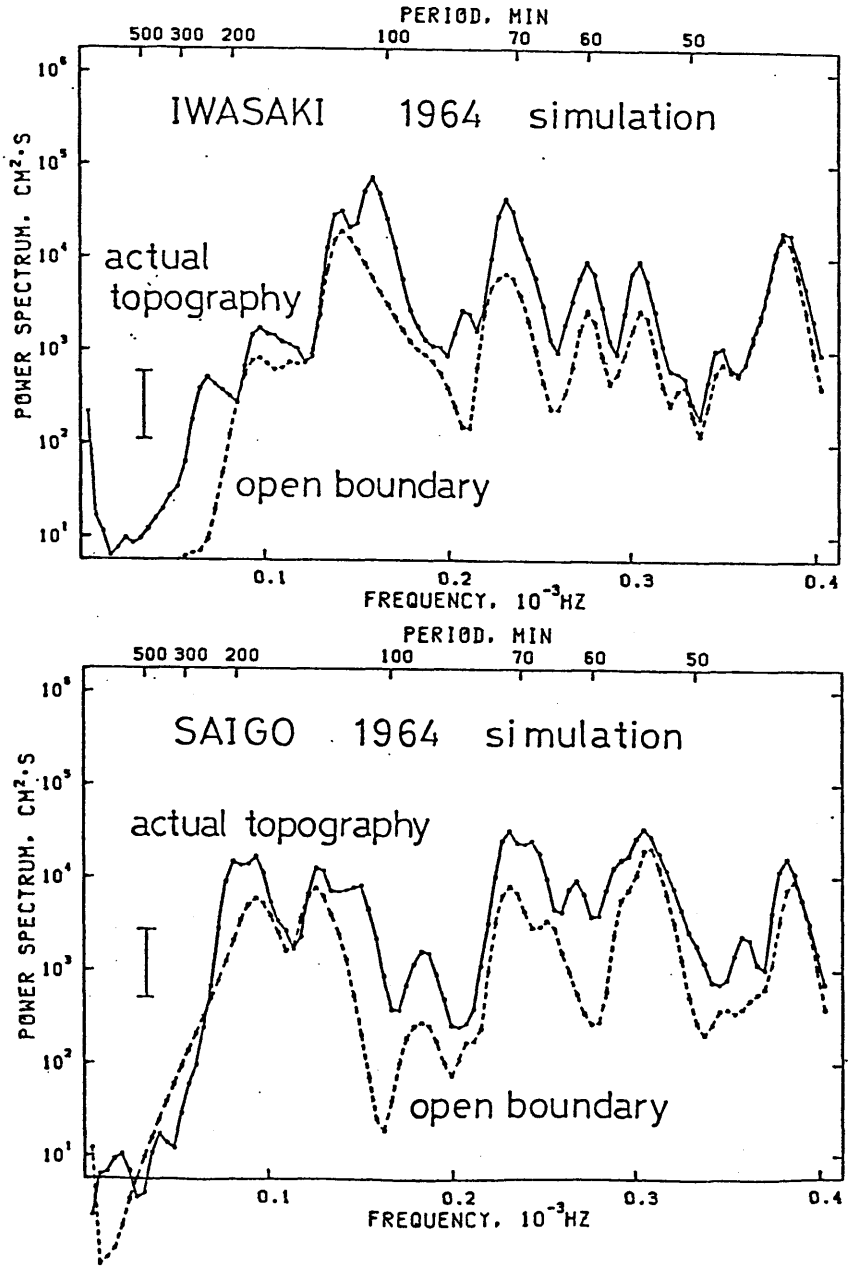

Figure 7. The spectra for the two sets of numerical computation for the 1964 Niigata earthquake tsunami. The solid lines show the computation in the marginal region with the artificial radiation boundary. The dashed lines are the results for the whole Japan Sea taken from Fig.5.

Fig.8

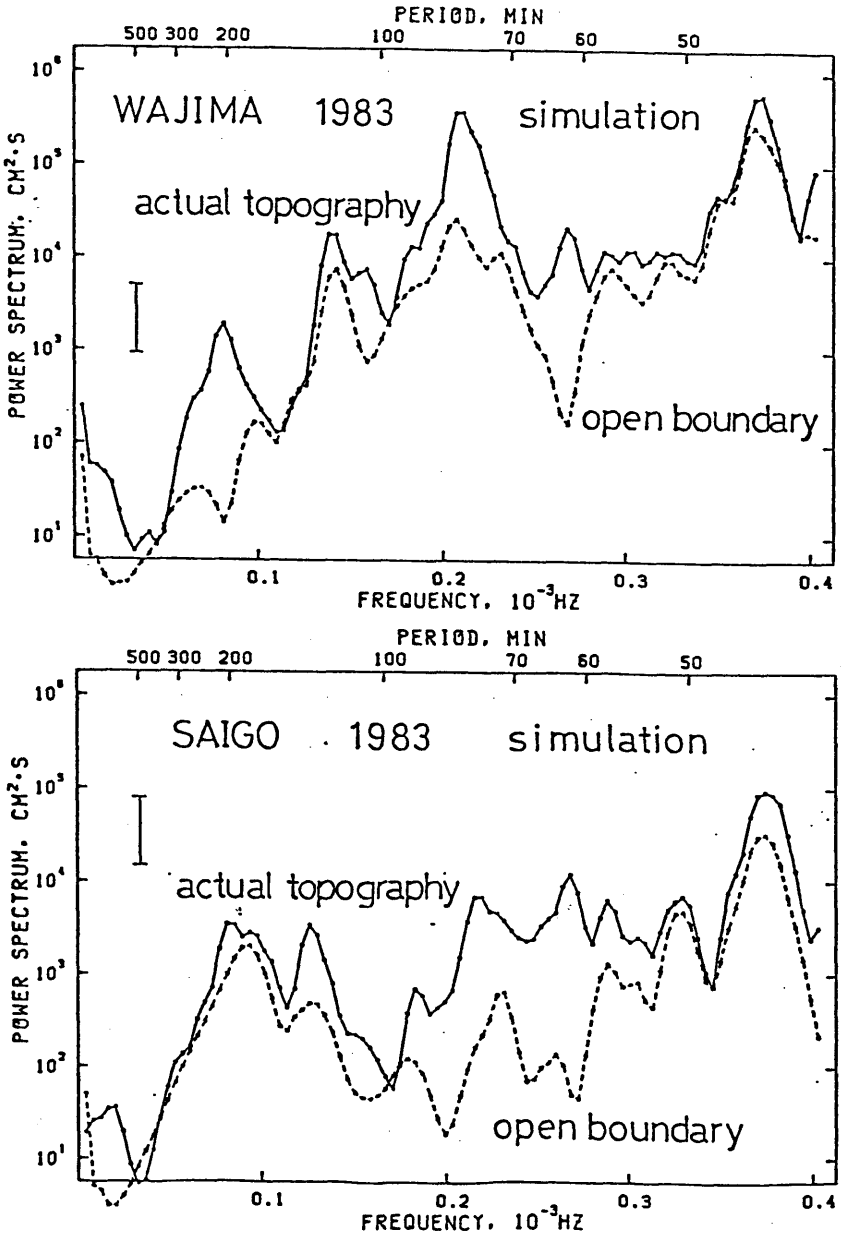

Figure 8. The spectra for the two sets of numerical computation for the 1983 Japan Sea earthquake tsunami. The solid lines show the computation in the marginal region with the artificial radiation boundary. The dashed lines are the results for the whole Japan Sea taken from Fig.6.

Chapter 2

Computation of Tsunami Waveforms by a Superposition of Normal Modes

Abstract

Computation of tsunami waveforms for actual topography is usually made by a time-stepping finite-difference method which needs a long computation time and must be repeated for different initial conditions. We propose here an alternative computation by a superposition of normal modes. Although the eigenvalue problem to obtain the normal mode solutions needs more memories, once we get the solution, the waveforms can be computed merely summing up the normal modes with weights determined by the initial condition. We present the waveforms for a simple water basin computed by the both methods. The results show that the new method is useful for a completely or almost closed basin including the tsunami source.

Tsunamis, as far as approximated as linear long-waves, propagate at a speed depending on the ocean depth. The bathymetry greatly affects the propagation (SATAKE, 1987). Tsunami waveforms, therefore, have been computed by a finite-difference method on actual topography (AIDA, 1978; SATAKE and SHIMAZAKI, 1987). Although it is not a great task to make such a computation if we use a supercomputer, it must be repeated as the initial condition at the source is changed. We propose here an alternative method in which the tsunami waveforms are represented as a superposition of normal modes. This method is valid for a completely or partially closed basin which includes the source area. The great advantage of this method is that once we get a set of normal mode solutions, the tsunami waveforms can be computed merely by summing up the eigenfunctions with the weight determined by the initial condition.

The basic equations describing linear long-waves are the equation of motion

$$\frac{\partial \mathbf{u}}{\partial t} = -g \nabla h \tag{1}$$

and the continuity equation

$$\frac{\partial h}{\partial t} + \nabla h \cdot \mathbf{u} = 0 \tag{2}$$

where $\mathbf{u}$ is the velocity of the wave, g the gravitational acceleration, and h is the water height above the surface (*e. g.* STOKER, 1957). A flow rate can be obtained by integrating the velocity in z (vertical) direction from the water bottom to the surface,

$$\mathbf{Q} = \int_0^d \mathbf{u}\, dz \tag{3}$$

where d is the water depth. By using $\mathbf{Q}$, *(1)* and *(2)* are expressed as

$$\frac{\partial \mathbf{Q}}{\partial t} = -gd \nabla h \tag{4}$$

and

$$\frac{\partial h}{\partial t} = -\nabla \cdot \mathbf{Q}. \tag{5}$$

These are the basic equations for the time-stepping finite-difference computation (AIDA, 1978). Differenciating *(2)* by time and substituting *(1)* into it, we obtain the wave equation of tsunami,

$$\frac{\partial^2 h}{\partial t^2} = g\nabla\cdot(d\nabla h). \tag{6}$$

When the depth is constant, we have the tsunami wave velocity $c = \sqrt{gd}$. If we assume that the motion is temporally periodic, the water height can be written as

$$h(\mathbf{x},t) = \Phi(\mathbf{x})\, e^{i\omega t} \tag{7}$$

in which $\Phi(\mathbf{x})$ describes the spatial distribution of water heights and ω is the angular frequency. Substituing *(7)* into *(6)*, we have

$$\nabla\cdot(d\nabla\Phi) = \lambda\Phi \qquad \text{where} \qquad \lambda = -\omega^2/g. \tag{8}$$

This is an eigenequation with the eigenvalue λ characterized by the eigenfrequency ω. Equation *(8)* can be solved by numerically differentiating the bathymetry. LOOMIS (1975) showed that the left hand side of *(8)* becomes symmetric if a staggered grid system is used.

Since the eigenvectors form a complete orthogonal set, any water distribution can be expressed as a linear combination of the eigenvectors. Therefore the tsunami waveforms can be written as a superposition of the normal modes,

$$h(\mathbf{x},t) = \sum_m C_m \Phi_m(\mathbf{x})\, \cos\omega_m t \tag{9}$$

where C_m is the weight for each mode. We have assumed that the velocity is initially zero. If the initial water height distribution at $t = 0$,

$$h_0(\mathbf{x}) = \sum_m C_m \Phi_m(\mathbf{x}), \tag{10}$$

is known, the coefficient for each mode can be obtained as follows. If we multiply Φ_k to the both sides of *(10)* and integrate it over the basin and by using the orthogonality of the eigenfucntion Φ, we have

$$C_k = \int h_0(\mathbf{x})\ \Phi_k(\mathbf{x})d\mathbf{x}. \tag{11}$$

Thus we have the weight of each mode for the superposition. Since $h_0(\mathbf{x})$ has non-zero values in the source area only, the integration in *(11)* can be evaluated only near the source region. The above procedure is analogous to the excitation of the normal modes of the elastic Earth by an earthquake source (SAITO, 1967; GILBERT 1970). In the case of the elastic Earth, however, an external force is applied, which is equivalent to the initial value probelm with a known initial velocity. For tsunami problem, an initial displacement is given instead.

As a simple example, we computed the waveforms by the two methods, the time-stepping finite-difference method and the superposition of normal mode solutions. A rectangular basin with a uniform depth with two different boundaries is considered (FIG.1). Model A is a completely closed basin and one side is open to outer sea in Model B. At the closed boundary, the total reflection of the waves are assumed in the both models; the flow rate **Q** is zero in the finite-difference method and the spatial derivative of the eigenfunction, $\nabla\Phi$, is zero in the modal approach. Different conditions are assumed for the case of the open boundary. In the finite-difference method, the radiation condition in which the waves go out of the region at a velocity on the boundary is adopted. In the modal approach, the open boundary is considered as a node where the eigenfunction is zero, or $\Phi = 0$.

The computed waveforms by the two methods are shown in FIG.2. The waveforms

agree well for Model A. For Model B, some disagreements are found in the later part of the waves because of the different boundary condition.

From a viewpoint of computational efficiency, both methods have advantages and disadvantages. Finite-difference method requires relatively moderate-sized memories of about ten times of the number of grids for the depth, water height and flow rate. The computation time is long, although which can be shorten by the use of supercomputer, and the computation must be repeated as the initial condition is changed. On the other hand, the modal approach requires large amount of memories, an order of a square of the number of grids to solve the eigenvalue problem. However, once the eigenvalue problem is solved and the eigenfunctions with eigenvalues, or modal solutions, are stored, the remaining computation is merely summing up the modal solutions with the weights determined by the initial condition. Since the integral in *(11)* is computed only near the source region, it is not a great task. If the source region and the output points of the waves are specified, the eigenfunction at the other points can be deleted, so that the memory can be saved. SATO and HARUMI (1972) proposed to solve the eigenvalue problem by the finite-difference method, which is exactly the opposite way to this paper. Because of a recent development of computer technology, the situation for numerical computation has drastically changed.

Normal mode solution with the radiation condition can be obtained by introducing the adjoint system (LANCZOS, 1961; GELLER *et al.*, 1985). This method requires more numerical computation and more memories. Our example showed that for a partially open region such as a bay, the nodal condition at the boundary is practically sufficient especially for the initial part of the waveforms.

References

AIDA, I., Reliability of a tsunami source model derived from fault parameters, *J. Phys. Earth,* **26**, 57-73, 1978.

GELLER, R. J., R. M. NOACK, and A. L. FETTER, Normal mode solutions for absorbing boundary conditions, *Geophys. Res. Lett.* **12**, 145-148, 1985.

GILBERT, F., Excitation of the normal modes of the Earth by earthquake sources, *Geophys. J. R. astr. Soc,* **22**, 223-226, 1970.

LANCZOS, C., *Linear Differential Operators,* D. Van Nostrand Company Limited, London, 1961.

LOOMIS, H. G., Normal modes of oscillation of Honolulu harbor, Hawaii, *Hawaii. Inst. Geophys. Rep.,* **HIG-75-20**, 20 pp., 1975.

SAITO, M., Excitation of free oscillations and surface waves by a point source in a vertically heterogeneous Earth, *J. Geophys. Res.,* **72**, 3689-3699, 1967.

SATAKE, K., Effects of bathymetry on tsunami propagation: application of ray tracing to tsunamis, *Pure Appl. Geophys. (in press),* 1987 *(Appendix of this thesis).*

SATAKE, K. and K. SHIMAZAKI, Free oscillation of the Japan Sea excited by earthquakes 1: observation and wave-theoretical approach, *Geophys. J. R. astr. Soc. (submitted),* 1987 *(Chapter 2.1 of this thesis).*

SATO, Y. and K. HARUMI, A method for determining the eigenfrequency of a mechanical system by simulation, *J. Comp. Phys.,* **9**, 194-206, 1972.

STOKER, J. J., *Water Waves,* Interscience Publishers, New York, 1957.

Fig.1

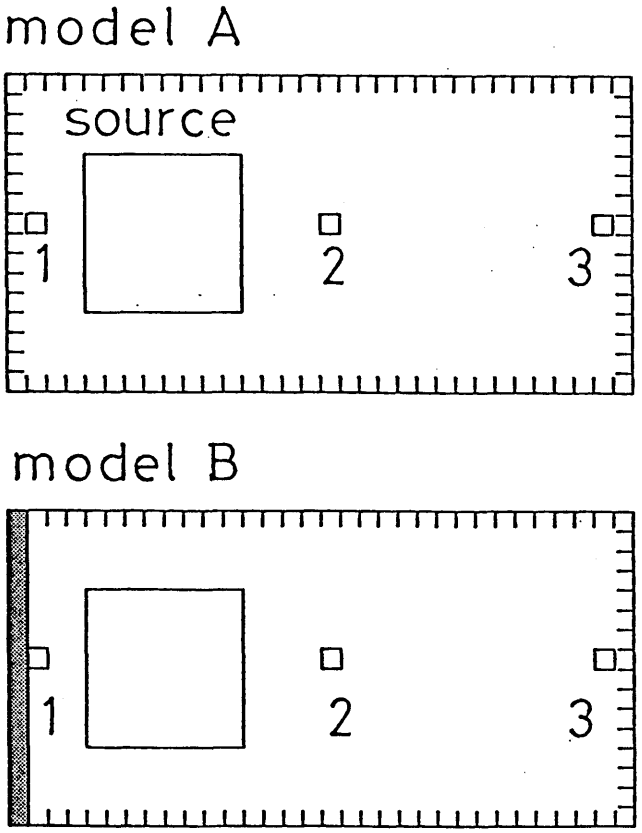

Figure 1. Grids used for the computations for two models. Sources where a uniform rise of the water is assumed and the numbered output stations for the waveforms are shown. Hatches in Model B is the boundary to the outer sea.

Fig.2

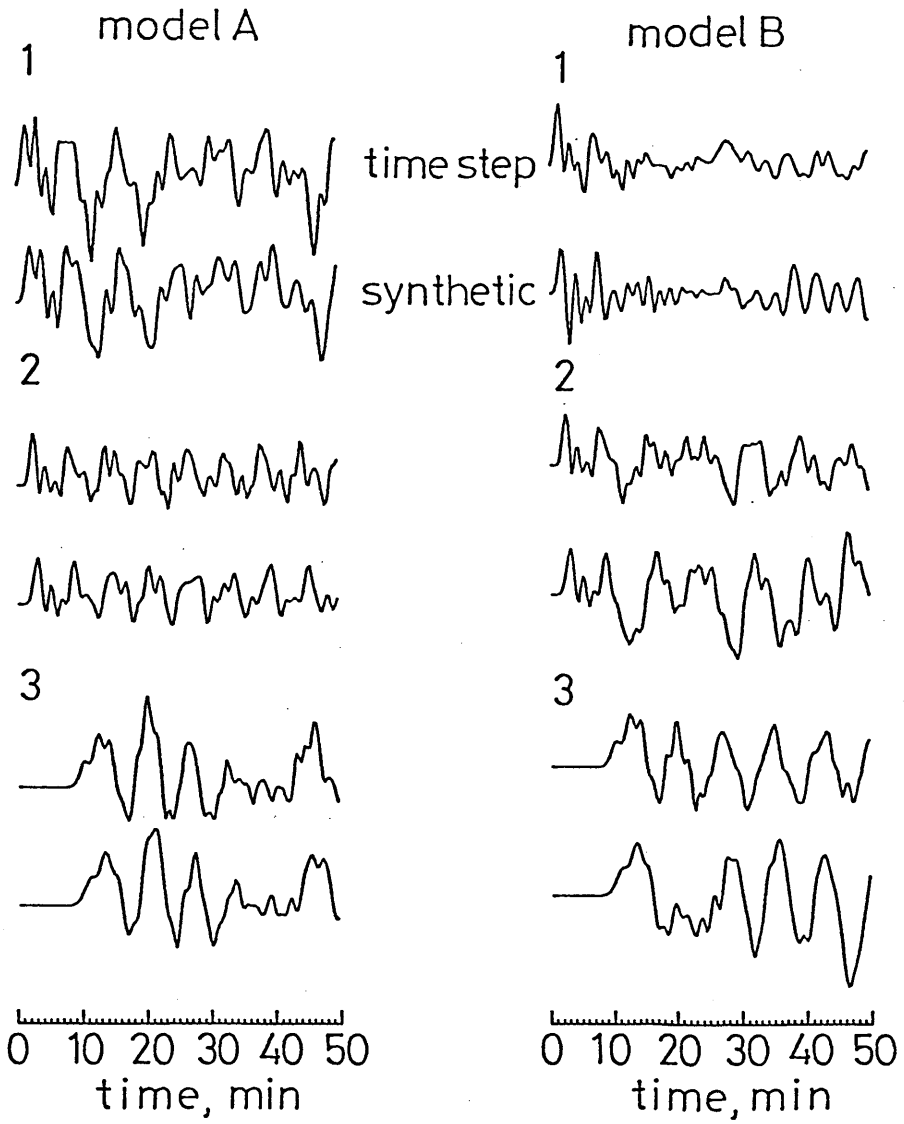

Figure 2. Waveforms computed by the time-stepping finite-difference method and the synthetic waves by a superposition of normal modes for the two models. The numbers correspond to the output points in Fig.1.

Chapter 3

Modal Approach and Synthetic Tsunamis

Summary

The free oscillations of the Japan Sea excited by the 1964 Niigata and the 1983 Japan Sea earthquakes are examined by taking modal approach. Normal mode solutions with periods longer than 50 min are obtained numerically for the actual bathymetry provided by the meshes of 20 km in size. The obtained eigen vectors, or water height distributions, show that the modes with longest eigen periods are determined by the size and depth of the whole Japan Sea. Many modes with shorter eigen periods are regionally trapped ones in a shallow part such as continental shelf where the amplitude of eigen vectors is large. The Niigata earthquake excites mainly the regional modes while the Japan Sea event equally excites both kinds of the modes. The different excitation is attributed to the different water depth at the source; the Niigata earthquake occurred on a continental shelf of about 100 m deep whereas the depth at the source area of the Japan Sea event is about 2500 m. The synthetic tsunami is computed by a superposition of the normal modes. The spectra agree well with the observed ones in the period range of 50 to 210 min.

1 Introduction

Tsunamis accompanied by large earthquakes in the almost closed Japan Sea are observed on tide gauge records for more than two days because of the multiple reflections at the coasts. They seem to have excited the free oscillation of the Japan Sea. In a previous paper (Satake & Shimazaki 1987a; hereafter we call it Paper I), we reproduced the free oscillation by finite-difference computations on the actual bathymetry given by the grid size of 5 km. The observed and simulated spectra agree well in the period range between 42 min and 3.5 hrs. We further tried to separate the regional oscillations on shallow parts such as a continental shelf and the whole oscillations characterized by the size and geometry of the Japan Sea by making a computation for the south-eastern half of the Japan Sea with an artificial radiation boundary.

The tsunami waveforms in a completely or almost closed basin can be represented by a superposition of normal modes (Satake & Shimazaki 1987b). The normal mode solutions can be computed numerically for the actual bathymetry. In this paper, the normal mode solutions of the Japan Sea are computed to examine the characteristics of the free oscillation. Further, the synthetic tsunamis from two large earthquakes occurred in the Japan Sea are presented by a superposition of the normal modes and compared with the observations.

Synthesizing tsunami waveforms from the normal mode solutions is analogous to the long-period seismology. Long-period seismic surface waves are represented by a superposition of normal mode solutions (*e.g.* Kanamori 1970). In case of the elastic Earth, the normal mode solutions have been obtained for spherically symmetric Earth models (*e.g.* Gilbert & Dziewonski 1975) but recent studies aimed to obtain the solution for laterally heterogeneous Earth models (Morris *et al.* 1987).

2 Tsunamis in the Japan Sea

The Japan Sea is an almost closed basin with an area of about $10^6 km^2$ and the mean depth of 1500 m. Four straits, Tatar, Soya, Tsugaru, and Tsushima (or Korea) straits, connect the Japan Sea with the outer oceans (Fig.1). Large earthquakes regularly occur along the eastern margin of the Japan Sea (Satake 1986). Among them, recent two large earthquakes accompanied by tsunamis, the 1964 Niigata (Satake & Abe 1983) and the 1983 Japan Sea (Satake 1985) earthquakes, are examined in this study. The tide gauge records at Fukaura, Iwasaki and Saigo (locations are given in Fig.4) are used. After the 1964 tsunami, the station Iwasaki was moved 5 km northward to Fukaura. Thus these two stations are considered to be effectively the same.

The tide gauge records at the two stations for the 1983 Japan Sea earthquake tsunami are shown in Fig.2. The upper trace in each pair shows the original record for 48 hrs after the event digitized from the tide gauge record with a 1 min sampling interval. The lower trace in each station is the band-pass filtered record for the pass-band between 50 min and 5 hrs to remove the tide and short-period oscillation due to a local topography such as small bay or harbor. All the records show decaying oscillations which continue more than two days. The short-period limit of the pass-band, 50 min, corresponds to the fundamental period of the oscillation of a bay with a size of 23.5 km if the depth is 100 m (*e.g.* Dietrich *et al.* 1980). We are not interested in the local effect smaller than this size and will use the mesh size of 20 km.

We first determine the attenuation coefficient from the tide gauge records. The energy decay of the tsunami wave is expressed as

$$E(t)=E_0\, e^{-2\gamma t} \tag{1}$$

where $E(t)$ is the variance or a dynamic component of the energy, E_0 the tsunami energy index, and γ the attenuation coefficient (Van Dorn 1984). The variances are computed from the filtered records for each 5 hrs after the earthquake and are plotted in Fig.3. In spite of

fairly large scattering at Iwasaki and Fukaura, the variance generally decreases with time. The attenuation coefficient γ is determined from a least-squares fitting of a line shown in the figure. Abnormal values in the first and last 5 hrs segments are not used. The attenuation coefficient γ is obtained as 0.022 ± 0.004 (1/hr) by averaging the four slopes in Fig.3. The decay time of the amplitude to become $1/e$ of the original water height, or $1/\gamma$, is 45 hrs. For the 1964 Niigata earthquake tsunami, Hatori (1965) also estimated the attenuation coefficient as 0.043 from a crest-height level change. Van Dorn (1987) obtained 0.058 for the 1983 Japan Sea tsunami by the same method of ours but using the original waveforms. The smaller attenuation coefficient obtained in this study is due to the filtering, indicating that the attenuation is smaller for the lower frequency band.

3 Modal solution of the free oscillation

The normal mode solution of an irregular basin with a variable depth can be obtained numerically (Loomis 1975, Satake & Shimazaki 1987b). The wave equation for tsunami is written as

$$\frac{\partial^2 h}{\partial t^2} = g \nabla \cdot (d \nabla h) \tag{2}$$

where h is the water height, g the gravitational acceleration, and d is the water depth. The Coriolis term is neglected since a half pendulum day at the latitude 40° is about 19 hrs (*e.g.* Dietrich *et al.* 1980).

Since we are interested in the free oscillation, we assume that h changes periodically with time, that is

$$h(\mathbf{x},t) = \Phi(\mathbf{x})\, e^{i\omega t} \tag{3}$$

where $\Phi(\mathbf{x})$ represents a spatial distribution of the water height and ω is the angular

frequency. By substituting *(3)* into *(2)*, we have

$$\nabla\cdot(d\,\nabla\Phi) = \lambda\,\Phi \quad \text{where} \quad \lambda = -\omega^2/g \ . \tag{4}$$

This is an eigen equation with the eigen value λ and the eigen vector Φ. We can obtain the eigen period $\omega/2\pi$ of the normal modes from the eigen value λ. The left hand side of *(4)* can be obtained by numerically differenciating the actual bathymetry. Loomis (1975) showed that if a proper grid scheme is employed, the left hand side of *(4)* becomes a symmetric matrix. The eigen value problem of a real symmetric matrix can be solved easily with a high accuracy.

Figure 4 shows the grid system. The grid size is 20 km and the Japan Sea is divided into 2538 meshes. Since we have to solve an eigen value problem which requires an order of a square of the number of meshes, the memory size of computer limits the mesh size. We use the staggered grid system so that the left hand side of *(4)* is symmetric. At a land-sea boundary, the depth d is zero. At three straits except Tatar, the nodes are prescribed, that is, Φ is assumed to be zero. Such meshes are shown as hatched in the figure. Since the Tatar strait is very shallow, less than 10 m deep, it is considered to be the land boundary.

The eigen value problem is solved by a supercomputer by using the Housholder and bysection methods. The dimension of matrix is 2521, since 17 meshes out of 2538 are nodal points, and the smallest 100 eigen values and eigen vectors are obtained. The CPU time was 1 min 20 sec by a supercomputer HITAC S-810/20.

The obtained eigen frequencies are plotted in Fig.5. Actually this figure shows the coefficients for each mode which are computed from the initial condition to be explained in the next section. The eigen periods is 874.1 min (14.6 hrs) for the longest mode, 712.1 min (11.9 hrs) for the second longest mode, 358.9 min (6.0 hrs) for the third and 279.7 min (4.7 hrs) for the fourth longest mode. The first few periods are in the tidal range so it is difficult to distinguish them from the tides. The Coriolis effect which we have neglected

may be dominant for those modes. The 100-th eigen period is 50.5 min, about a shortest limit of the period range of our interest. Kawakami (1927) made a very rough estimate of the longest eigen period. Assuming that the Japan Sea is a bay with a uniform depth, he obtained 13.7 hrs for the longest period, which roughly agrees with our computation of the longest period, 14.6 hrs.

The spatial distributions of the eigen vectors for several modes are shown in Fig.6. In the first mode, the node is that prescribed at the Tsushima strait. In the second mode, another node exists at the northern part of the Japan Sea. The third mode has two nodes at the northern-most and the central part besides the prescribed one. In the 6-th to 8-th modes, several nodes are seen in the Japan Sea. The eigen vectors are determined by the size and geometry of the whole Japan Sea for these modes with long eigen periods. For those modes with eigen periods around 80 min (Fig.6 c), the pattern of the eigen vector is very complicated. The regionalized loops at marginal shallow parts are seen in these modes, indicating that these modes are characterized by the regional shallow parts. These modes are easily excited by earthquakes on their loops as is discussed later.

4 Synthetic tsunami

Since the eigen vectors form a complete orthogonal set, any water distribution can be expressed as a linear combination of the eigen vectors. Thus the tsunami can be written as a superposition of normal modes,

$$h(\mathrm{x},t) = \sum_k C_k \, \Phi_k(\mathrm{x}) \, e^{-\gamma t} \cos \omega_k t \tag{5}$$

where the subscript k denotes the eigen frequency or eigen vectors of the k-th mode. The coefficient or weight C_k is determined from the initial water height distribution h_0 by using the orthogonality of the eigen vectors Φ (Satake & Shimazaki 1987b),

$$C_k = \int h_0(\mathrm{x})\ \Phi_k(\mathrm{x})\mathrm{dx}. \qquad (6)$$

Since h_0 is zero outside the tsunami source area, the integration can be performed over the source area only. Actually the number of meshes for the source area is 28 for the 1983 Japan Sea earthquake and 8 for the 1964 Niigata earthquake.

The initial water height distribution h_0 is assumed to be the same as the vertical crustal movement computed from the fault parameters. The fault models of Satake & Abe (1984) for the 1964 Niigata earthquake and that of Satake (1985) for the 1983 Japan Sea earthquake are used. For the attenuation coefficient γ, the value obtained in the preceding section is used.

The coefficient C_k's thus calculated are plotted in Fig.5 for the 100 modes. Two features are seen in this figure. First, the weights for the modes excited by the 1964 Niigata earthquake are larger than those excited by the 1983 Japan Sea earthquake. The potential energy of the crustal deformation is 1.6×10^{20} erg for the Niigata earthquake and 4.2×10^{20} erg for the Japan Sea earthquake (Satake 1985). Although the potential energy of the Niigata earthquake is smaller, less than half of the Japan Sea event, the excitation of the free oscillation is larger. Second feature is that the excitation of the modes with eigen periods between 100 and 60 min is larger than the other modes for the Niigata earthquake whereas the Japan Sea event equally excites most of the modes at all the frequency range. These features are a direct consequence of a spatial relation between the eigen vectors and the initial water heights (see *(6)*) and will be discussed in the next section.

The synthetic tsunami is computed at a 1 min interval for 48 hrs by *(5)* and the power spectra, more precisely power spectral density, are plotted in Figs.7 and 8 for the two earthquakes. The power spectra obtained in Paper I for the observed tsunami, in the same way as the synthetic tsunami, are also plotted in the figure. The range of the 90 % confidence limit of the power spectra estimated by smoothing (Bendat & Piersol 1971) is

shown by a bar. For both earthquakes, the power level and the overall pattern of spectra of the observed and synthetic waveforms agree well in the period range of 50 to 210 min. The discrepancy at the low frequency is due to the tidal and Coriolis effects. The agreement between the synthetic and observed spectra is worse for the 1964 Niigata event because the shallow source area is represented by the meshes of 20 km in size.

5 Discussion & Conclusion

As already pointed out, the excitation of the modes with the eigen periods between 100 and 60 min is larger for the Niigata earthquake. The eigen vector of these modes (Fig.6) have large amplitudes on regional continental shelves where the source of the Niigata event lies. Shallow water depth, about 100 m deep, of the source area of the Niigata event contributes the excitation of these regional modes. The Japan Sea event, on the other hand, equally excite most of the modes (Fig.5), since the water depth of the source area is deeper, about 2500 m.

The above difference is consistent with the conclusion of Paper I. Two kinds of finite-difference computations for the whole Japan Sea and for the south-eastern half of the Japan Sea with an artificial radiation boundary are compared in Paper I. The spectra from both computations are similar for the Niigata event, indicating that the spectra are mainly determined by the regional modes trapped in the half of the Japan Sea. For the 1983 Japan Sea event, there is a significant discrepancy between the two spectra, indicating that the modes of the whole Japan Sea are essential component of the spectra.

For the boundary condition for the computation of the normal mode solutions, we assumed that three straits are nodes where the eigen vector or the water height is zero. Strictly speaking, we should assume a radiation boundary condition at these straits as was used in Paper I. However, this condition cannot be easily incorporated in the eigen value

problem (Geller *et al.* 1985). Satake & Shimazaki (1987b) showed that the synthetic waveform calculated by assuming nodes for an open boundary is very similar to the exact waveform for an almost closed basin. The boundary condition is not sensitive when the open boundary is very small as compared with the whole region such as a case of the Japan Sea, except for the lowest modes. Actually, we also solved the same eigen value problem for several different boundary conditions for the four straits. The modal solutions for these boundary conditions have essentially similar features obtained in this study; the eigen vector is determined by the geometry of the whole Japan Sea for the lower modes whereas for the higher modes the amplitude is large at the regional shallow parts. The eigen periods of the several lowest modes differ significantly depending on the boundary conditions.

In conclusion, the modal solution for the Japan Sea shows that the eigen vector for the lower modes is determined by the whole Japan Sea and that the eigen vector for the higher modes is affected by regional bathymetry and is large at the regional shallow parts. The excitation of these modes depends on the location of the earthquake. The 1964 Niigata event mainly excites regional modes since the source area is in a shallow sea. On the other hand, the 1983 Japan Sea earthquake equally excites most of the modes because the water depth of the source area is deep. Synthetic spectra computed by a superposition of the normal modes can reproduce major features of the observed spectra.

Acknowledgements

This chapter is a manuscript submitted to *Geophysical Journal of the Royal astronomical Society* with Kunihiko Shimazaki. Discussions with Hiroo Kanamori, Harold Loomis, Toshiyuki Hibiya and Yoshinobu Tsuji are helpful. The numerical computations were made at Computer Centre, University of Tokyo using HITAC S-810/20 and M680 computer system.

References

Bendat, J.S. & Piersol, A.G., 1971. *Random Data: Analysis and measurement procedures.*, John Wiley & Sons.

Dietrich, G., Kalle, K., Krauss, W., & Siedler, G., 1980. *General oceanography* (translation from German), John Wiley & Sons.

Geller, R. J., Noack, R. M. & Fetter, A. L., 1985. Normal mode solutions for absorbing boundary conditions, *Geophys. Res. Lett.* **12**, 145-148.

Gilbert, F., & Dziewonski, A. M., 1975. An application of normal mode theory to the retrieval of structure parameters and source mechanism from seismic spectra. *Phil. Trans. R. Soc. Lond.* **A 278**, 187-269.

Hatori, T., 1965. On the tsunami which accompanied the Niigata earthquake of June 16, 1964. - Source deformation, propagation, and tsunami run-up. *Bull. Earthq. Res. Inst. Tokyo,* **43**, 129-148.

Kanamori, H., 1970. Synthesis of long-period surface waves and its application to earthquake source studies -Kurile Islands earthquake of October 13, 1963. *J. Geophys. Res.,* **75**, 5011-5027.

Kawakami, N., 1927. On the secondary undulations of tides in the Japan Sea. *Umi to Sora,* **7**, 91-94 (in Japanese).

Loomis, H. G., 1975. Normal modes of oscillation of Honolulu harbor, Hawaii. *Hawaii Inst. Geophys. Rep.* **HIG-75-20**, 20 pp.

Morris, S. P., Geller, R. J., Kawakatsu, H., & Tsuboi, S., 1987. Variational free oscillation computations for three laterally heterogeneous earth models. *Phys. Earth Planet. Inter.* (in press).

Satake, K., 1985. The mechanism of the 1983 Japan Sea earthquake as inferred from long-period surface waves and tsunamis. *Phys. Earth Planet. Inter.*, **37**, 249-260.

Satake, K., 1986. Re-examination of the 1940 Shakotan-oki earthquake and the fault

parameters of the earthquakes along the eastern margin of the Japan Sea. *Phys. Earth Planet. Inter.*, **43**, 137-147.

Satake, K. & Abe, K., 1983. A fault model for the Niigata, Japan, earthquake of June 16, 1964. *J. Phys. Earth,* **31**, 217-223.

Satake, K. & Shimazaki, K., 1987a. Free oscillation of the Japan Sea excited by large earthquakes: observation and wave- theoretical approach. submitted to *Geophys. J. R. astr. Soc. (Chapter 2.1 of this thesis)*

Satake, K. & Shimazaki, K., 1987b. Computation of tsunami waveforms by a superposition of normal modes. to be submitted to *J. Phys. Earth. (Chapter 2.2 of this thesis)*

Van Dorn, W. G., 1984. Some tsunami characteristics deducible from tide records. *J. Phys. Ocean.*, **14**, 353-363.

Van Dorn, W. G., 1987. Tide gage response to tsunamis II: (Other oceans and smaller seas). *J. Phys. Ocean.* submitted.

Fig.1

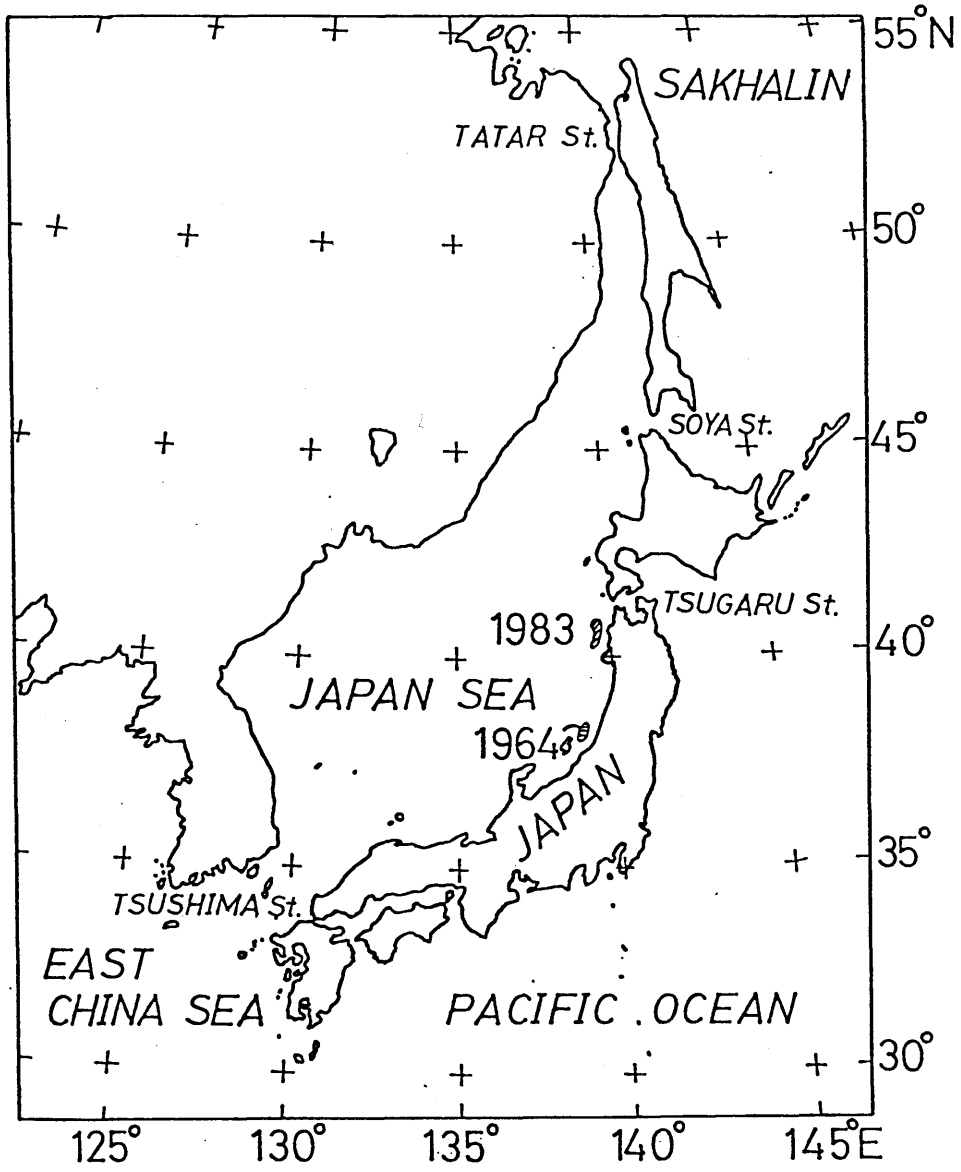

Figure 1. Map showing the location of the Japan Sea. The source areas of the two earthquakes used in this study are also shown.

Fig.2

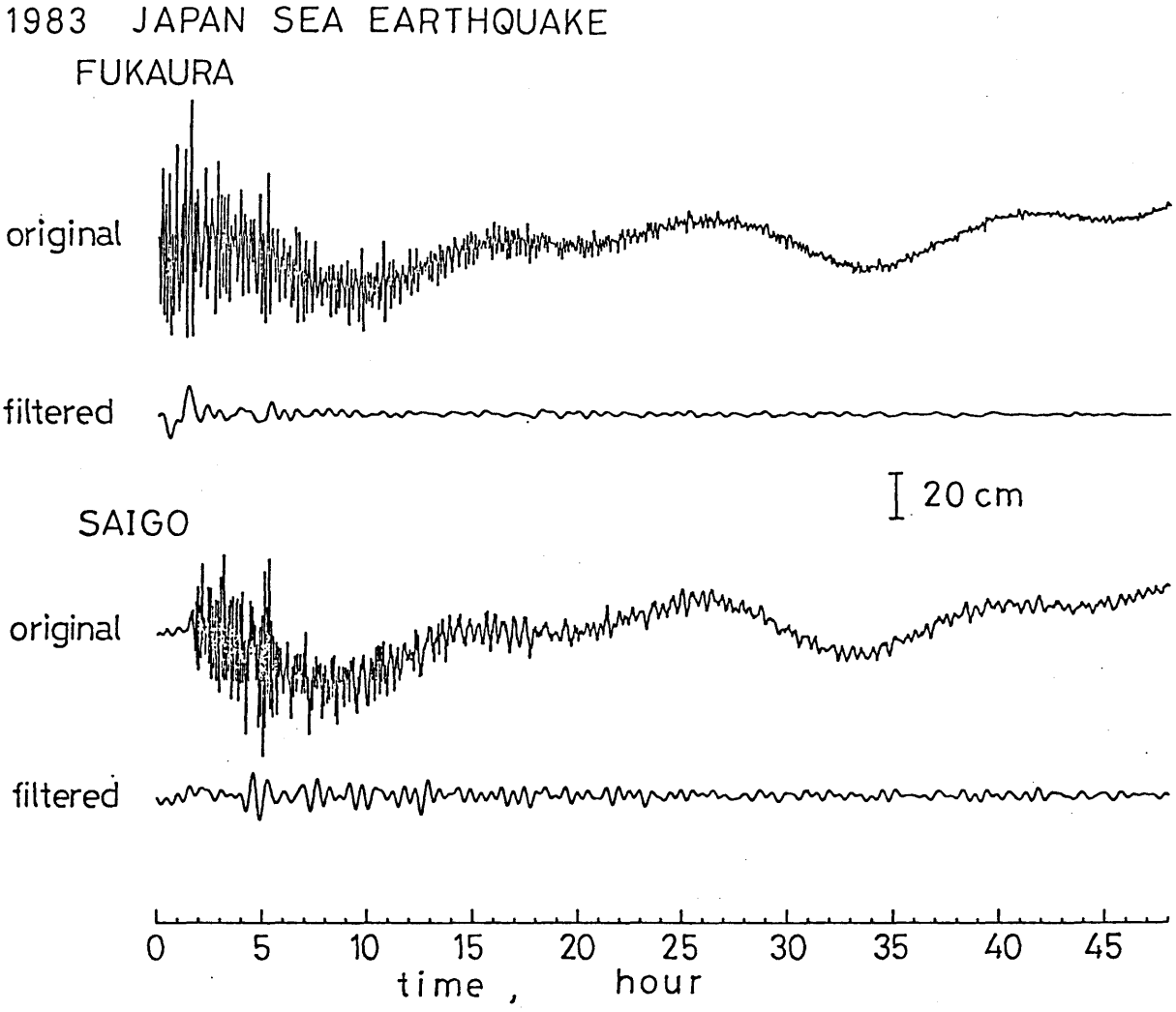

Figure 2. Digitized tide gauge records at Fukaura (*top*) and Saigo (*bottom*) from the 1983 Japan Sea earthquake. The upper trace in each station is the original record while the lower one is band-passed with a pass-band between 50 and 300 min.

Fig.3

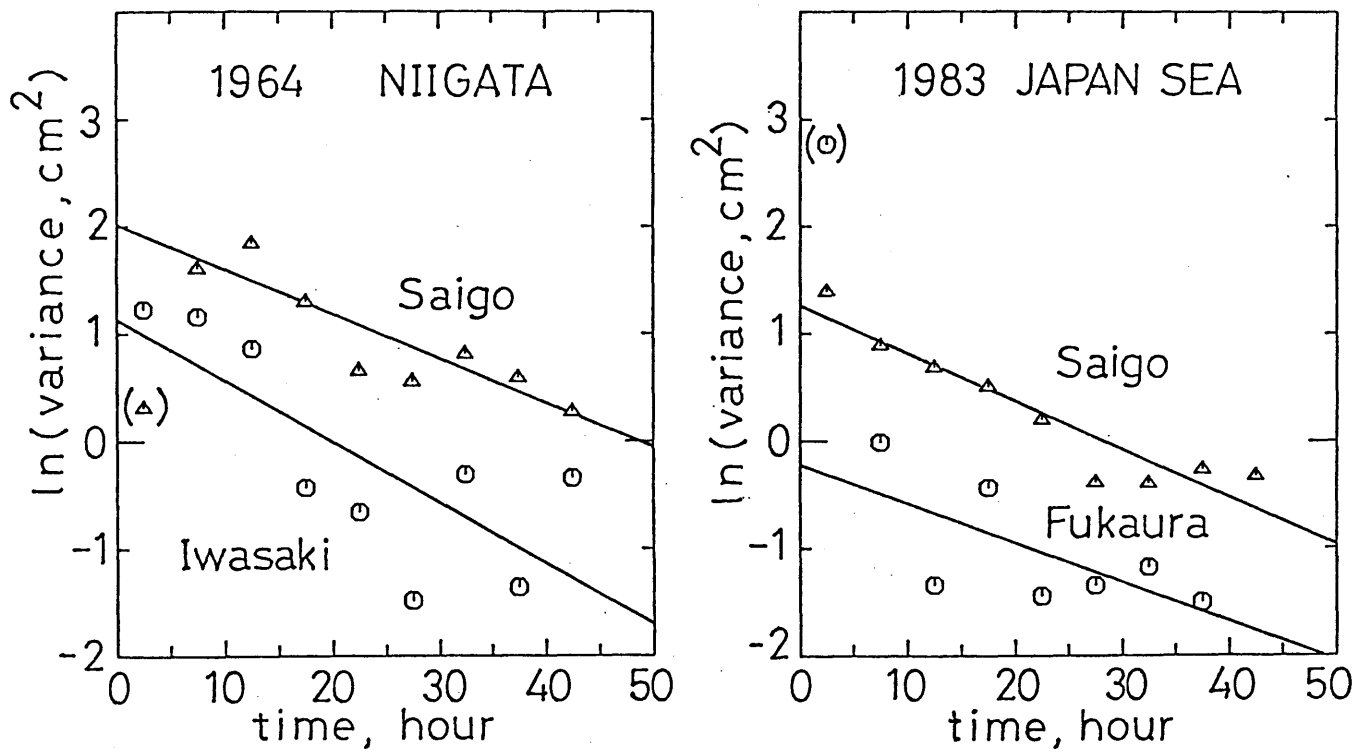

Figure 3. Energy or variance of the filtered tsunami waveforms for each 5 hrs interval for the two tsunamis at the two stations. Solid lines indicate least-squares regressions for the estimation of the attenuation coefficients. Abnormal values in the parenthesis or absent in the graph are not used for the regression.

Fig.4

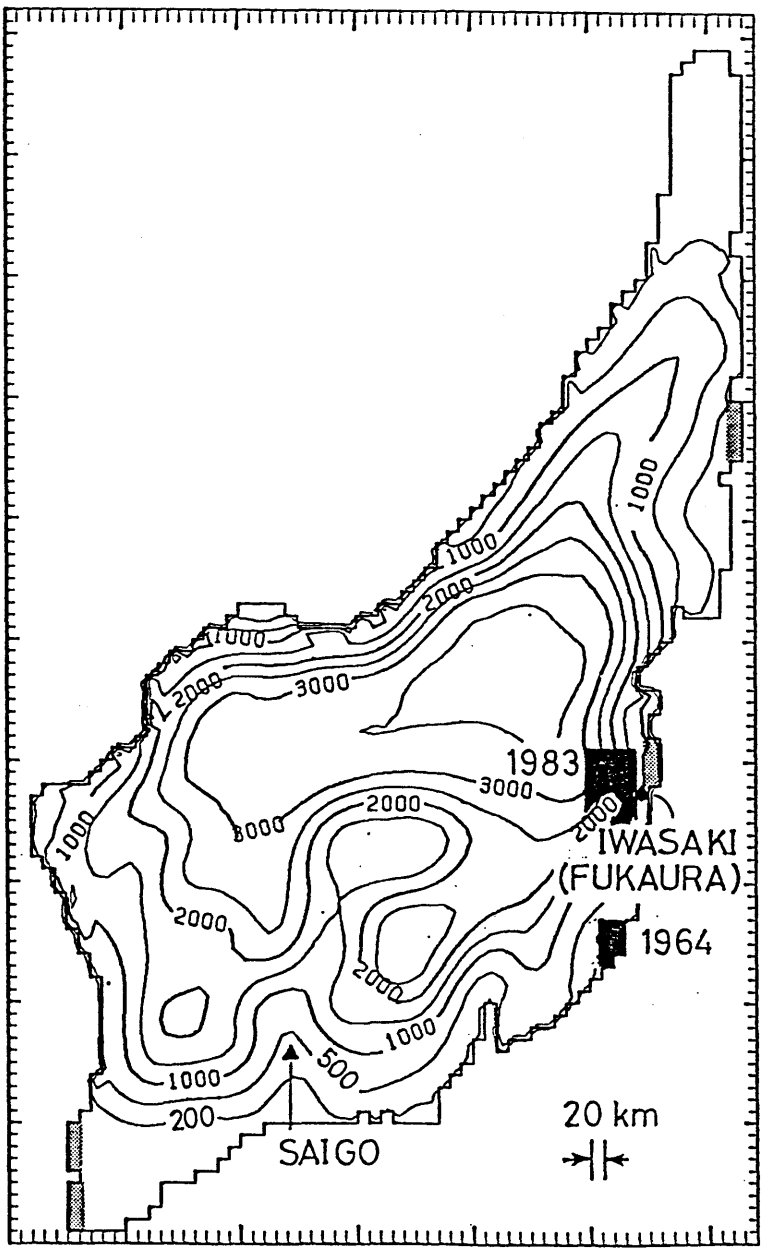

Figure 4. The grids and their depths used for the computation of normal modes. Two tide gauge stations are shown by solid triangles. Hatched meshes show the prescribed nodes and the solid meshes are the source area of the 1964 Niigata and the 1983 Japan Sea earthquakes.

Fig.5(a)

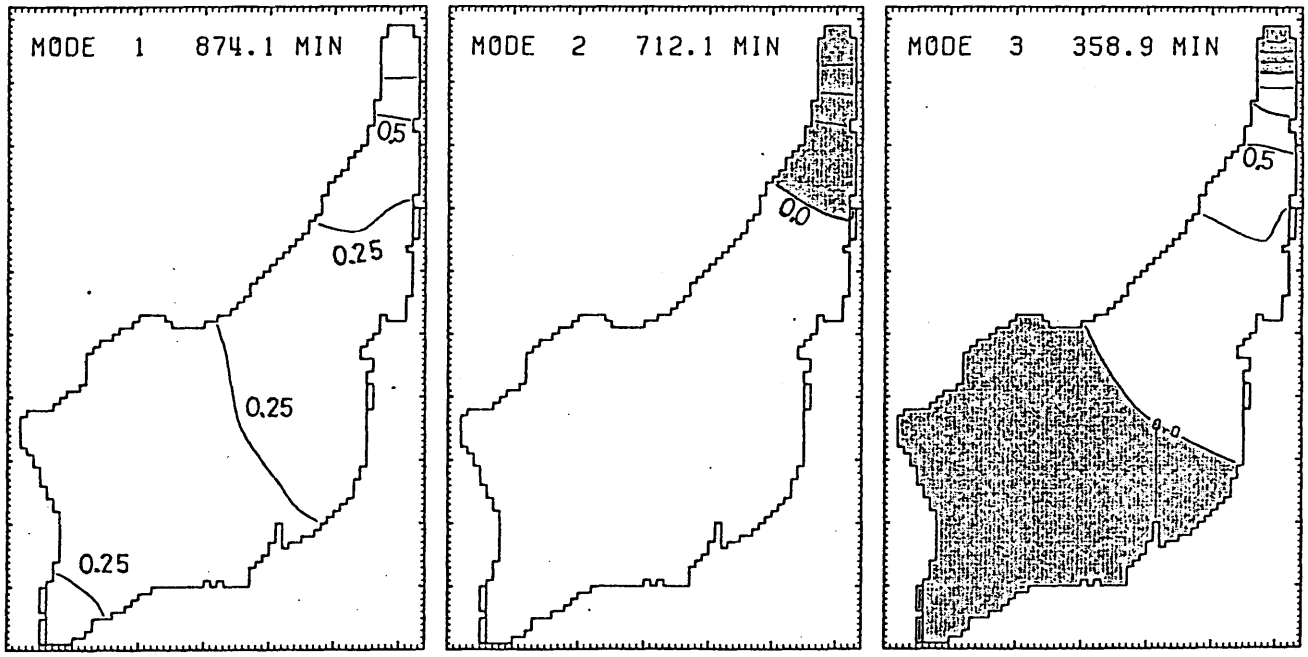

Figure 5. Plot of eigen vectors for several modes. *(a)*: the lowest three modes, *(b)*: the 6-th to 8-th modes, *(c)*: 35-th, 39-th and 46-th modes. Contour interval is 0.25 for the normalized eigen vectors by the largest component. Open and hatched areas show positive and negative values of the eigen vector component, respectively. Note that the sign of the eigen vector is indefinite, so it is given arbitrary.

Fig.5(b)

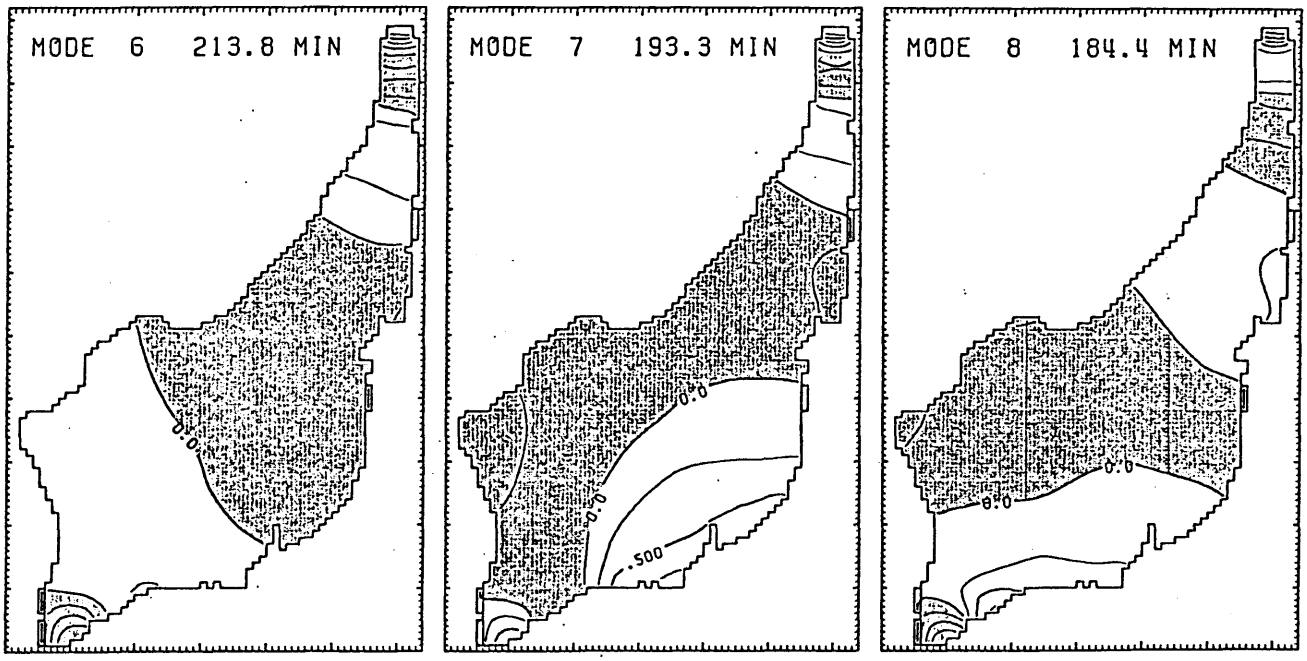

Fig.5(c)

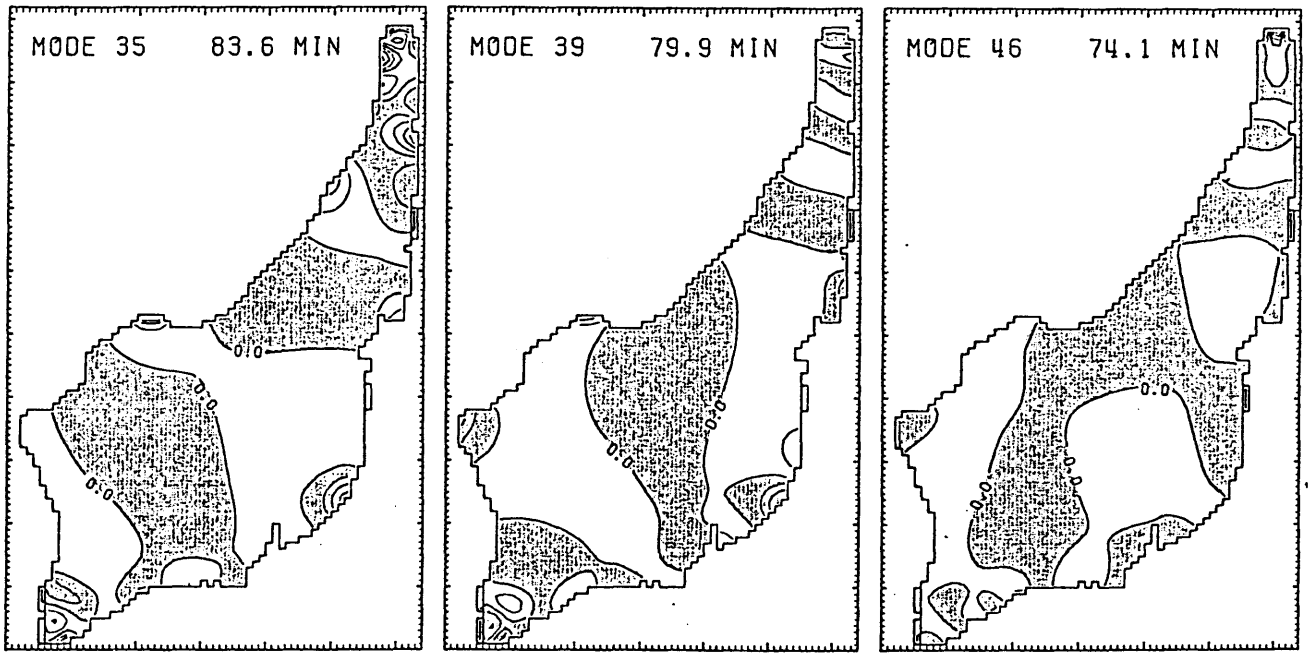
MODE 35 83.6 MIN
0.0
0.0
0.0
MODE 39 79.9 MIN
0.0
0.0
0.0
MODE 46 74.1 MIN
0.0
0.0
0.0

Fig.6

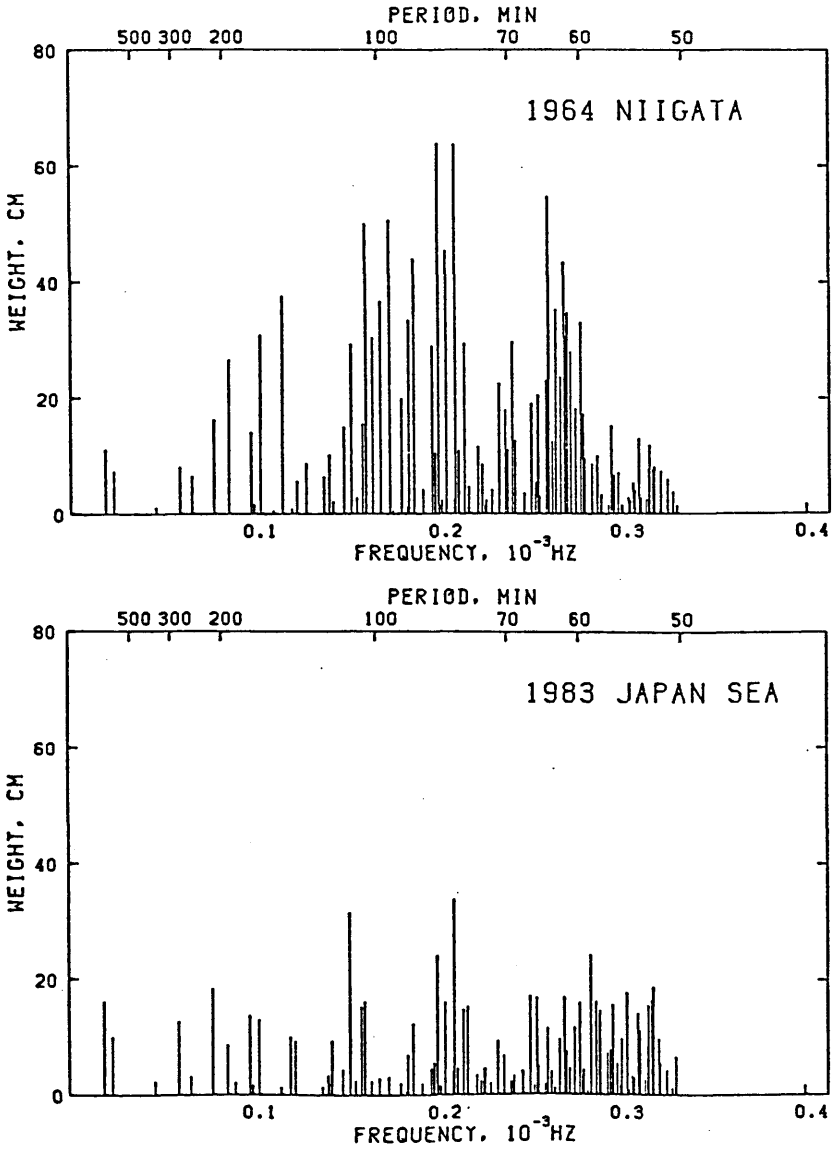

Figure 6. The weights of each mode excited by the two earthquakes. These weights are used for synthesizing the tsunami waveforms by a superposition of normal modes.

Fig.7

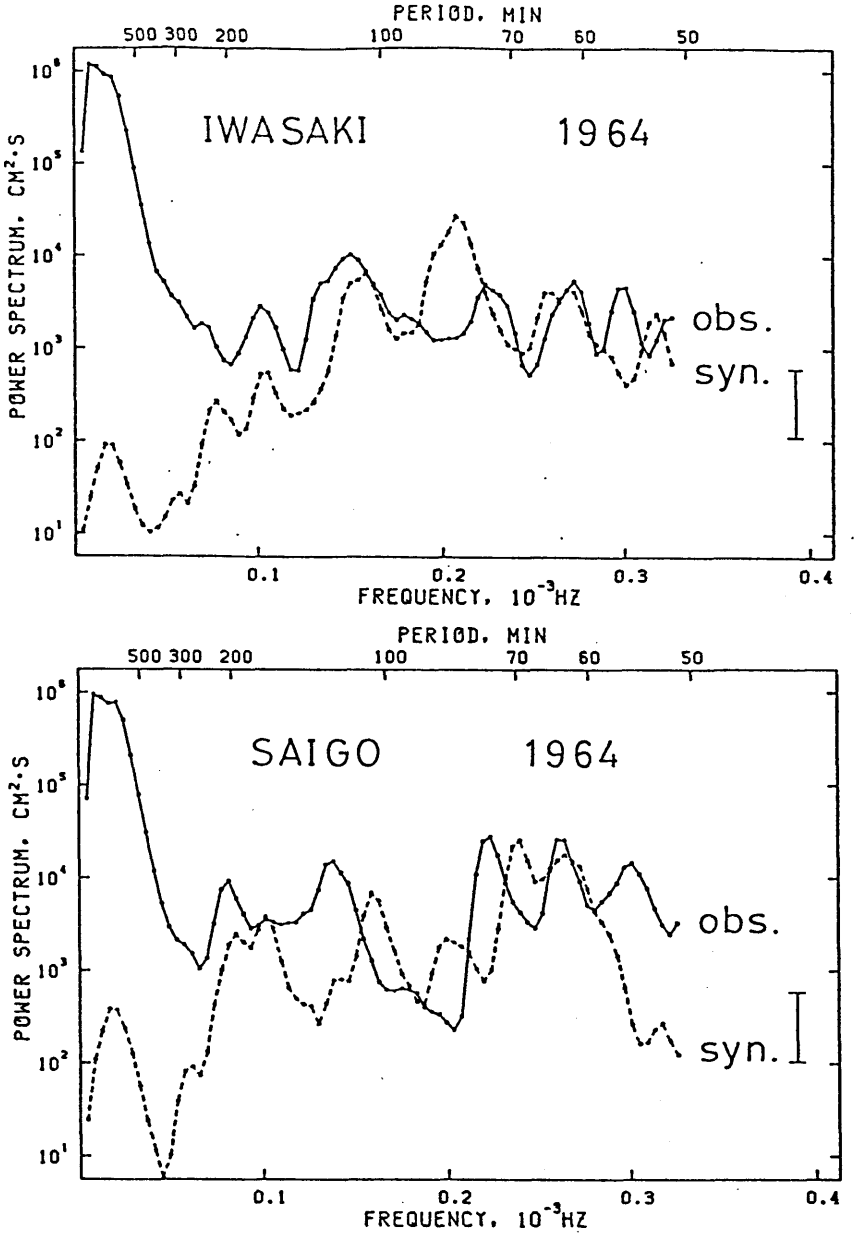

Figure 7. Comparison of the observed and synthesized spectra for the 1964 Niigata earthquake tsunami at Iwasaki and Saigo. Solid lines show the observed spectra while the dashed lines show synthesized ones. The vertical bar at the left indicates the range of the 90 % confidence level.

Fig.8

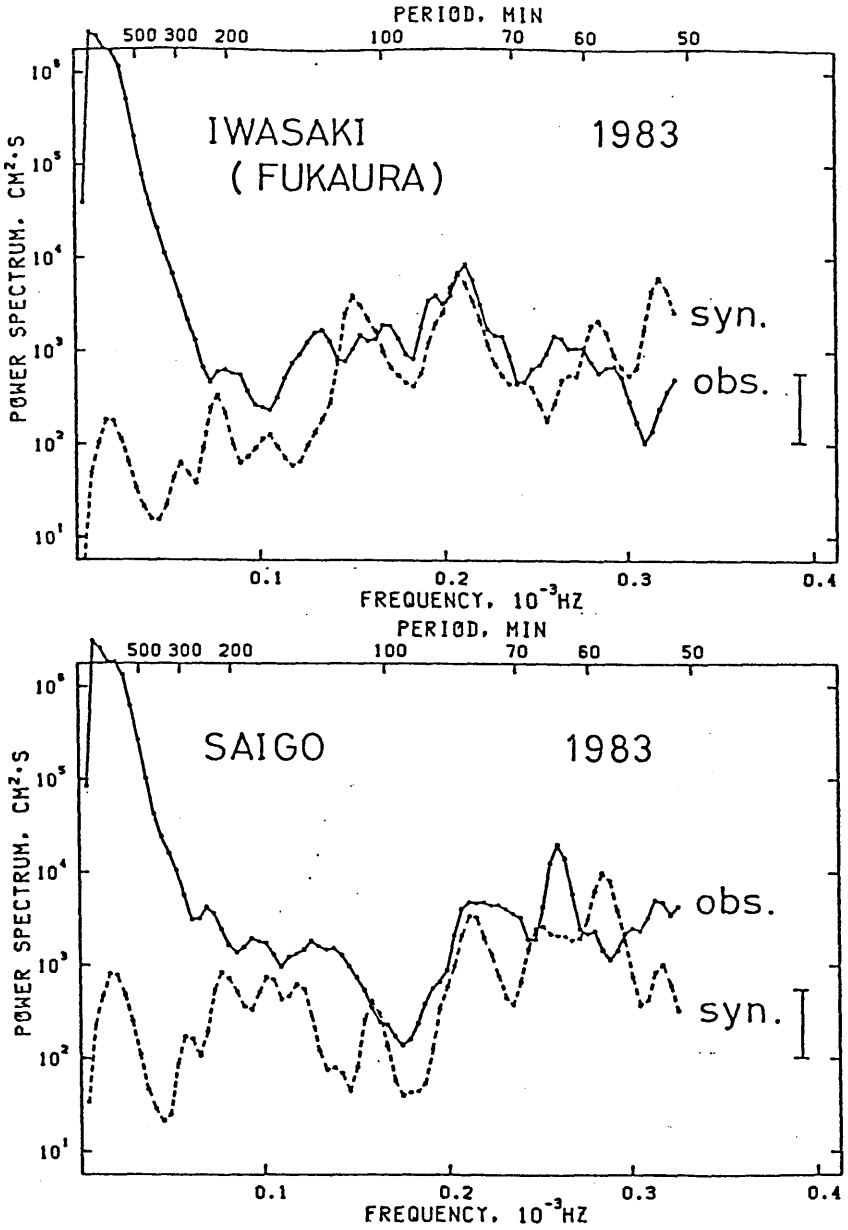

Figure 8. Comparison of the observed and synthesized spectra for the 1983 Japan Sea earthquake tsunami at Iwasaki and Saigo. The symbols are the same as those of Fig.7.

Chapter 4

Detectability of Very Slow Earthquake from Tide Gauge Records

Abstract

A very slow earthquake or crustal deformation with a rise time longer than the period of the free oscillation of the Earth is difficult to observe as a propagating wave on seismograms in the far-field. However, we propose that it may be detected by the free oscillation of an ocean basin, because the free oscillation of the Japan Sea excited by large earthquakes are detected from tide gauge records. A simulation is made for a hypothetical earthquake with a very long source process time (1 hr) to examine the detectability. The result indicates that if the amount of slip is almost the same as that for a magnitude 7 class earthquake, it is detectable in the present tide gauge observation system. However, the smaller is the slip, the more difficult is to detect the movement because of the limited dynamic range of the existing tide gauge and the presence of the tide. If a slow deformation precedes a large earthquake, tide gauge records would be useful for earthquake prediction, so an improvement of the observation system is desirable.

1. Introduction

The long-period characteristics of an earthquake source is an important problem in earthquake seismology. Slow movement at the source has been reported using surface waves (Kanamori and Stewart, 1979) or free oscillations of the Earth (Kanamori and Anderson, 1975). Recent development and deployment of very long-period seismographs are helpful for such studies. However, the longest period of free oscillation of the elastic Earth so far detected is about an hour and it is difficult to detect movements with a duration of an hour or longer. On the other hand, it is sometimes suggested that earthquakes are preceded by precursory slow movements with a duration of several hours to days (*e.g.* Mogi, 1985). Thus the detection of slow movements is also important in view of earthquake prediction.

Shimazaki (1976) proposed to use the ocean as a resonator and the tide gauge as a detector of slow movement. The free oscillation of an ocean basin has a period characterized by the depth and size of the basin. Normal mode solutions of the world's oceans indicate that the eigen periods are up to 80 hours (Platzman *et al.*, 1981) while the longest period of the normal modes in the Japan Sea is about 15 hours (Satake and Shimazaki, 1987c). If such free oscillations, sometimes called seiches in oceanographical terminology, are caused by movements of the ocean bottom, it may be possible to detect such movement using tide gauge records. The use of tide gauge records to detect crustal movements has been discussed (*e.g.* Tsumura, 1970). However, those are static treatments. The approach taken here is a dynamic one.

We have already shown that the observed spectra can be reproduced by a finite-difference computation on actual bathymetry (Satake and Shimazaki, 1987a) or by a superposition of numerically obtained modal solutions (Satake and Shimazaki, 1987c). In this paper, we make a simulation of a hypothetical slow deformation and discuss the

detectability of very slow earthquakes or crustal movements by observing the free oscillation of the Japan Sea. Such a large computation is possible by using supercomputer which has become available recently.

2. Free oscillation of the Japan Sea

The Japan Sea, the marginal sea of the Japanese Islands, has an area of about $10^6 km^2$, a mean depth of 1500 m and is an almost completely closed basin (Fig.1). Large earthquakes occurred periodically along the eastern margin of the Japan Sea (Hatori and Katayama, 1977; Satake, 1986). Recent two large earthquakes, the 1964 Niigata earthquake (M_W 7.6; Abe, 1975; Satake and Abe, 1983) and the 1983 Japan Sea earthquake (M_W 7.9; Satake 1985), are accompanied by destuctive tsunamis. One of the characteristic features of these tsunamis is the long duration which is attributed to the free oscillation of the Japan Sea.

Satake and Shimazaki (1987a) showed that finite-difference computations for the whole Japan Sea reproduce the observed spectra of tsunamis accompanied by the 1964 Niigata and the 1983 Japan Sea earthquakes. They mainly compared the spectra in a period range of 50 min to 3.5 hrs and showed that the peaks of the spectra represent the free oscillation of the Japan Sea. Satake and Shimazaki (1987c) further obtained the normal mode solutions of the Japan Sea and showed that the eigen vector, or water height distribution, for modes with longer eigen periods is determined by the whole Japan Sea while for those having shorter eigen periods, the amplitudes are regionally large at the shallow parts such as continental shelves. They also showed that the synthesized spectra by a superposition of normal modes (Satake and Shimazaki, 1987b) for the Niigata and the Japan Sea tsunamis agree well with the observed ones.

The power spectrum, more precisely power spectral density, of the 1964 Niigata

earthquake tsunami observed at Iwasaki (Fig.1) is shown in Fig.2 with the spectra from the tide gauge records before the earthquake. All the spectra in this paper are obtained by making FFT on records for 48 hrs. The power spectra for frequencies below 0.4 mHz (corresponding to a period of 42 min) are shown. The vertical bar in the figure shows the range of the 90 % confidence level estimated by smoothing the spectrum (Bendat and Piersol, 1971). The spectra for two different time intervals before the earthquake show almost the same features, indicating that these can be regarded as noise spectra for this station. The power spectrum after the event is about 100 times larger than, or 20 dB above, the noise level in the frequency range above 0.08 mHz (about 3.5 hrs). Below this frequency, the spectra are very similar for the three time intervals, indicating that they have no relations with the tsunami but represent the tides. Several distinct peaks exist around 0.15, 0.23, 0.27 and 0.3 mHz. These peaks represent modes of the free oscillation of the Japan Sea excited by the earthquake.

3. Detectability of very slow movements

We consider a hypothetical event by changing the actual source process time τ of 0.5 min of the Niigata earthquake to 60 min. We assume that the location, source mechanism, and amount of slip are the same as those of the Niigata event and make a finite-difference computation. It is known that the longer the source process time, the less efficient is the generation of tsunamis (Kajiura 1970). However, because of the closed nature of the Japan Sea, the result should be different. The spectrum of the tsunami from the slow deformation is shown in Fig.3. Also shown in the figure are the computed spectrum for the actual earthquake in which τ of 0.5 min is used (Satake and Shimazaki, 1987a) and the noise level of this station taken from Fig.2. The power spectrum of the slow earthquake is not very different from that of the case τ = 0.5 min at low frequency. However, at high frequency,

the power spectrum naturally becomes lower than that for an ordinary event.

The larger discrepancy at higher frequency can be interpreted as follows by considering the excitation of the free oscillation. The observed tsunami wave $f(t)$ is represented as a convolution of an impulse response $h(t)$ and a time function $g(t)$,

$$f(t) = h(t) * g(t).$$

Since the source process time, 0.5 min, is much shorter than the wave period considered here, the movement can be regarded as an instantaneous motion, hence the spectrum for τ = 0.5 min can be considered as an impulse response. On the other hand, the assumed source time function $g(t)$ for the slow deformation is a box-car function with height $1/\tau$ and width τ, so that the total deformed volume remains constant. Therefore, the resultant spectrum is represented as

$$F(\omega) = H(\omega) \cdot G(\omega)$$

where $F(\omega)$, $H(\omega)$ and $G(\omega)$ are the Fourier transform of $f(t)$, $h(t)$ and $g(t)$, respectively. The Fourier transform of a box-car function is (*e.g.* Bracewell, 1978),

$$G(\omega) = \sin x / x \qquad \textit{where} \quad x = \omega\tau/2 = \pi\tau/T.$$

Here ω and T are the angular frequency and the period of wave we consider. The power spectrum of the slow deformation (τ = 60 min) is, therefore, interpreted as $|G(\omega)|^2 = |\sin x / x|^2$ multiplied by the power spectrum of the impulse response which is approximated as the power spectrum for τ = 0.5 min. Two distinct peaks exist in Fig.3 at around 110 min and 72 min. If we take 110 min as T, then $|G(\omega)|^2$ is computed as 0.33. For T= 72 min, $|G(\omega)|^2$ is 0.036. These agree with the difference between the two spectra shown in Fig.3.

Based on the above interpretation we can estimate the detectability of the slow deformation. The peak at 110 min for τ = 60 min is about 100 times larger than the noise level.

Therefore the peak is detectable even if the amount of slip is as small as a tenth of the Niigata earthquake because of the linearity of the tsunami equations. The peak at 72 min will be severely affected by the source process time itself if it is near 60 min. Although the peak for τ = 0.5 min is about 300 times in power above the noise level, the simulated peak for τ = 60 min is only 10 times above it. Thus one-third of the slip of the Niigata earthquake is the detectable limit at this peak.

When the source process time τ is longer than 60 min, the detectability can be estimated by examining the function $\sin x / x$. Since the two peaks for τ = 0.5 min are about 300 times above the noise level, it is detectable as far as $|\sin x / x|^2$ is 1/300. The corresponding x is 0.95 π. Since $x = \pi\tau/T$, τ is 105 min for a peak at T = 110 min and τ is 68 min for a peak at T = 72 min. In other words, a slow deformation whose duration up to 105 min is detectable using the peak at 110 min or up to 68 min in duration using the peak at 72 min if the amount of slip is the same as that of the Niigata earthquake. Because the function $|\sin x / x|^2$ becomes almost zero for x larger than π, it is difficult to detect a slow deformation with duration longer than a period of signals. This is the reason why the free oscillation of the elastic Earth cannot be used for the detection of a very slow earthquake. However, there exist modes with longer eigen periods for the free oscillation of closed ocean basin such as the Japan Sea, so it is possible to use them for the detection of very slow earthquakes if we could remove the tidal effects.

4 Discussion

We have seen in the previous section the possibility of the detection of very slow movements. The detectability can be further improved in various ways such as removing the tides or noise from tide gauge records. As mentioned before, since modal solutions exist in the tidal range, it is possible to use such modes if the tides are removed. It is

necessary to remove the tides only, so band-pass filtering is not appropriate. An effort to make the noise level lower is also important.

The present tide gauge system has an analog recorder usually with a pen. Great advantages are expected if a digital recording system is employed; the dynamic range is wider, the analysis can be made easily or even automatically. Such a digital recording and telemetering system is installed at several Japanese tide gauge stations. The response of a tide gauge well is also important and should be examined (Satake *et al.*, 1987), although it is unlikely that the low frequency signal treated in this paper is severely affected by the response of the well.

Besides the problems of the tide gauge system mentioned above, there are several problems toward the earthquake prediction by detecting slow movements from tide gauge records. Locating the slow deformation is one of them. Once we have detected such a slow movement from the spectra of the tide gauge records, it has to be located for the purpose of earthquake prediction. This will be a subject of a future study.

References

Abe, K., 1975. Re-examination of the fault model for the Niigata earthquake of 1964. *J. Phys. Earth,* **23**, 349-366.

Bendat, J.S. and Piersol, A.G., 1971. *Random Data: Analysis and measurement procedures.* John Wiley & Sons.

Bracewell, R.N., 1978. *The Fourier transform and its applications.* McGraw-Hill.

Hatori, T. and Katayama, M., 1977. Tsunami behavior and source areas of historical tsunamis in the Japan Sea. *Bull. Earthq. Res. Inst. Univ. Tokyo,* **52**, 49-70 (in Japanese).

Kajiura, K., 1970. Tsunami source, energy and the directivity of wave radiation. *Bull. Earthq. Res. Inst. Univ. Tokyo,* **48**, 835-869.

Kanamori, H. and Anderson, D.L., 1975. Amplitude of the earth's free oscillations and long-period characteristics of the earthquake source. *J. Geophys. Res.,* **80**, 1075-1078.

Kanamori, H. and Stewart, G. S., 1979. A slow earthquake. *Phys. Earth Planet. Inter.,***18**, 167-175.

Mogi, K., 1985. *Earthquake prediction.* Academic press.

Platzman, G.W., Curtis, G.A., Hansen, K.S. and Slater, R.D., 1981. Normal modes of the world ocean. Part II: Description of modes in the period range 8 to 80 hours. *J. Phys. Oceanogr.,* **11**, 579-603.

Satake, K., 1985. the mechanism of the 1983 Japan Sea earthquake as inferred from long-period surface waves and tsunamis. *Phys. Earth Planet. Inter.,* **37**, 249-260.

Satake, K., 1986. Re-examination of the 1940 Shakotan-oki earthquake and the fault parameters of the earthquakes along the eastern margin of the Japan Sea. *Phys. Earth Planet. Inter.,* **43**, 137-147.

Satake, K. and Abe, K., 1983. A fault model for the Niigata, Japan, earthquake of June 16, 1964. *J. Phys. Earth,* **31**, 217-223.

Satake, K., Okada, M., and Abe, K., 1987. Tide gauge response: measurement and its effect on tsunami waveforms. to be submitted to *Proc. PACON'88 (Chapter 1.2 of this thesis).*

Satake, K. and Shimazaki, K., 1987a. Free oscillation of the Japan Sea excited by earthquakes 1: observation and wave-theoretical approach. submitted to *Geophys. J. R. astr. Soc. (Chapter 2.1 of this thesis).*

Satake, K. and Shimazaki, K., 1987b. Computation of tsunami waveforms by a superposition of normal modes. to be submitted to *J. Phys. Earth (Chapter 2.2 of this thesis).*

Satake, K. and Shimazaki, K., 1987c. Free oscillation of the Japan Sea excited by earthquakes 2: modal approach and synthetic tsunamis. to be submitted to *Geophys. J. R. astr. Soc. (Chapter 2.3 of this thesis).*

Shimazaki, K., 1976. Long-period power spectra of tsunamis in the Japan Sea (abstract). *EOS Trans. Am. Geophys. Union.,* **57**, 290.

Tsumura, K., 1970. Investigations of mean sea level and its variations along the coast of Japan (part 2) -Changes in ground level at various places in Japan as deduced from tidal data and earthquake prediction -. *J. Geod. Soc. Japan,* **16,** 239-275.

Fig.1

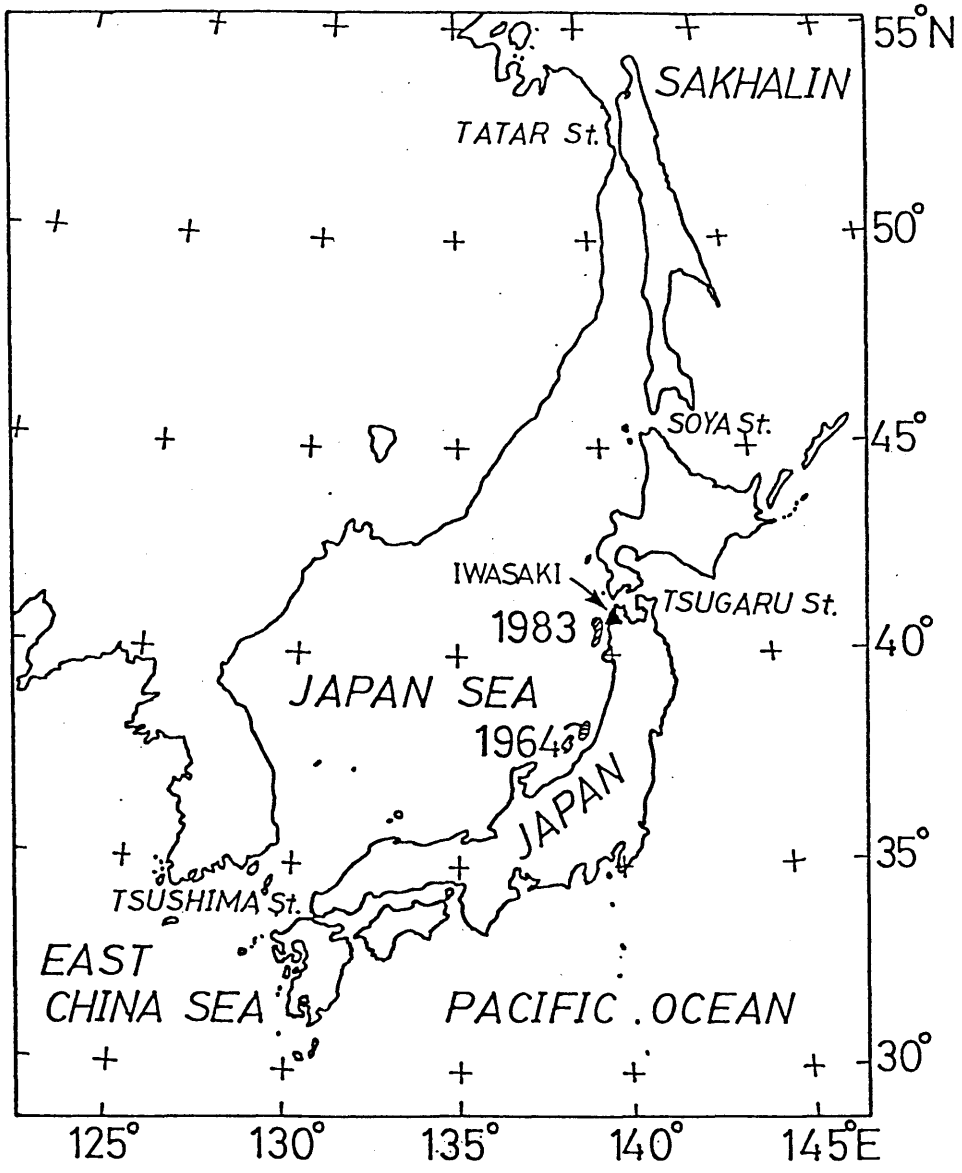

Figure 1. Map showing the location of the Japan Sea. The source areas of the 1964 Niigata and the 1983 Japan Sea earthquakes and location of the tide gauge station Iwasaki are shown.

Fig.2

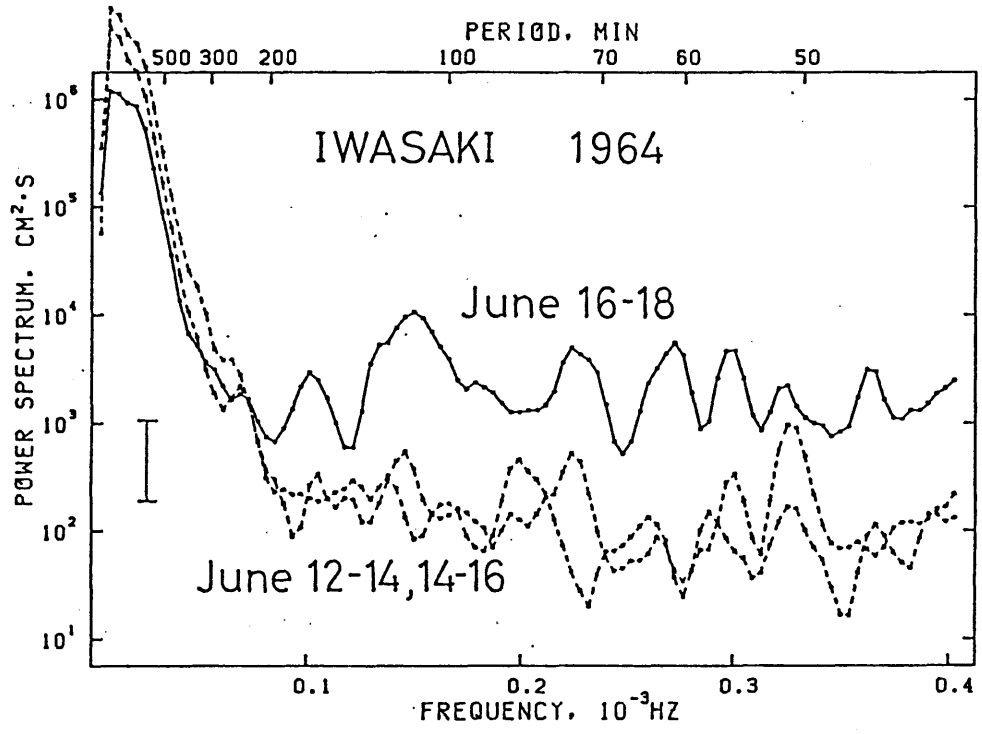

Figure 2. The spectra of the tide gauge records at Iwasaki at the time of 1964 Niigata earthquake of June 16. The solid line shows the spectrum after the event while two dashed lines are the spectra before the event indicating the noise level. The vertical bar at the left indicates the range of the 90 % confidence level.

Fig.3

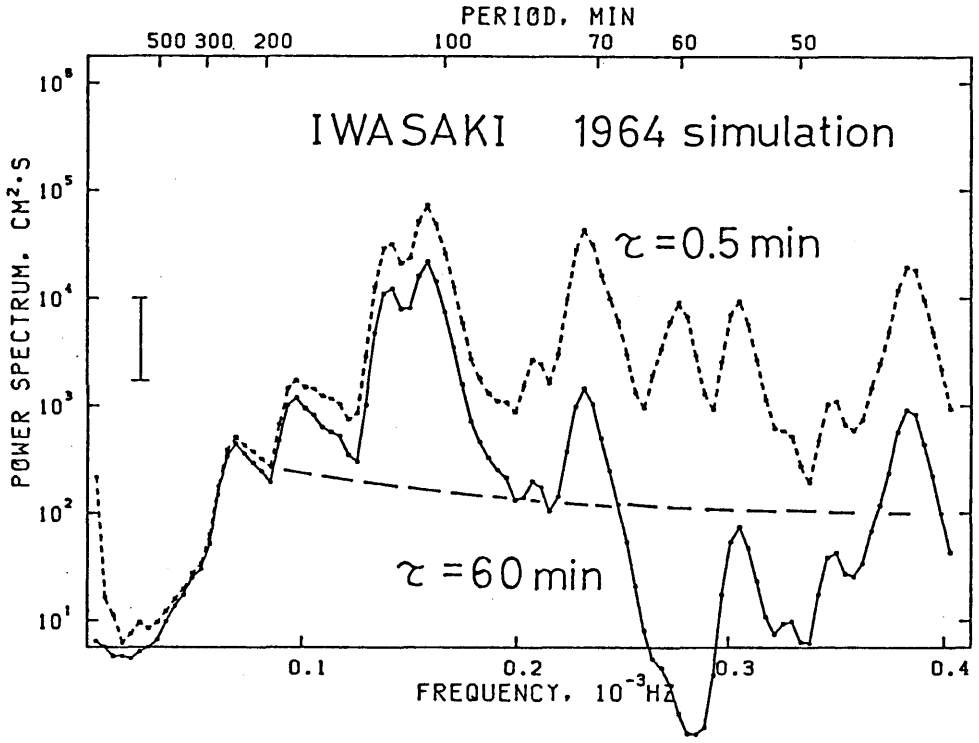

Figure 3. The spectra of the finite-difference computations at Iwasaki for the Niigata earthquake with the source process times 0.5 min and 60 min. Dashed line represents the noise level taken from Fig.2.

Appendix

Effects of Bathymetry on Tsunami Propagation: Application of Ray Tracing to Tsunamis

Abstract

Ray tracing of seismic surface waves is applied to tsunami propagation to examine bathymetric effect along its propagation path. Computations are made for trans-Pacific tsunamis and for near-field tsunamis in the Japan Sea. For tsunamis across the Pacific Ocean, the comparison to a uniform ocean shows that focusing and defocusing due to bathymetry are significant for some combinations of source and receiver. For example, the refraction of rays is predominant at the East Pacific Rise for the tsunami from Chile. The tsunamis in the Japan Sea are strongly affected by the shallow Yamato Rise. The predicted arrival time and amplitude distribution generally agree with the observations from an actual tsunami. Since the computation can be made very quickly, the method is useful for preliminary analysis of tsunami propagation such as in an operational warning system or in the determination of computational area for finite-difference computation.

Introduction

Large earthquakes are sometimes accompanied by destructive tsunamis. Arrival times and amplitudes of tsunamis, important information in view of hazard reduction as well as geophysical research, are affected by various factors which can be grouped into three: those related to the source, the propagation path, and shore effects. The source effect includes directivity due to fault orientation (Kajiura, 1970; Ben-Menahem and Roseman, 1972) and fault parameters such as dip angle or slip amount (Yamashita and Sato, 1974). The propagation path includes the effects of Earth's sphericity (Miyoshi, 1955), local bathymetry near the source (Miyoshi, 1968) and scattering of tsunamis by sea-mounts (Tsuji, 1977). The resonance of bay or harbor or run-up (Murty, 1977) may be included in the shore effects. The effect of propagation path is determined by ocean bathymetry, since tsunamis from large earthquakes can usually be treated as non- dispersive linear long-waves so that the velocity is given as $\sqrt{gh}$ where g is the gravitational acceleration and h is the water depth. The bathymetric effect can be evaluated by refraction diagrams which are usually made manually (*e.g.* Murty, 1977). Efforts to construct them numerically have also been made but applied to only regional problems (*e.g.* Griswold, 1963). Recent developments in computer technology allow extensive numerical computations. At the same time, fine bathymetric data are also available today.

In this paper, ray tracing of seismic surface waves on the spherical Earth is applied to tsunami propagation in the whole Pacific Ocean and the Japan Sea to examine the bathymetric effect. The major advantage of the ray tracing is that ray paths are visible in a short computation time. Focusing and defocusing due to bathymetry is seen and the amplitude and arrival time can be estimated from it. For more accurate evaluation of amplitude or waveform comparable to observation, finite-difference computation of hydrodynamic equations must be made (*e.g.* Satake, 1985). Since ray path is known by ray tracing, the area

needed for the finite-difference computation can be determined before the computation. The short computation time of ray tracing is encouraging for the use in an operational tsunami warning system if bathymetric effect is dominant compared to other effects. There are also several disadvantages, however. In shadow zones it is impossible to evaluate the tsunami arrival time or the amplitude except for the fact that the amplitude may be smaller than the other regions. The reflected waves cannot be evaluated. The intrinsic nature of ray tracing, as discussed in the next section, also limits the application.

Method and Data

Ray tracing is a short wavelength approximation. It is valid for smoothly changing inhomogeneity (ocean bathymetry for tsunamis) and the change must be small within a wavelength (*e.g.* Aki and Richards, 1980). Ray tracing is invalid near caustics. Since the Earth's sphericity must be considered when we treat tsunami waves traveling long distance, ray tracing equations for seismic surface waves are used. They are,

$$\frac{d\theta}{dT} = \frac{1}{nR}\cos\zeta$$

$$\frac{d\phi}{dT} = \frac{1}{nR\sin\theta}\sin\zeta$$

$$\frac{d\zeta}{dT} = -\frac{\sin\zeta}{n^2R}\frac{\partial n}{\partial\theta} + \frac{\cos\zeta}{n^2R\sin\theta}\frac{\partial n}{\partial\phi} - \frac{1}{nR}\sin\zeta\cot\theta$$

where θ and ϕ are colatitude and longitude of the ray at time T, n is the slowness ($=1/\sqrt{gh}$), R is the radius of the Earth, and ζ is the ray direction measured counterclockwise from the south (Aki and Richards, 1980). The above equations are solved by the Runge-Kutta-Gill method. Integration is performed by the mid-point method using interpolated velocities; the detail of the method is the same as that of Sobel and von Seggern (1978).

Different kinds of bathymetric data are used depending on the travel distance of tsunami as shown in Fig. 1. For trans- Pacific tsunamis, 10′×10′ bathymetric data are made from ETOPO5 provided by NGDC (Loughridge, 1986). For tsunamis in the Japan Sea, the ocean depth is given as 6′×6′ grid since the travel distance is short and the source area is small. All of the data are smoothed to satisfy the short wavelength condition mentioned above. Moving average is made with neighboring 10° × 10° for the Pacific Ocean and 1° × 1° for the Japan Sea data. The ray tracing represents tsunamis with wavelength of a few hundreds of km for the trans-Pacific, and a few tens of km for the Japan Sea tsunamis. Only the ocean part is smoothed and the land-sea boundaries are unchanged. Trials for several kinds of smoothing including a homogeneous depth showed that rays are unstable for the less smoothed bathymetric data.

Ray Tracing of Trans-Pacific Tsunamis

Figure 2 shows the ray tracing of trans-Pacific tsunamis. Rays are generated with 2° interval in azimuth. The time step for computation is 1 min and the tick marks indicate each 1 hour from the origin time. Rays stop when they reach 1000 m depth. The ray tracing for a uniform depth assuming that the whole Pacific Ocean is 5400 m deep is also shown for comparison. Rays travel along great circle if the ocean depth is uniform.

For tsunami from Chile, the convergence of rays near Japan due to the Earth's sphericity has been pointed out by Miyoshi (1955) because the arc distance between Japan and Chile is about 150°. This feature can be seen in the case of the uniform depth. However, the ray tracing for actual batymetry shows that the refraction of rays at the East Pacific Rise is predominant. Compared to the uniform depth, more rays arrive at California and less at the Aleutian Islands. Rays arrive at Hawaii in 15 hrs and at Japan in 22 hrs, well reproducing the 1960 Chilean tsunami (Takahashi and Hatori, 1961).

For tsunami from the Aleutians, less rays arrive at Chile than in the uniform depth case. No significant difference is seen at the other places. The tsunami arriving at Chile from Japan show similar characteristics to that from Chile arriving at Japan, indicating a reciprocity. Rays from Japan focus at Hawaii and defocus at California and Solomon. Rays from Solomon focus at California but defocus at Japan. Significant focusing is seen at Japan and the Philippines and defocusing between them for the tsunami from Hawaii. Some modification of the bathymetric data are made for the Hawaiian source; the islands are replaced with the ocean to eliminate a shadow of the island near the source. This map can be used for an inverse diagram in which arrival times from circum-Pacific sources to Hawaii can be estimated.

In order to quantify the focusing and defocusing, ray density ρ_{ray} is defined as the ratio of ray numbers along the coast for actual bathymetry to that for uniform depth (Lay and Kanamori, 1985). The latter can be computed from the azimuthal interval of the ray take-off and the distance between the source and the observation site, since rays travel along the great circle on a uniform ocean. The rays are generated with 1° interval in azimuth for the actual bathymetry for an accurate counting. Figure 3 shows the ρ_{ray} for the five tsunamis at six coastal regions. Solid circles indicate that rays focus compared to the uniform depth, open circles show defocusing, and plus signs mean no significant difference between the actual and uniform depths. All of the features mentioned above are tabulated in this figure. The reciprocity between source and receiver is maintained except for the case between Solomon and Chile. The reason for this exception is that the source is given as a point whereas rays are counted along the coasts about 2000 km in length. A close look at Fig.2 shows that the ray paths are different between Solomon and Chile depending on the ray direction.

The point source assumption adopted in this paper may not be valid enough to estimate amplitude of tsunami from great earthquakes. The directivity due to fault orientation

(Ben-Menahem and Roseman, 1972) is also predominant as well as bathymetric effect. However, the computed arrival times roughly reproduce the observation as seen in the Chilean case.

Ray Tracing of Tsunamis in the Japan Sea

As examples of near-field tsunamis, ray tracing is applied to tsunamis in the Japan Sea. Figure 4 shows the ray tracing for two earthquakes: 1983 Japan Sea (Satake, 1985) and 1940 Shakotan-Oki (Satake, 1986) earthquakes. Rays are generated with 1° interval in azimuth from point sources. The integration is made with 1 min step and the tick marks in the figure indicate each 10 min from the origin time. Computation is stopped when rays reach a shallow depth (10 m).

For both events, the rays are strongly refracted at shallow region located in the center of the Japan Sea, the Yamato Rise (Fig.1). Focusing of rays is seen at Noto Peninsula, Oki Islands, North Korea, and coastal range of USSR. Actually the observed tsunami height was larger at these areas (Miyabe, 1941; JMA, 1984; Tsuji *etal.*, 1985).

To examine the effects of source size and location, the point source is shifted to northern, southern, and eastern end of the source area of the 1983 event (Satake, 1985) and the ray tracing is repeated. The results are shown in Fig.5. The number of outgoing rays is maximum in the case of northern end of the fault, and smaller for southern and eastern ends. However, the ray paths are very similar for all three sources. As far as ray paths are concerned, a point source assumption is valid for this earthquake. These maps are also useful to determine the computational area for a finite-difference computation. For example, if the waveform at Noto Peninsula is desired, the computational area must extend to the west by a few degrees because the rays are coming from north-west direction to Noto Peninsula. The observed and predicted travel times are compared at several tide gauge stations for the

1983 Japan Sea tsunami. The result is shown in Fig.6. For Japanese stations, the agreement is generally good, if we consider the coarse velocity grid. Discrepancy in northern stations near the source might be due to the point source assumption. The error in bathymetric data also affects the discrepancies in Korean and Russian stations for which our data quality is poor. The tsunami velocity is very small at a shallow depth near coast, so that a large error in travel time might arise there.

Tsunami height is sometimes estimated by using simple Green's law (*e.g.* Murty, 1977);

$$H_1 = (b_0/b_1)^{1/2}(h_0/h_1)^{1/4}H_0$$

where b is the distance between two neighboring rays and H is the tsunami height with subscripts 0 and 1 indicating at the source and at the observing site, respectively. Considering the bathymetric effect, the Green's law can be modified as

$$H_1 = (\rho_{ray}\sin\Delta_0/\sin\Delta)^{1/2}(h_0/h_1)^{1/4}H_0$$

where Δ is the arc distance between the source and observer, Δ_0 is the source radius in which uniform vertical displacement H_0 is assumed. By using this equation, the amplitudes are also predicted and compared with observations in Fig.6. In this particular example, we adopt h_0= 2000 m, h_1= 10 m, Δ_0= 60 km, and H_0= 123 cm (Abe, 1985; Satake, 1985). For the observed value, arrival times and maximum peak-to-peak amplitudes are read from the tide gauge records. The reading of maximum amplitude is limited within an hour from the first arrival of tsunami to eliminate the reflection or the resonance caused by local topography. Except for one station (No.1) where the local effect might be large, the predicted and the observed amplitudes agree well. Although the method is theoretically invalid after rays intersect, the agreement is good for such stations as Nos.6-8. The amplitude as well as the travel time agreement indicates that the arrival time and the amplitude of the earlier part of tsunami wave are determined by the long-wavelength bathymetry along the propagation

path in the case of near-field tsunami. This is encouraging for the application of the present method to operational tsunami warning system.

Conclusion

By introducing ray tracing to tsunami, the bathymetric effect along its propagation is estimated. For tsunamis across the Pacific Ocean, focusing and defocusing are dominant compared to the uniform ocean for some combination of source and receiver. The tsunamis in the Japan Sea are strongly affected by Yamato Rise. Both arrival time and amplitude are reproduced by ray tracing, indicating that those are mainly determined by the bathymetry. Ray tracing of tsunamis is useful for preliminary analysis such as a determination of computational area of finite-difference computation or an operational tsunami warning system since the prediction can be made within a minute after the epicenter is determined.

Acknowledgements

I thank Katsuyuki Abe and Yoshinobu Tsuji, both at Earthquake Research Institute, University of Tokyo and Bruce Turner at the Pacific Tsunami Warning Center, NOAA for reading the manuscript and giving me valuable comments. The bathymetric data for the Pacific Ocean are made from the data base ETOPO5 compiled by National Geophysical Data Center and provided by the data base system at Earthquake Prediction Observation Center, Earthquake Research Institute. Numerical computation was made at Computer Centre, University of Tokyo, using the graphic library NCARG originally developed at National Center for Atmospheric Research. This work was partially supported by the Grand-in-Aid for Scientific Research from Ministry of Education, Science and Culture, Japan (No.61020009).

References

Abe, K.(1985), Quantification of major earthquake tsunamis of the Japan Sea, Phys. Earth Planet. Inter. 38, 214-223.

Aki, K. and Richards, P.G., Quantitative seismology (W.H.Freeman, San Francisco 1980).

Ben-Menahem, A. and Roseman, M. (1972), Amplitude patterns of tsunami waves from submarine earthquakes, J. Geophys. Res. 77, 3097-3128.

Griswold, G.M. (1963), Numerical calculation of wave refraction, J. Geophys. Res. 68, 1715-1723.

Japan Meteorological Agency (JMA), Report on the Nihonkai-chubu earthquake, 1983 (in Japanese, Tech. Rep. JMA 1984).

Kajiura, K. (1970), Tsunami source, energy and the directivity of wave radiation, Bull.Earthq. Res. Inst. Univ. Tokyo 48, 835-869.

Lay, T. and Kanamori, H.(1985), Geometric effect of global lateral heterogeneity on long-period surface wave propagation, J. Geophys. Res. 90, 605-621.

Loughridge, M.S. (1986), Relief map of the Earth's surface, EOS, Trans. Amer. Geophys. Union 67, 21.

Miyabe, N. (1941), Tunami associated with the earthquake of August 2, 1940 (in Japanese), Bull. Earthq. Res. Inst., Univ. Tokyo 19, 104-114.

Miyoshi, H. (1955), Directivity of recent tsunamis, J. Ocean. Soc. Japan 11, 151-155.

Miyoshi, H. (1968), Re-consideration on directivity of the tsunami (I) (in Japanese), Zisin 21, 121-138.

Murty, T.S., Seismic sea waves -tsunamis (Bull. Fish. Res. Board Canada 198, 1977).

Satake, K. (1985), The mechanism of the 1983 Japan Sea earthquake as inferred from long-period surface waves and tsunamis, Phys. Earth Planet. Inter. 37, 249-260.

Satake, K. (1986), Re-examination of the 1940 Shakotan-oki earthquake and the fault

parameters of the earthquakes along the eastern margin of the Japan Sea, Phys. Earth Planet. Inter. 43, 137-147.

Sobel, P.A. and von Seggern, D.H. (1978), Application of surface-wave ray tracing, Bull. Seismol., Soc. Am. 68, 1359-1380.

Takahashi, R. and T. Hatori, A summary report on the Chilean tsunami of May 1960, In Report on the Chilean Tsunami, (ed. Comm. Field Invest. Chilean Tsunami) (Tokyo, 1961) pp. 23-34.

Tsuji, Y. (1977), A study on the scattering wave induced by tsunami passing over a sea mount or rise (in Japanese), Marine Sciences Monthly 9, 45-53.

Tsuji, Y., Baek,W.S., Chu,K.S. and An H.S., Report of the 1983 Nihonkai-chubu earthquake tsunami along the east coast of the Republic of Korea (in Japanese), Rev. Res. Disaster Prevention 90, (National Research Center for Disaster Prevention, 1985).

Yamashita, T. and Sato, R.(1974), Generation of tsunami by a fault model, J. Phys. Earth 22, 415-440.

Fig.1

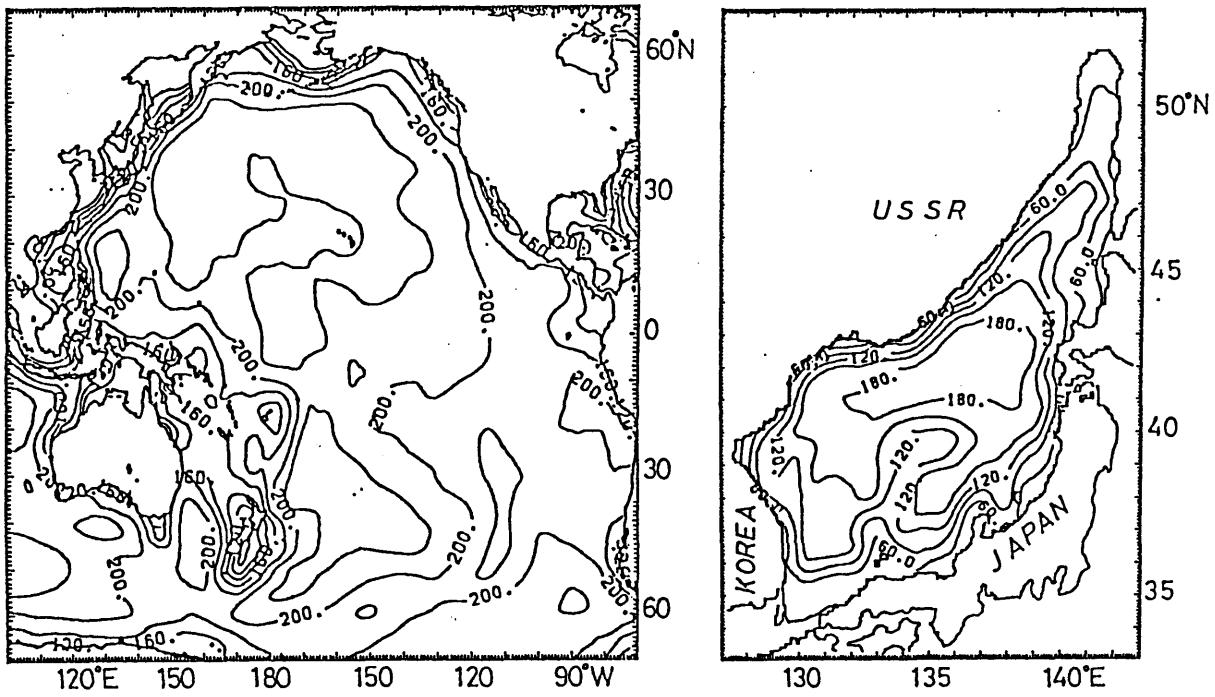

Figure 1. Bathymetric data used for ray tracing calculations. (*left*) Pacific Ocean (*right*) Japan Sea. Numerals indicate tsunami velocity in m/s.

Fig.2

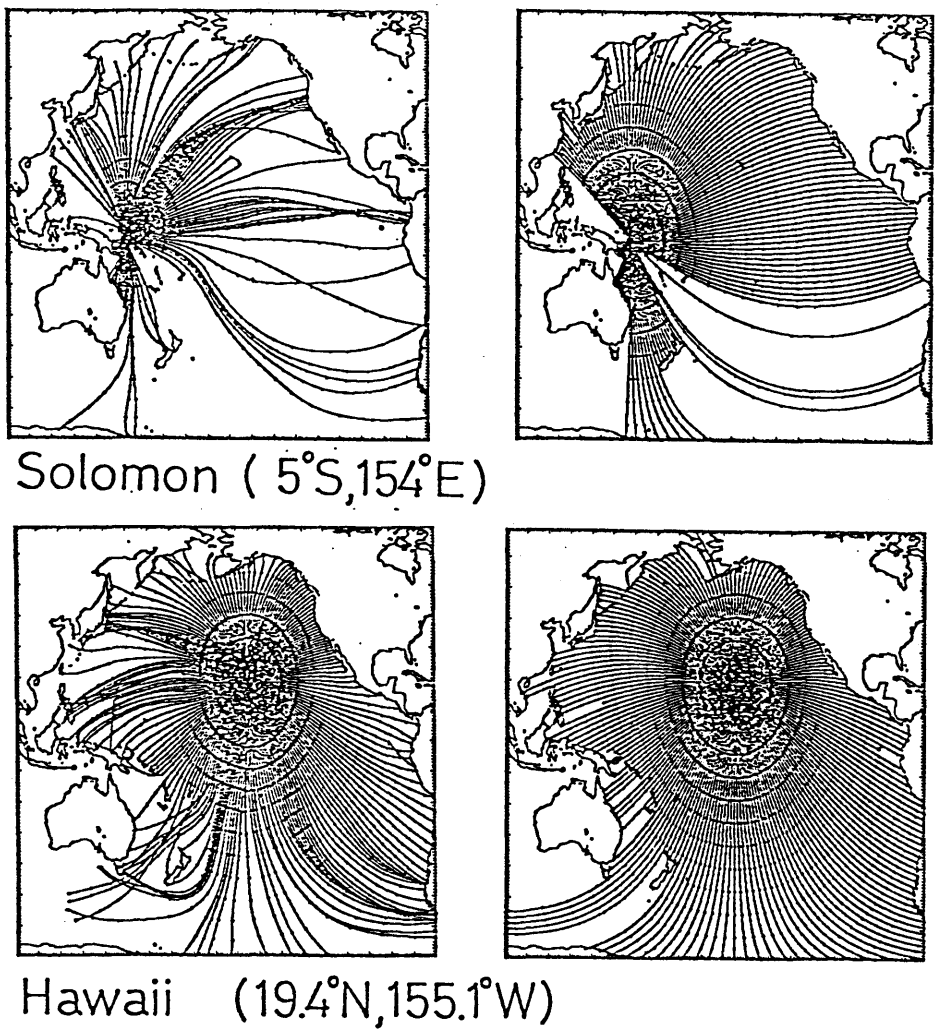

Figure 2. Ray tracing for trans-Pacific tsunamis. Rays are generated with 2° interval in azimuth from point sources. Tick marks indicate each 1 hour from the origin time. (*left*) Calculation for actual bathymetry, (*right*) calculation for uniform (5400 m) ocean depth.

Fig.2 (*continued*)

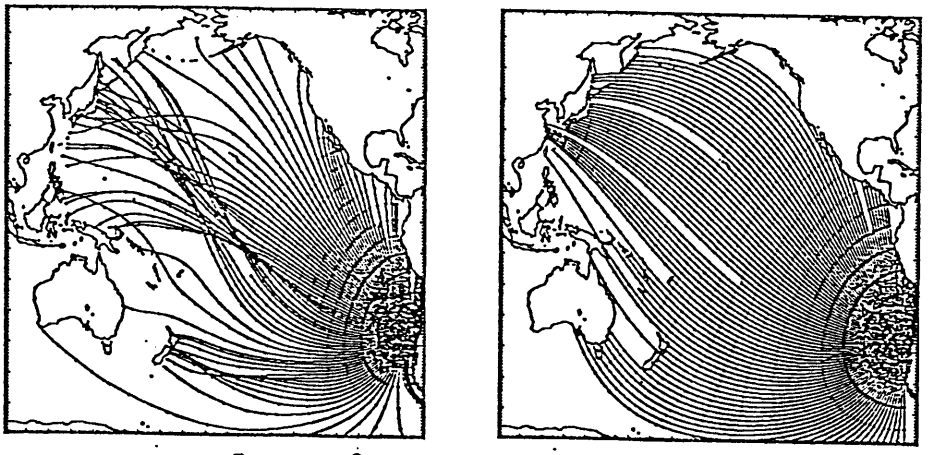

Chile (35°S, 76°W)

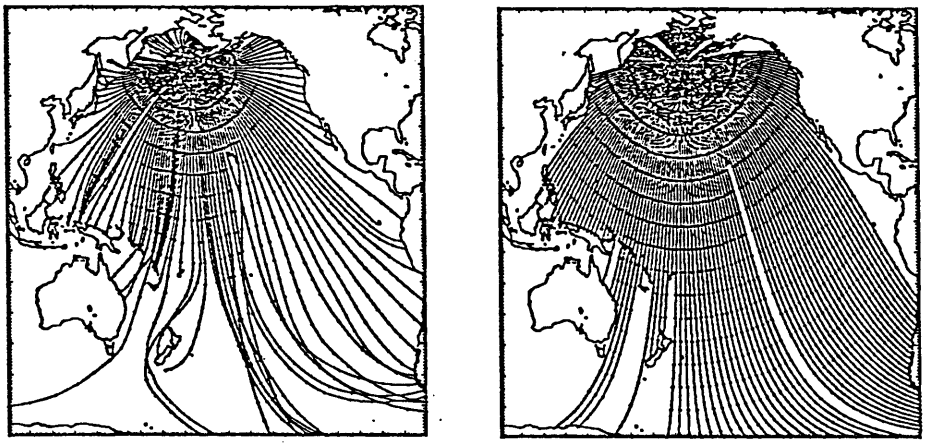

Aleutian (51°N, 176°W)

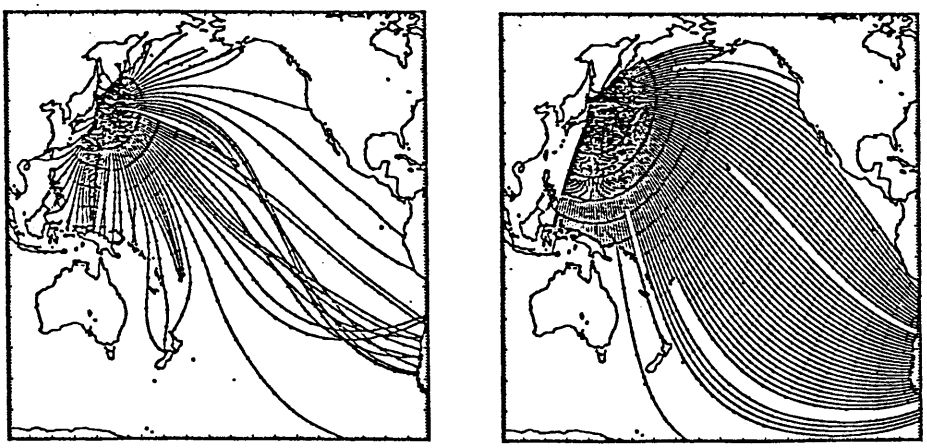

Japan (39°N, 143°E)

Fig.3

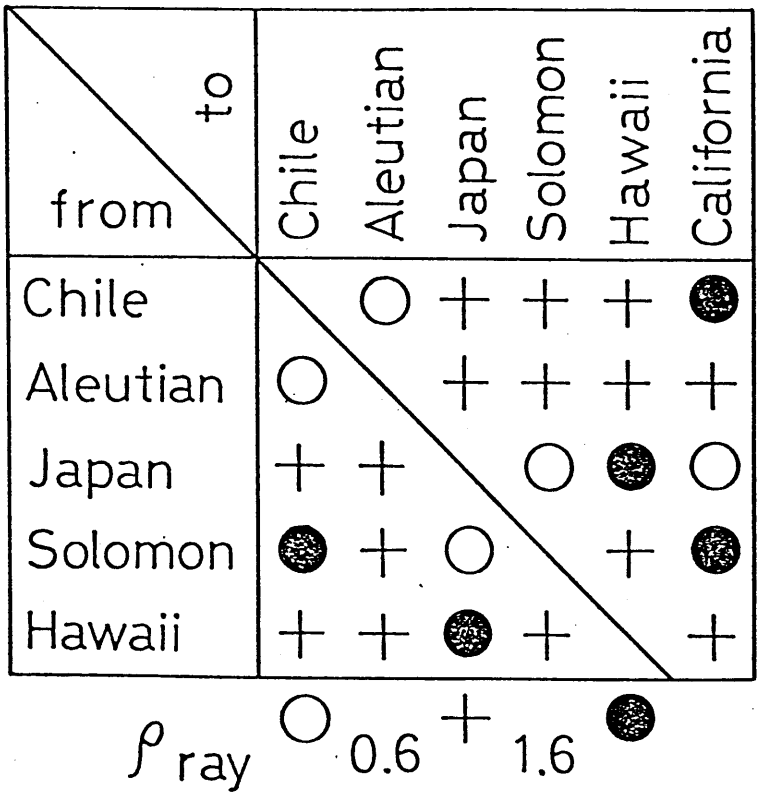

Figure 3. Ray density at six coastal regions from five sources. Solid circles mean that more rays are coming compared to a uniform ocean, open circles less rays, and plus signs mean no significant difference between the actual and uniform ocean.

Fig.4

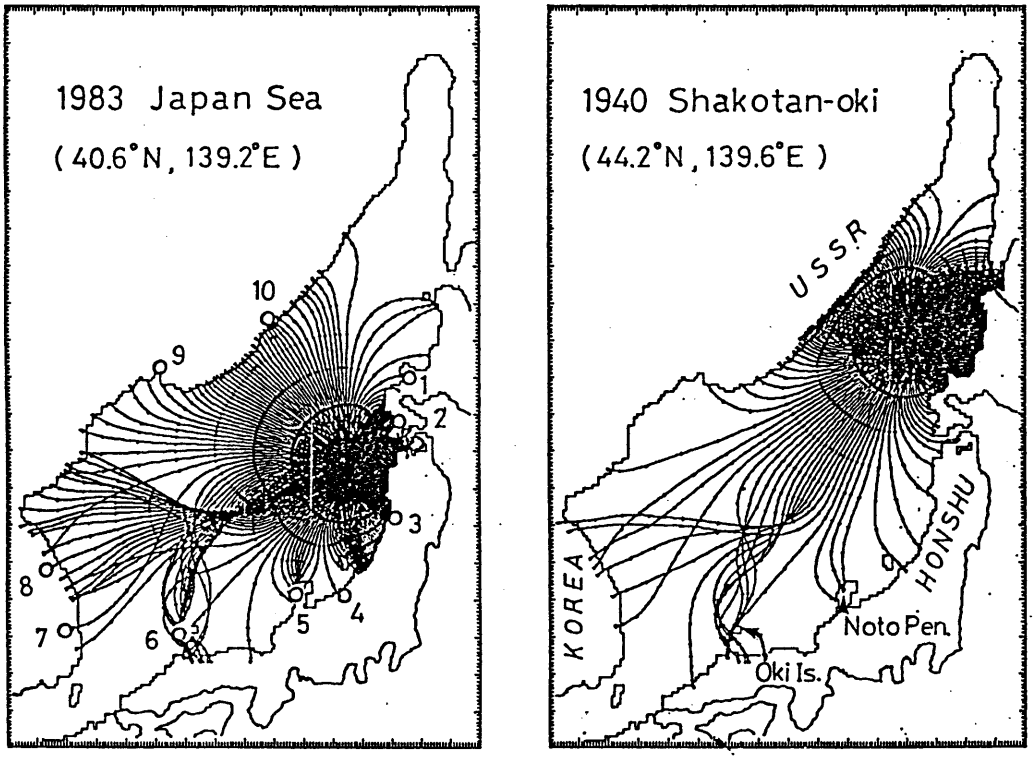

Figure 4. Ray tracing for tsunamis in the Japan Sea. Rays are generated with 1° interval in azimuth from point sources. Tick marks indicate each 10 min from the origin time. Numbered circles in the 1983 tsunami correspond to the tide gauge stations in Fig.6.

Fig.5

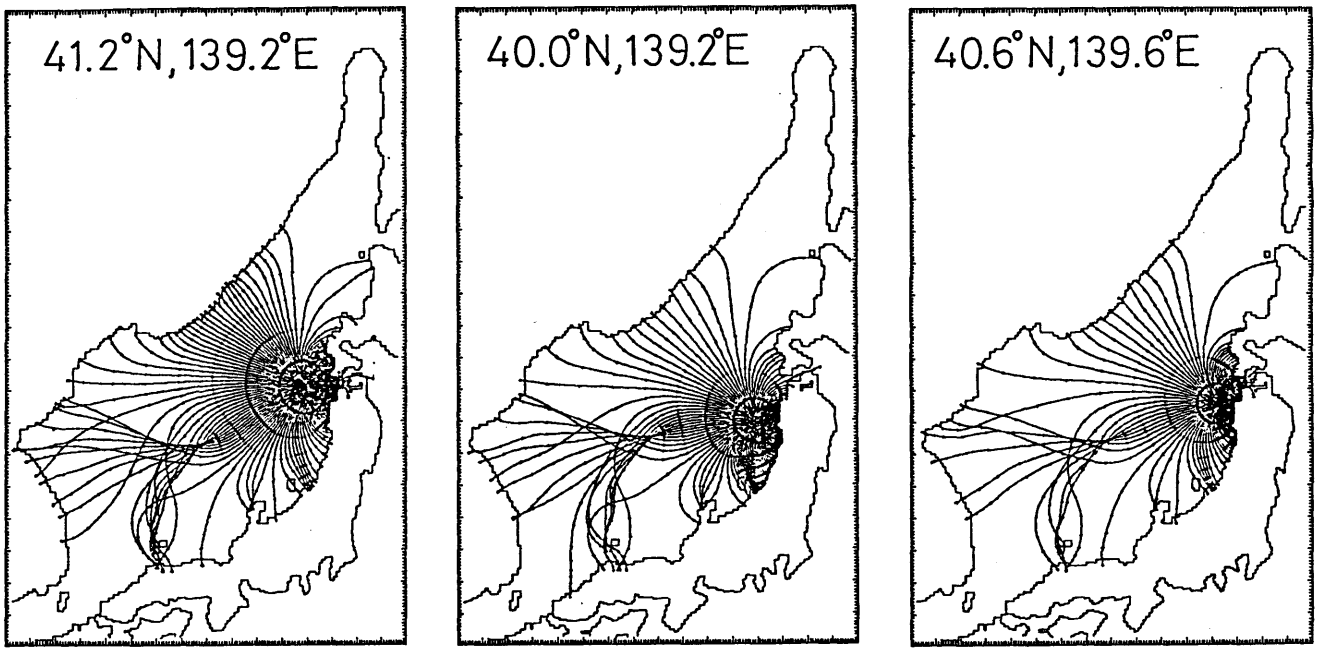

Figure 5. Ray tracing from three end points of the 1983 Japan Sea earthquake fault. Ray interval is 2° in azimuth.

Fig.6

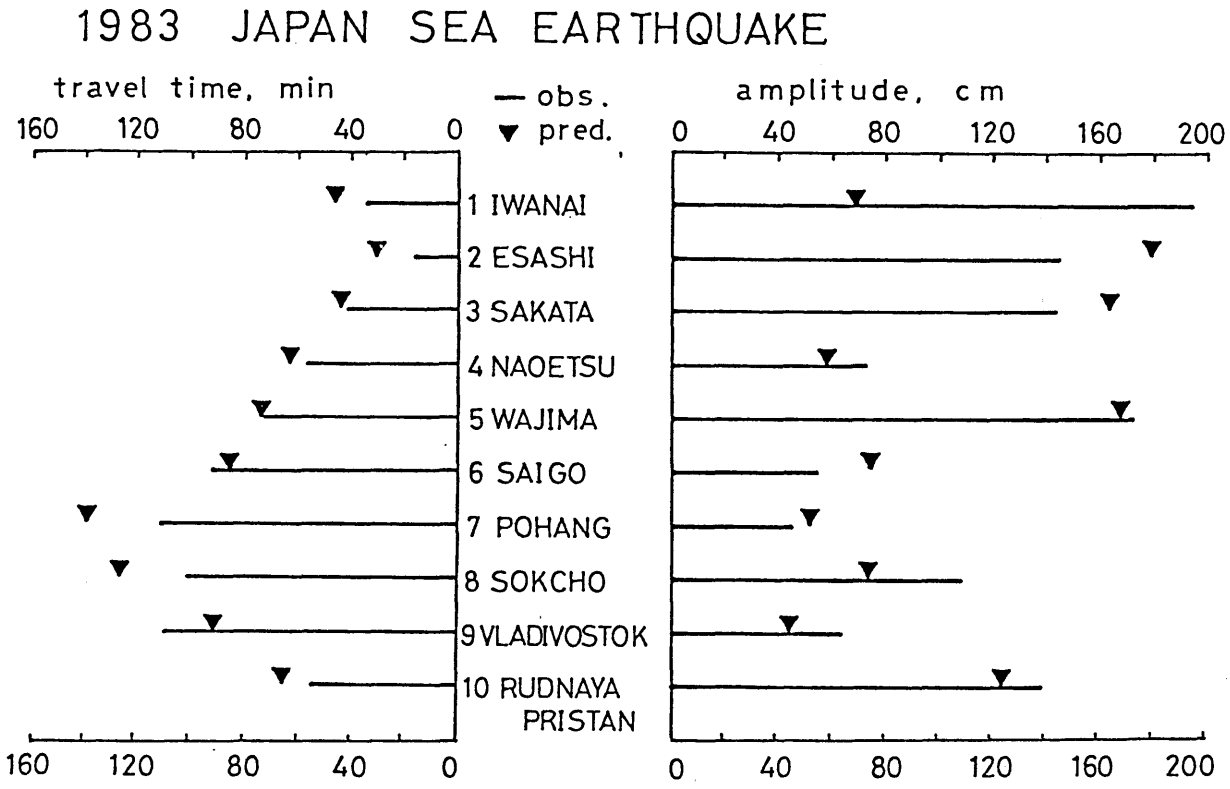

Figure 6. Comparison of predicted and observed values for travel time and amplitude for the 1983 Japan Sea tsunami. The location of each station is indicated in Fig.4.